ANALYSIS OF SOME WAX DEPOSITION EXPERIMENTS IN A CRUDE OIL CARRYING PIPE

by

ARNE D. HANDAL

THESIS

for the degree

Master of Science

in Computational Science and Engineering

(Master i Anvendt matematikk og Mekanikk)

Faculty of Mathematics and Natural Sciences
University of Oslo

October 2008

Det matematisk- naturvitenskapelige fakultet
Universitetet i Oslo

Analysis of some Wax Deposition Experiments in a Crude Oil Carrying Pipe

by

Arne Handal

Preface

During my bachelor's degree at the University in Bergen I finished a technical education in drilling and well technology at Bergen Maritime Vgs. In this period I also worked offshore for Odfjell Drilling and had a unique opportunity to combine a practical and theoretical experience. I realized soon that I had found my niche and decided to specialize in applied mathematics related to relevant problems in the oil industry. In the spring 2006 I got in contact with Research Director (StatoilHydro) Ruben Schulkes who is also Professor (2) at UiO. He suggested an interesting subject for my thesis and came up with the idea of doing analysis of wax deposition experiments performed by StatoilHydro. I have been privileged with two important mentors, Ruben Schulkes and Professor Arnold Bertelsen. Arnold Bertelsen and his strong knowledge in fluid mechanics have been of large importance. Finally, I want to thank Dr.ing. Rainer Hoffmann in StatoilHydro and his most kind assistance related to questions I have had about the wax experiment performed under his responsibility.

Arne D. Handal
Trondheim, August 29, 2008

Contents

Chapter 1

Introduction

1.1 Wax - Relevance of the Problem

Several crude oils contain significant amounts of wax. The different waxes have in a pure state definite freezing (melting) and boiling temperatures. During production, transportation and storage, the crude will attain temperatures lower than the freezing temperatures of the waxes. At these temperatures, called wax appearance temperatures (WAT), waxes start to form crystals in the fluid and deposits on the vessel walls. Wax build up can totally block a pipeline. In the worst cases, production must be stopped in order to replace the plugged portion of the pipeline (see Figure 1.1). The cost of this replacement and downtime is estimated approximately $30,000,000 per incident (Lee & Fogler 2007). In the North Sea an off-shore platform had to be abandoned at a cost of about $100,000,000 (Lee & Fogler 2007). Elf Aquitaine reported some years ago that the direct cost of removing a pipeline blockage from a sub sea pipeline is at least $5,000,000, and that the production loss during the 40 days downtime for the removal process is additional $25,000,000 (Singh 2000). In 1994 Mineral Management Society (USA) reported that fourteen sub sea pipelines were plugged in the Gulf of Mexico due to wax deposition, and this number has increased since then (Singh 2000). All these examples indicate that wax deposition can cause considerable economic losses, and the need and importance of wax predicting models follows. This has lead many engineers and scientists around the world to study wax deposition and to develop wax prediction models for the oil industry.

1.2 Physical Considerations

The fluid mixture produced from a reservoir is called crude and consists of several hydrocarbon components which can be divided into two main groups; light and heavy hydrocarbons. The light hydrocarbons like gas have carbon number C1-C4, while the liquid components gasoline, kerosene and diesel have carbon number C5-C17, and the heavier hydrocarbons consist of paraffins and napthenes. Paraffins are alkanes given by the chemical formula C_nH_{2n+2} with carbon number ranging from 18 to 65 or even higher (Srivastava et al. 1993). One of the features of high molecular weight paraffins is their low solubility in most of the oil solvents at room temperatures. At reservoir temperatures the solubility of these compounds is sufficiently high to keep them fully dissolved in the mixture, and the crude behaves as a Newtonian fluid with a low viscosity (Singh 2000). Once the crude leaves the reservoir, its temperature begins

Figure 1.1: A completely blocked pipe from the Norwegian shelf

The black material is wax that has blocked an offshore production line. There is no other solution but to cut the pipe, which is an extremely expensive cost with regard to loss of production, establishment of a new line connected to the well, challenges with restarting production etc. The picture is taken by StatoilHydro.

to drop due to colder environments. On its way, the oil temperature decreases, and at a sudden point the paraffin molecules precipitate out of the solution. This will occur when the bulk temperature reaches the critical WAT, or cloud point. Both terms are describing the temperature at which wax begins to crystallize from a distillate fuel. Paraffins precipitate when the bulk temperature decreases below the WAT. Crystal formation of wax particles is an exothermal process where paraffin molecules precipitate out of the oil solution and release thermal energy to the environments. It is believed that paraffins diffuse against the inner pipe surface as a consequence of the colder surface compared to the bulk flow temperature. This mechanism is often described by the famous Fick's law for a binary (two medium) system (Svendsen 1993).
Historically wax deposition problems have been known to the oil industry for several decades, and in the beginning researchers tried to relate the phenomenon to already well-known physical mechanisms. Mechanisms as molecular diffusion, shear dispersion, Brownian diffusion and gravity settling have been widely discussed considering the wax deposition process. Several hundreds of experiments indicate that molecular diffusion is the best descriptive mechanism to the problem of deposition (Brown et al. 1993; Svendsen 1993;
Singh 2000; Lee & Fogler 2007).
It is believed that a number of events will occur when crude, rich of wax, form on a cold inner pipe surface. We will not go into details because of the less relevance to our work, but it is important to mention what scientists seem to anticipate about this issue. In their

opinion solid waxes in sufficient quantities can significantly affect oil viscosity and cause non-Newtonian behaviour. Solid waxes can further interact to form a matrix that entraps the liquid phase and effectively gels the fluid (Kok & Saracoglu 2000). The liquid is light hydrocarbons assumed to diffuse out of the gel while the heavier hydrocarbons are assumed to diffuse into the gel (Singh 2000; Lee & Fogler 2007). In this way the deposit reaches an increased wax fraction over time. Therefore the deposit is often called gel instead of wax. In our work we will consistently use the terms wax or deposit. We regard an oil condensate that has a low content of waxes and consider the fluid as Newtonian.

Figure 1.2: Wax almost blocking the pipe

The inner radius available for flow has been significantly diminished because of the thick layer of wax that occupies most of the cross section in the pipe.

1.3 Some Earlier Works and Modeling

Ramirez-Jaramillo and C.Lira-Galeana (2004) have developed and tested a simulating wax deposition model in pipelines based on work done by Singh (2000), Svendsen (1993), Elphingstone (1999) etc. Results found in model pipelines indicate that deposition occurs due to radial mass diffusion driven by a concentration gradient induced by a temperature gradient. They conclude that the Reynold numbers and the mass Peclet number profoundly influence the mass deposition rate. They found a steep increase in the solid deposition with Reynolds number up to $Re \approx 100$, where a more gradual increase is observed for higher Reynolds number. A further observation in their study was a decrease in the mass deposited when $Re > 2000$. They state that the reason for this phenomenon from the fact that the shear forces acting on the deposit layer will become larger with higher Reynolds number. At some point the shear forces will remove deposit on the wall and thereby decrease its thickness. When estimating the average molecular diffusion coefficient, they found that there is an important connection

between the mass Peclet number and the radial mass flux. A substantial dependence of the deposited mass layer-thickness on the determined average diffusion coefficient were observed.

S.Todi et al., (2006) have performed experimental and modeling studies of wax deposition in crude-oil-carrying pipelines. They studied the deposition phenomena in relation to particle transport at all types of heat fluxes (positive (cooling), negative (heating) and zero). They considered laminar flow with low Reynolds number and found that deposition of the crude tested will occur independently of the three different types of heat fluxes, as long as the temperature of the deposition surface is below the WAT. They also found that the distribution of the wax particles is established as a result of Brownian diffusion and shear dispersion. During the experiments they observed very thin layers, and the pressure transducers did not register the decrease in diameter. Confirmation of deposition was via a visual notice of inner pipe wall deposition.
Ramachandran Venkatesan and H. Scott Fogler, (2004) studied and tested the well-known Colburn analogy for the heat and mass- transfer in turbulent pipe flow. For the crudes tested they presumed the systems to be in thermodynamic equilibrium in the sense that the kinetics of paraffin precipitation are much faster compared to the transport rates. They further showed that the Sherwood number must be less than the Nusselt number for a sub cooled system[1]. From the Colburn analogy they achieved a larger Sherwood number than the Nusselt number, and this caused an over-predicted mass-transfer rate. Venkatesan and Fogler consequently showed that the Colburn analogy is very wrong for a few selected oils.
B. A. Krasovitskii and V. I. Maron, (1980) developed a mathematical model for prediction of wax deposition in turbulent pipeline flow. An interesting aspect of their work is that they transformed the balance equations to the form of the Stefan problem[2]. They found that wax continuously occupy more of the free pipe surface along the pipeline when the bulk temperature reaches, or is lower than, the WAT. They noted that whereas the layer grows monotonically along the pipe when its thickness is small, a maximum appears at some local cross section of the pipe when the layer is thick. This is connected to the fact that when there is considerable wax-thickness, the heat dissipation capacity increases and thereby rises the bulk temperature. Accordingly, the temperature of the layer increases and thereby decreases the migration flow of paraffins. For large time scales (several days) they also observed that there is a minimum concentration of waxes corresponding to the maximum thickness of the layer and vice versa.
Svendsen, (1993) has given an important contribution to the understanding of wax deposition in both closed and open pipeline systems through his mathematical model based on analytical and numerical methods. His model is widely referred to by other researchers. In the introduction he makes it clear from the assumptions that a negative radial temperature gradient must be present in the flow. He assumes that with a zero gradient, approximately no deposition will occur. He further assumes that the temperature of the wall must be below the precipitation temperatures, and that the roughness of the wall must be large enough so that wax crystals can stick to it. In any case the model predicts that wax deposition can be considerably reduced even when the wall temperature is below the WAT, provided the liquid/solid phase transition is small at the wall temperature. He finally concludes that whether the model is good must be determined experimentally.

[1] A subcooled system means the center-line temperature is less than, or equal to the WAT.
[2] The Stefan Problem (after J. Stefan, 1835-1893) is originally based on the study of differential equations with moving boundaries, describing the formation of ice in the polar seas (L.I. Rubinstein, 1972).

Singh, (2000) developed and tested a mathematical model describing the wax deposition process in a laboratory flow-loop. He found that an increase in the wall temperature results in a decrease in the thickness of the deposit, and consequently an increase in the wax content of the deposit. He also observed that an increase in the flow rate has a similar effect; a decrease in the thickness and an increase in the solid wax fraction. The results from his mathematical models presented in his work show an excellent agreement with the experimental data. There is an interesting discussion related to some of the results. For three different flow-loop tests of laminar flow, the wax deposit virtually stopped after a certain period of time. From his point of view this condition arises as a result of the insulating effect of the wax deposit, i.e., the thermal resistance of the wax deposit is sufficient to prevent further deposition in the flow-loop. Singh seems to have noticed a connection between the flow rate, the inner wall temperature, and the thickness of wax. He writes that for a higher flow rate, the rate of heat transfer is higher; hence, the rate of increase of the interface temperature is higher. His research seems to have been an important contribution to the understanding, and predication of wax deposition. On the same level as Svendsen he is widely referred to by others. Through his thesis for the doctorate he built up a well described model for the physics related to the wax deposition processes.

1.4 About This Work

It is a challenging task to predict flow and temperature fields of a multicomponent fluid flowing turbulent in a hydrocarbon production pipe line. Many complicated physical processes take place, among them, wax deposition, the topic of this thesis. The models of Svendsen (1993) and Singh (2000) include wax deposition, but more experimental data are needed to assess the accuracy and applicability of these and other available models. Such data were obtained in a series of experiments carried out at StatoilHyro's Research Department in Porsgrunn (Norway). Data from these experiments have, with the most kind assistance from employees in that department, been made available for analysis and discussion in this thesis. The thermal boundary conditions is an important issue in wax deposition modeling. As a prerequisite for the analysis and discussion of the appropriate thermal boundary during wax deposition, Graetz problem is considered in Chapter 2 and the results are summarized in Chapter 3. In the end of Chapter 2, we also introduce the basic balance equations related to wax deposition.

Data from the wax deposition experiments at StatoilHydro's Research Department are analyzed, presented and discussed in Chapter 4 and elsewhere in the remainder of thesis. It turns out that the friction number formula is important for the calculation of wax layer thickness from pressure drop measurements. Further, the importance of the thermal boundary conditions are clearly demonstrated in the analysis. Dimensional analysis is also used in Chapter 5.

Chapter 2

Heat Transfer

2.1 Graetz problem

Graetz problem is a thermal entrance problem first studied by Graetz in 1885 (see White 2006). The fluid properties are assumed constant. Fully developed, laminar and time independent flow in a circular pipe is considered. A sudden change in wall temperature is imposed at some defined axial location. The temperature distribution of the incoming fluid with constant temperature will be modified downstream from this location. The problem is to find the modified temperature distribution.

2.1.1 Formulation of the Problem

A cylindrical coordinate system (r, θ, x) (see Figure 2.1) is appropriate for the boundary value problem indicated above. In accordance with the assumptions above, the axial velocity is given by the Poiseuille profile :

$$u(r) = \frac{\beta}{4\mu}\left(r_0^2 - r^2\right) \quad where \quad \beta = -\frac{\partial p}{\partial x} \tag{2.1}$$

The complete energy equation is approximated by :

$$u\frac{\partial T}{\partial x} \cong \frac{k}{\rho \cdot c_p}\frac{1}{r}\frac{\partial}{\partial r}\left(r\frac{\partial T}{\partial r}\right) \tag{2.2}$$

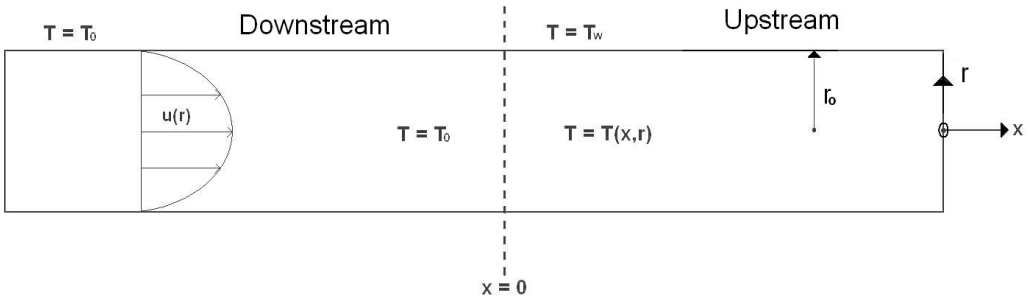

Figure 2.1: Illustration of Graetz Problem

where axial diffusion and dissipation have been neglected in relation to axial advection and radial diffusion as we presume $P_e \gg 1$ and $P_r E_c \ll 1$ (see A.1-A.8). With definitions Peclet number $P_e = \frac{u_o L}{\kappa_f}$, Prandtl number $P_r = \frac{k_f}{\rho C_p}$, and Eckert number $E_c = \frac{u_o^2}{C_p(T_o - T_w)}$.

The boundary conditions are :

$$T(0, r) = T_o \tag{2.3}$$

$$T(x > 0, r_o) = T_w \tag{2.4}$$

Graetz defined the following dimensionless variables :

$$T^* = \frac{T_w - T}{T_w - T_o}, \quad r^* = \frac{r}{r_o}, \quad x^* = \frac{2 \cdot k}{\rho \cdot c_p \cdot u_o \cdot {d_o}^2} \cdot x, \tag{2.5}$$

where the average velocity and the inner diameter is given by :

$$u_o = \frac{\beta {r_0}^2}{8\mu} \quad and \quad d_o = 2r_o \tag{2.6}$$

Combining (2.1), (2.5) and (2.6) with (2.2) gives:

$$\frac{\partial T^*}{\partial x^*} = \frac{1}{r^* \left(1 - r^{*2}\right)} \frac{\partial}{\partial r^*} \left(r^* \frac{\partial T^*}{\partial r^*} \right) \tag{2.7}$$

The dimensionless boundary conditions become :

$$T^*(0, r^*) = 1 \tag{2.8}$$

$$T^*(x^* > 0, 1) = 0 \tag{2.9}$$

2.1.2 Solution of the Problem

Since x^* and r^* are independent variables and equation (2.7) is linear, separation of variables is attempted by introducing :

$$T^*(x^*, r^*) = f(r^*) \cdot g(x^*) \tag{2.10}$$

If we now multiply both sides of equation (2.7) with $\frac{1}{T^*}$ and substitute equation (2.10), we will obtain a new equation where we have only x^* dependence on the right side of the equal sign and only r^* dependence on the left side. This can not be fulfilled except when both sides give a common constant. Here we call this constant λ, and therefore :

$$\frac{\frac{dg(x^*)}{dx^*}}{g(x^*)} = \frac{1}{r^*(1 - r^{*2})} \left(\frac{df}{dr^*}(r^*) + r^* \frac{d^2 f}{dr^{*2}} \right) = -\lambda^2 \tag{2.11}$$

where equation (2.11) gives the two separate equations :

$$\frac{dg}{dx^*} + \lambda^2 g = 0 \tag{2.12}$$

and:

$$r^* \frac{d^2 f}{d^2 r^*} + \frac{df}{dr^*} + \lambda^2 r^* \left(1 - r^{*2}\right) f = 0 \tag{2.13}$$

The general solution of (2.12) is :

$$g(x^*) = Ae^{-\lambda^2 x^*} \tag{2.14}$$

With the boundary conditions in mind, we realize we have an eigenvalue problem to solve giving a sequence of eigenvalues $\{\lambda_n\}$ and eigenfunctions $\{f_n(r^*)\}$, if we define $f_n(r^*) = f_n(r^*;\lambda_n)$. The combination of (2.14) and (2.10) with the eigenfunctions $\{f_n(r^*)\}$ in mind, we have :

$$T^*(x^*, r^*) = \sum_{n=0}^{\infty} A_n f_n(r^*) e^{-\lambda_n^2 x^*} \tag{2.15}$$

Where the index n indicate that we have restricted values of λ_n, which are the representing eigenvalues related to the Graetz functions f_n. The entrance condition (2.8) gives :

$$\sum_{n=0}^{\infty} A_n f_n(r^*) = 1 \tag{2.16}$$

and the eigenvalues are determined by the condition (2.9) giving :

$$f_n(1, \lambda_n) = f_n(1) = 0 \tag{2.17}$$

Graetz showed that the eigenfunctions f_n are orthogonal over the interval $r^* \in [0, 1]$ with weight $r^*(1 - r^{*2})$ (White 2006). Therefore we have :

$$\int_0^1 r^*(1 - r^{*2}) f_m(r^*) dr^* = \begin{cases} \int_0^1 r^*(1-r^{*2}) f_m^2(r^*) A_n dr^* & ; \ n=m \\ 0 & ; \ n \neq m \end{cases} \tag{2.18}$$

giving:

$$A_n = \frac{\int_0^1 r^*(1 - r^{*2}) f_n(r^*) dr^*}{\int_0^1 r^*(1 - r^{*2}) f_n^2(r^*) dr^*} \tag{2.19}$$

Rewriting equation (2.13) by introducing the transformations :

$$Z = \lambda r^{*2} \quad and \quad W(Z) = e^{\frac{Z}{2}} f(r^*) \tag{2.20}$$

we arrive at the Kummer equation :

$$Z \frac{d^2W}{dZ^2} + (1 - Z)\frac{dW}{dZ} + \left(\frac{\lambda}{4} - \frac{1}{2}\right) W = 0 \tag{2.21}$$

The general solution for this special case is given by the Kummer‘s function (Abramowitz & Stegun 1964) which has a regular singularity at $Z = 0$ and an irregular singularity at ∞. An independent solution of (2.21) is :

$$W(Z) = C \cdot M(\frac{1}{2} - \frac{\lambda}{4}, 1, Z), \quad where \quad C = constant \tag{2.22}$$

where :

$$M(a, 1, Z) = 1 + \sum_{k=1} \frac{(a)_k}{(k!)^2} Z^k, \quad a = \frac{1}{2} - \frac{\lambda}{4} \tag{2.23}$$

and:

$$(a)_k = a(a+1)(a+2)...(a+k-1), \qquad k \geq 1 \tag{2.24}$$

The boundary conditions give :

$$M(a,1,\lambda) = 0 \tag{2.25}$$

and:

$$\sum_{n=0}^{\infty} A_n f_n(r^*) = \sum_{n=0}^{\infty} A_n e^{-\frac{1}{2}\lambda_n r^{*2}} \left(1 + \sum_{k=1}^{K} \frac{(a_n)_k}{(k!)^2} \lambda_n^k r^{*2k}\right) = 1 \tag{2.26}$$

If we define :

$$(a_n)_k = (\frac{1}{2} - \frac{\lambda_n}{4}) \cdot (\frac{1}{2} - \frac{\lambda_n}{4} + 1) \cdot (\frac{1}{2} - \frac{\lambda_n}{4} + 2) \cdot ... \cdot (\frac{1}{2} - \frac{\lambda_n}{4} + k - 1) \tag{2.27}$$

The coefficients are :

$$A_n = \frac{\int_0^1 \left(1 - r^{*2}\right) e^{-\frac{1}{2}\lambda_n r^{*2}} \left(1 + \sum\limits_{k=1}^{K} \frac{(a_n)_k}{(k!)^2} \lambda_n^k r^{*2k}\right) dr^*}{\int_0^1 \left(1 - r^{*2}\right) e^{-\lambda_n r^{*2}} \left(1 + \sum\limits_{k=1}^{K} \frac{(a_n)_k}{(k!)^2} \lambda_n^k r^{*2k}\right)^2 dr^*} \tag{2.28}$$

2.1.3 Solving the Coefficients

The coefficients A_n are evaluated using series of expansion of the integrals involved (see equation 2.28). Partial integration is applied to generate the series. Details of this task are given in (A.1-A.3. We write the expression for the coefficients as :

$$A_n = \frac{\int_0^1 r^* e^{-\beta_n r^{*2}} dr^* + \int_0^1 \sum\limits_{k=1}^{K} \left(\frac{(a_n)_k}{(k!)^2} \lambda_n^k r^{*2k+1}\right) e^{-\beta_n r^{*2}} dr^* - \int_0^1 r^{*3} e^{-\beta_n r^{*2}} dr^*}{(...)} - \frac{\int_0^1 \sum\limits_{k=1}^{K} \left(\frac{(a_n)_k}{(k!)^2} \lambda_n^k r^{*2k+3}\right) e^{-\beta_n r^{*2}} dr^*}{(...)} \tag{2.29}$$

where the denominator (...) is given by :

$$\begin{aligned}(...) = &\int_0^1 r^* e^{-2\beta_n r^{*2}} dr^* + 2 \int_0^1 \sum_{k=1}^{K} \left(\frac{(a_n)_k}{(k!)^2} \lambda_n^k r^{*2k+1}\right) e^{-2\beta_n r^{*2}} dr^* \\ &+ \int_0^1 \sum_{k=1}^{K} \left(\frac{(a_n)_k}{(k!)^2} \lambda_n^k r^{*2k+\frac{1}{2}}\right)^2 e^{-2\beta_n r^{*2}} dr^* - \int_0^1 r^{*3} e^{-2\beta_n r^{*2}} dr^* \\ &- 2 \int_0^1 \sum_{k=1}^{K} \left(\frac{(a_n)_k}{(k!)^2} \lambda_n^k r^{*2k+3}\right) e^{-2\beta_n r^{*2}} dr^* - \int_0^1 \sum_{k=1}^{K} \left(\frac{(a_n)_k}{(k!)^2} \lambda_n^k r^{*2k+\frac{3}{2}}\right)^2 e^{-2\beta_n r^{*2}} dr^*\end{aligned} \tag{2.30}$$

and : $\beta_n = \frac{\lambda_n}{2}$
If we continue to process the equation given over, we might express the coefficients as following :

$$A_n = \frac{C_n}{D_n} \tag{2.31}$$

The numerator :

$$\begin{aligned} C_n = \frac{1}{2\beta_n}\left(1 - e^{-\beta_n}\right) + e^{-\beta_n}\sum_{i=0}^{S}(2\beta_n)^i \sum_{k=1}^{K}\tilde{A}_{n,k}\frac{1}{\prod_{j=0}^{i}(2k+2j+2)} \\ - e^{-\beta_n}\sum_{i=0}^{S}\frac{(2\beta_n)^i}{\prod_{j=0}^{i}(2j+4)} - e^{-\beta_n}\sum_{i=0}^{S}(2\beta_n)^i\sum_{k=1}^{K}\tilde{A}_{n,k}\frac{1}{\prod_{j=0}^{i}(2k+2j+4)} \end{aligned} \tag{2.32}$$

The denominator :

$$\begin{aligned} D_n = \frac{1}{4\beta_n}\left(1 - e^{-2\beta_n}\right) + 2e^{-2\beta_n}\sum_{i=0}^{S}(4\beta_n)^i\sum_{k=1}^{K}\tilde{A}_{n,k}\frac{1}{\prod_{j=0}^{i}(2k+2j+2)} \\ + e^{-2\beta_n}\sum_{i=0}^{S}(4\beta_n)^i\sum_{a=1}^{K}\sum_{b=1}^{K}\tilde{A}_{n,a}\tilde{A}_{n,b}\frac{1}{\prod_{j=0}^{i}(2(a+b)+2j+2)} \\ - e^{-2\beta_n}\sum_{i=0}^{S}(4\beta_n)^i\sum_{a=1}^{K}\sum_{b=1}^{K}\tilde{A}_{n,a}\tilde{A}_{n,b}\frac{1}{\prod_{j=0}^{i}(2(a+b)+2j+4)} \\ - e^{-2\beta_n}\sum_{i=0}^{S}\frac{(4\beta_n)^i}{\prod_{j=0}^{i}(2j+4)} - 2e^{-\beta_n}\sum_{i=0}^{S}(4\beta_n)^i\sum_{k=1}^{K}\tilde{A}_{n,k}\frac{1}{\prod_{j=0}^{i}(2k+2j+4)} \end{aligned} \tag{2.33}$$

where:

$$\tilde{A}_{n,\gamma} = \frac{(a_n)_k}{(k!)^2}Z_n^k, \quad and \quad \gamma = k, a, b \tag{2.34}$$

It is necessary to do further calculations to determine the upper boundaries S and K. The upper boundary K is found by numerical calculations of equation (2.35). This is done by finding the roots/eigenvalues and evaluate their precision based on existing tables (Shah & London 1978; White 2006).

$$1 + \sum_{k=1}^{K}\frac{(a_n)_k}{(k!)^2}\lambda_n^k = 0 \tag{2.35}$$

For this case we have found it sufficient with an upper boundary $K = 40$.
How to derive S is dependent on the value of n, or how many eigenvalues we want to include to our solution. When n increases, so does S. See A.2 for further details.

Table 2.1: Eigenvalues of Graetz Problem

n	λ_n	S	A_n
0	2.7043644	40	+1.476435
1	6.6790315	40	−0.806124
2	10.6733795	40	+0.588761
3	14.6710785	40	−0.475850
4	18.6698719	40	+0.405019
5	22.6691438	75	−0.355757
6	26.6686716	75	+0.319169
7	30.6684241	75	−0.290745
8	34.6686899	75	+0.267952
9	38.6704098	75	−0.249322

The coefficients A_n given in the Table 2.1 above indicate that the solution will converge slowly, and it is therefore necessary to involve a sufficient number of eigenvalues to achieve an accurate solution for $x^* = 0$. This can be confirmed by evaluating the dimensionless temperature function (2.38) for $x^* = 0$ and $r^* = 0$. The sum must converge to one according to the boundary condition (2.8).

2.1.4 Dimensionless Temperature Profile

We have found an analytical expression for the coefficients and we can now gather the most important results from our analysis. Equation (2.15) gives the dimensionless temperature profile, but for completeness we chose to repeat it here :

$$T^*(x^*, r^*) = \sum_{n=0}^{\infty} A_n f_n(r^*) e^{-\lambda_n^2 x^*} \tag{2.36}$$

By combining the transformations (2.20) with the given solution to the Kummer equation, we achieve an expression for the function $f_n(r^*)$:

$$f_n(r^*) = e^{-\frac{1}{2}\lambda_n r^{*2}} \left(1 + \sum_{k=1}^{K} \frac{(a_n)_k}{(k!)^2} \lambda_n^k r^{*2k}\right) \tag{2.37}$$

The dimensionless temperature can therefore be expressed as :

$$T^*_{Graetz}(x^*, r^*) = \sum_{n=0}^{\infty} A_n e^{-\lambda_n\left(\frac{1}{2}r^{*2} + \lambda_n x^*\right)} \left(1 + \sum_{k=1}^{K} \frac{(a_n)_k}{(k!)^2} \lambda_n^k r^{*2k}\right) \tag{2.38}$$

In this chapter we will compare the dimensionless cup-mixing temperatures[1] considering laminar flow. We therefore derive the dimensionless cup-mixing temperature based on the Graetz temperature (2.38) (see A.4) :

$$\begin{aligned} T^*_{Graetz-cup-mix} &= 4\int_0^1 r^*\left(1-r^{*2}\right)T^*dr^* = 4\sum_{n=0}^{\infty} A_n \exp(-\lambda_n^2 x)\frac{(1-\exp(-\beta_n))}{2\beta_n} \\ &+ 4\sum_{n=0}^{\infty} A_n \exp(-\lambda_n^2)\sum_{i=1}^{S}(2\beta_n)^i \sum_{k=1}^{K}\widetilde{A}_{n,k}\frac{\exp(-\beta_n)}{\prod_{j=0}^{i}(2k+2+2j)} \\ &- 4\sum_{n=0}^{\infty} A_n \exp(-\lambda_n^2 x)\sum_{i=0}^{S}\frac{(2\beta_n)^i\exp(-\beta_n)}{\prod_{j=0}^{i}(4+2j)} \\ &- 4\sum_{n=0}^{\infty} A_n \exp(-\lambda_n^2)\sum_{i=1}^{S}(2\beta_n)^i \sum_{k=1}^{K}\widetilde{A}_{n,k}\frac{\exp(-\beta_n)}{\prod_{j=0}^{i}(2k+4+2j)} \end{aligned} \quad (2.39)$$

2.1.5 Accuracy of Dimensionless Temperature Profile

If we implement the equations (2.31)-(2.34) in Maple and derive the different coefficients, our program will only give the ten first coefficients precisely, but as we involve eigenvalues greater than λ_9 (see T able 2.1), our program reduces accuracy. Term three and four on the right side of equation (2.33) have eigenvalues in high powers, and as the eigenvalues become larger, the results are inaccurate and disturb the numerical calculations. We conclude that our implemented solution must be limited to the first ten eigenvalues.

2.1.6 Comment

The dimensionless temperature distribution are shown in Figures (2.2)-(2.7) below. From the figures we see a decreasing temperature for $x^* > 0$. The temperature on the wall is lower than the bulk temperature and causes a release of energy toward the wall. The surroundings absorb thermal energy as the fluid moves in the positive x^*-direction, until equilibrium is achieved. We notice the strong radial temperature gradient close to the wall for $0 < x^* < \frac{1}{10}$, and that the gradient becomes weaker as thermal equilibrium is approached as the fluid is being cooled and transported in the pipe. We notice small waves in the profiles where $x^* < \frac{1}{1000}$. This is due to the restricted number of eigenvalues involved. Including a larger number of eigenvalues will decrease the "wavy effect" of the profiles near $x^* = 0$. Equation (2.5) gave $x^* = \frac{x}{r_o Re Pr}$. We find that the Pr number for water vapor and (unused) engine oil are 1.06 and 233, respectively given a bulk flow temperature at 380K, and using tables A.4 and A.5 (Incropera & DeWitt 1996). If we assume constant volume flux and Reynolds number corresponding to laminar flow, this will indicate that the engine oil will be transported a distance 200 times longer than the water before the same temperature is reached.

[1] The cup-mixing temperature is defined in equation (2.47).

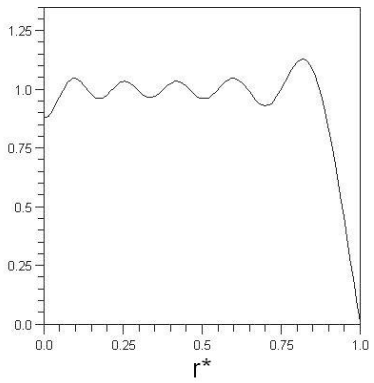

Figure 2.2: T^* when $x^* = 0$

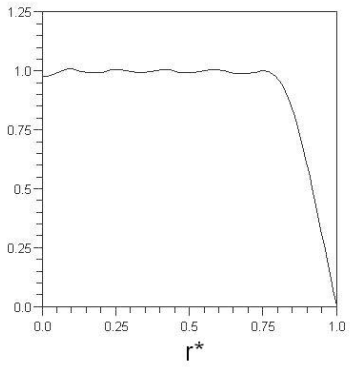

Figure 2.3: T^* when $x^* = \frac{1}{1000}$

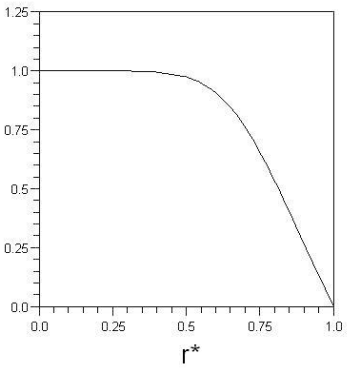

Figure 2.4: T^* when $x^* = \frac{1}{100}$

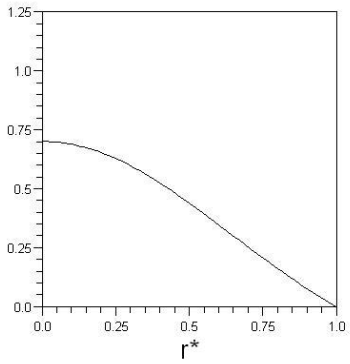

Figure 2.5: T^* when $x^* = \frac{1}{10}$

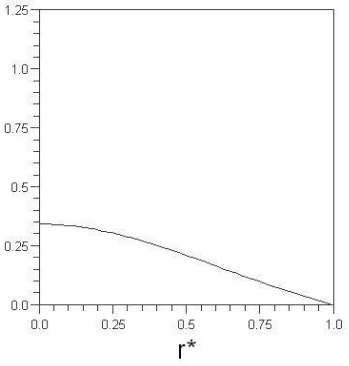

Figure 2.6: T^* when $x^* = \frac{1}{5}$

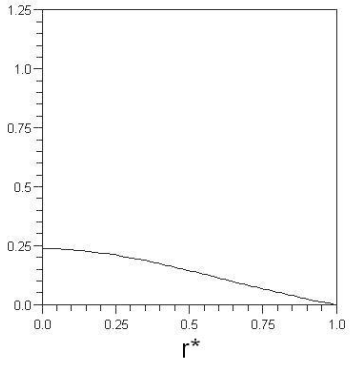

Figure 2.7: T^* when $x^* = \frac{1}{4}$

2.2 Heat Transfer in Pipe with Stationary Turbulent Flow

The general velocity field can be written as the following by introducing mean velocity and fluctuating velocities :

$$\mathbf{V} = \Big(V(r) + \mathbf{v}'_x(\mathbf{x},t)\Big)\,\mathbf{i}_x + \mathbf{v}'_r(\mathbf{x},t)\,\mathbf{i}_r + \mathbf{v}'_\theta(\mathbf{x},t)\mathbf{i}_\theta \tag{2.40}$$

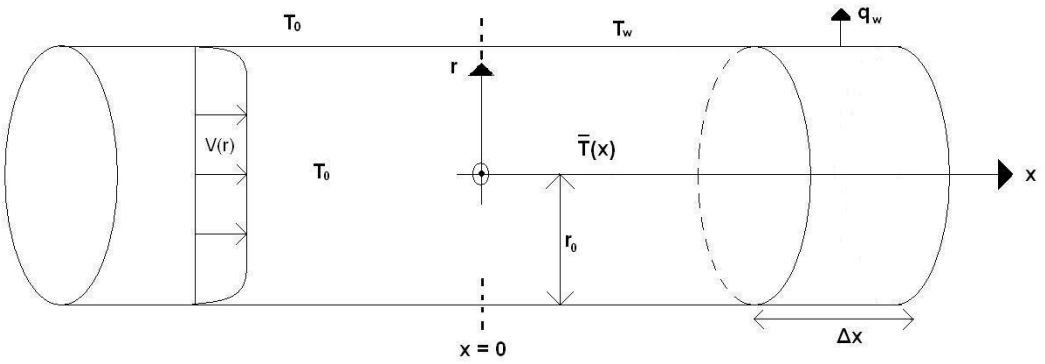

Figure 2.8: Stationary Turbulent Flow with Heat Exchange to the Environments

We presume the axial velocity component as dominating. If we further use Reynolds time averaging, which is appropriate for stationary turbulence, we achieve the mean velocity in the axial direction :

$$V(r) \tag{2.41}$$

Area-averaging the mean velocity still give a good approximation to V(r) over the cross section except near the wall (see 2.9). The velocity profile displayed in Figure 2.9 is derived from an analytical expression of the eddy diffusivity (Quarmby & Anand 1969). Based on this profile we further introduce an area-averaged velocity :

$$\overline{V} = \frac{2}{r_o^2}\int_0^{r_o} rV(r)dr \tag{2.42}$$

It is now of interest to investigate the loss of energy to the surroundings as a consequence of heat loss from the bulk flow through the pipe wall. Since the flow is turbulent, the time averaged thermal energy equation should be considered. When axial heat conduction and dissipation is neglected, the equation will be (see B.1-B.7) :

$$V\frac{\partial T}{\partial x} = \frac{1}{r}\frac{\partial}{\partial r}\left(r\frac{\partial}{\partial r}\left(\kappa + \kappa_t\right)\frac{\partial T}{\partial r}\right) \tag{2.43}$$

where κ and κ_t are the thermal diffusivities, molecular and turbulent, respectively. κ_t must be given to allow equation (2.43) to be solvable, for example as a correlation or by turbulence modeling. It follows from (2.43) that the radial component of the heat flux vector is given by :

$$q_r = -\rho C_p\left(\kappa + \kappa_t\right)\frac{\partial T}{\partial r} \tag{2.44}$$

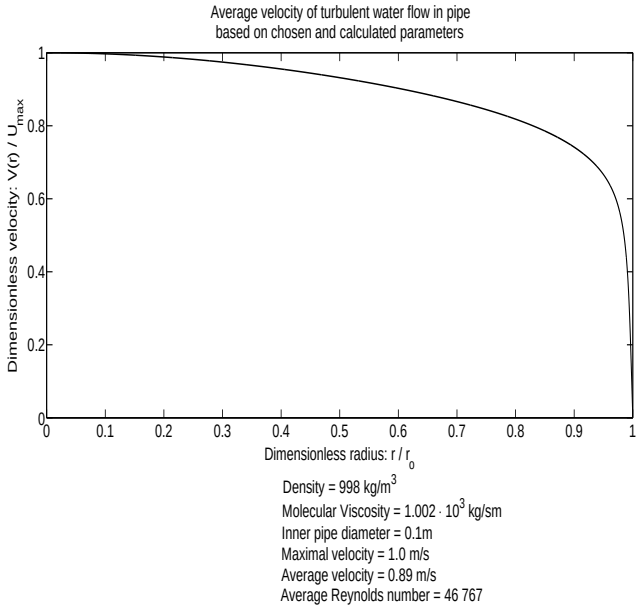

Figure 2.9: Turbulent Velocity Profile

where $\kappa_t(r = r_o) = 0$, and the heat flux at the wall is :

$$q_w = -k_f \left(\frac{\partial T}{\partial r} \right)_{r=r_o} \tag{2.45}$$

q_w is given by equation (2.45) for both laminar and turbulent flow, but the temperature distributions are different in the two cases. Here we do not intend to model κ_t and we can therefore not predict the heat flux at the wall for turbulent flow using (2.45). We will instead use Nusselt number correlations. First we define the mass flux (in axial direction) :

$$Q_m = 2\pi \int_0^{r_o} \rho V r dr \tag{2.46}$$

The Nusselt number and the cup-mixing temperature are defined by (White 2006) :

$$Nu = \frac{q_w d_o}{k(T_{cup-mix} - T_w)} \quad and \quad T_{cup-mix} = \frac{\int_A \rho V T_{av} dA}{\int_A \rho V dA} \tag{2.47}$$

The temperature $T_{cup-mix}$ is the the cup-mixing temperature defined as a mass flow (ρV) weighted cross sectional averaged temperature. We regard a physical system that is approximately independent of time in the sense that we have a constant inlet temperature. In reality the temperature in production lines along the seabed will be almost independent of time, and along the pipe we do not know exactly how the temperature will vary over the cross sections. In the definition of the cup-mixing temperature we have eliminated information of the cross sectional distribution of the temperature, and can therefore only derive a simplified one dimensional temperature distribution from the energy equation. There are several empirical

models for the Nusselt number in a smooth pipe with turbulent flow, and in the literature (Incropera & DeWitt 1996) the most recommended is the Pethukov model :

$$Nu = \frac{(\frac{f}{8})Re_{d_o}Pr}{1,07 + 12,7(\frac{f}{8})^{\frac{1}{2}}(Pr^{\frac{2}{3}} - 1)}, \quad Re_{d_o} = \frac{\overline{V} \cdot d_o}{\nu}, \quad Pr = \frac{C_p \cdot \mu}{k_f} \tag{2.48}$$

The Pethukov friction factor f is given by :

$$f = (0.790 \ln Re_{d_o} - 1.64)^{-2} \tag{2.49}$$

and the Petukhov model is adapted for Reynolds and Prandtl numbers within the respective intervals :

$$3 \cdot 10^3 < Re_{do} < 5 \cdot 10^6 \qquad 0.5 < Pr < 2,000 \tag{2.50}$$

For rough pipes a model developed by A.F. Mills could be considered (Mills 1979). To progress further with the energy balance equation (2.43), we area-average the equation using the definitions of the cup mixing temperature and the mass flux (see B.8-B.9), finding :

$$Q_m C_p \frac{\partial T_{cup-mix}}{\partial x} = -2\pi r_o q_w \tag{2.51}$$

By substituting the defined Nusselt number (2.47) and the heat flux (2.45) into (2.51) we find by integration :

$$T_{cup-mix} = T_w + (T_o - T_w) \exp\left(\frac{-\pi k_f Nu}{Q_m C_p} x\right) \tag{2.52}$$

where $T_{cup-mix}(x < 0) = T_o$ has been used as the boundary condition. To simplify the temperature equation we introduce the dimensionless parameters :

$$T^*_{cup-mix} = \frac{T_{cup-mix} - T_w}{T_o - T_w} \quad and \quad x^* = \frac{x}{2r_o} \tag{2.53}$$

Combining (2.51), (2.52) and (2.53) we find the following dimensionless temperature distribution :

$$T^*_{cup-mix} = \exp\left(\frac{-2r_o \pi k_f Nu}{Q_m C_p} x^*\right) \tag{2.54}$$

2.3 Heat Conduction Through Pipe Wall for Laminar and Turbulent Flow

We assume the flow for both laminar and turbulent conditions to be stationary and fully developed.

2.3.1 Laminar Flow

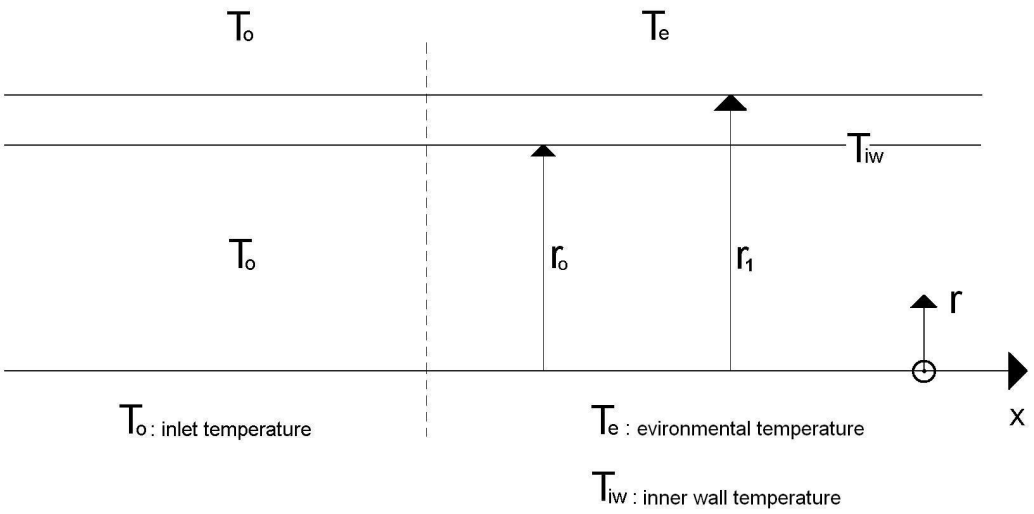

Figure 2.10: Influence of Pipe Wall Included

For laminar flow we have the velocity profile :

$$u(r) = \frac{\beta}{4\mu}\left(r_0^2 - r^2\right) \quad where \quad \beta = constant = -\frac{\partial p}{\partial x} \tag{2.55}$$

The mass flux can be derived exactly since we know the velocity profile :

$$Q_m = \frac{\pi \beta r_o^4 \rho}{8\mu} \tag{2.56}$$

A balance equation for the heat transfer through the wall is given by (see Figure 2.10) :

$$U_w(T_e - T_{iw})2\pi r_o \Delta x - k_w \frac{\partial T}{\partial r} 2\pi r \Delta x = 0 \tag{2.57}$$

where U_w is the heat transfer coefficient of the wall. Integration of (2.57) yields :

$$U_w \frac{r_o}{k_w} \int_{r_o}^{r_1} \frac{1}{r} dr = \int_{T_{iw}}^{T_e} \frac{dT}{T_e - T_{iw}} \tag{2.58}$$

We then achieve the heat transfer coefficient of the wall :

$$U_w = \frac{k_w}{r_o \ln\left(\frac{r_1}{r_o}\right)} \tag{2.59}$$

The overall heat transfer coefficient related to our system is (see (B.10-B.20)) :

$$\frac{1}{U_{tot}} = \frac{1}{h_f} + \frac{1}{U_w} \tag{2.60}$$

where h_f is the heat coefficient of the fluid inside the pipe given by :

$$h_f = \frac{k_f Nu}{2r_o} \tag{2.61}$$

The (mean) Nusselt number for forced convection of fully developed laminar flow inside a circular duct with constant wall temperature is given by (Hausen 1959) :

$$Nu = 3.657 + \frac{0.19\left(\mathrm{Re}\,\mathrm{Pr}\,\frac{2r_o}{L}\right)^{0.8}}{1 + 0.117\left(\mathrm{Re}\,\mathrm{Pr}\,\frac{2r_o}{L}\right)^{0.467}} \quad where \;\; Re < 2300 \tag{2.62}$$

L is the pipe length, and we consider a system where $L \gg 2r_o$. It is therefore a good approximation to use $Nu = 3.657$. We may now derive the overall heat transfer coefficient from the equations (2.60), (2.61) and (2.62). This can be used in our next statement; a balance equation for the loss of energy in the flow direction and for the transfer of thermal energy from the fluid through the pipe wall. The dimensions involved are energy per unit time and per unit length :

$$Q_m C_p \frac{\partial T_{cup-mix}}{\partial x} = 2\pi r_o U_{tot}(T_e - T_{cup-mix}) \tag{2.63}$$

Integration with boundary conditions (see Figure 2.11) gives :

$$T_{cup-mix} = T_e + (T_o - T_e)\exp\left(-\frac{16\mu U_{tot}}{\beta r_o^3 \rho C_p} x\right) \tag{2.64}$$

Let us simplify the temperature function by introducing the dimensionless variables :

$$T^*_{cup-mix} = \frac{T_{cup-mix} - T_e}{T_o - T_e} \quad and \quad x^* = \frac{x}{2r_o} \tag{2.65}$$

The dimensionless temperature for laminar flow is then :

$$T^*_{cup-mix} = \exp\left(-\frac{32\mu U_{tot}}{\beta r_o^2 \rho C_p} x\right) \tag{2.66}$$

2.3.2 Turbulent Flow

For turbulent flow conditions we can now express the general dimensionless temperature distribution along a pipe in a similar way as for the laminar. It is then important to use the overall heat transfer coefficient U_{tot} related to turbulent flow. There exist several empirical models of the heat transfer coefficient considering turbulent flow. We have already introduced the Pethukov Nusselt correlation from equations (2.48) and (2.49) and can therefore derive

the heat transfer coefficient of the fluid from (2.61). The expression for U_{tot} is established in (2.60), and it is straight forward to derive the overall heat transfer coefficient for turbulent flow conditions, as well. The temperature distribution is almost the same as (2.64) except for the mass flow and the overall heat transfer coefficient. The temperature for turbulent flow is therefore :

$$T_{cup-mix} = T_e + (T_o - T_e) \exp\left(-\frac{2\pi r_o U_{tot}}{Q_m C_p} x\right) \tag{2.67}$$

or in dimensionless form :

$$T^*_{cup-mix} = \exp\left(-\frac{4\pi r_o^2 U_{tot}}{Q_m C_p} x^*\right) \tag{2.68}$$

2.3.3 Deriving the Inner Wall Temperature

We find the inner wall temperature T_{iw} by assuming that the total heat exchange from the fluid to the environments must equal the transfer of thermal energy from the bulkflow to the pipe wall. Our balance equation becomes :

$$U_{tot}(T_e - T_{cup-mix}) = h_f(T_{iw} - T_{cup-mix}) \tag{2.69}$$

After some manipulation we achieve a result that can be used for both turbulent and laminar flow. We already know that the heat transfer coefficient related to the fluid is different for laminar and turbulent flow. The general inner wall temperature is :

$$T_{iw} = T_{cup-mix} - \frac{U_{tot}}{h_f}(T_{cup-mix} - T_e) \tag{2.70}$$

2.4 Influence of Pipe Wall Including an Uniform Insulation on the Inside

We assume that the insulation inside the pipe is of constant thickness everywhere on the inner wall. The overall heat transfer coefficient U_{tot} will then be expressed as below for the general case :

$$\frac{1}{U_{tot}} = \frac{1}{h_f} + \frac{1}{U_i} + \frac{1}{U_w} \tag{2.71}$$

We have included an insulating wall layer through the heat transfer coefficient U_i in the equation above. We derive U_i in the same way as we did for the heat transfer coefficient of the wall -establishing a balance equation for the heat transfer through the insulation (see Figure 2.11) :

$$U_i(T_w - T_{iw})2\pi r_o \Delta x - k_i \frac{\partial T}{\partial r} 2\pi r \Delta x = 0 \tag{2.72}$$

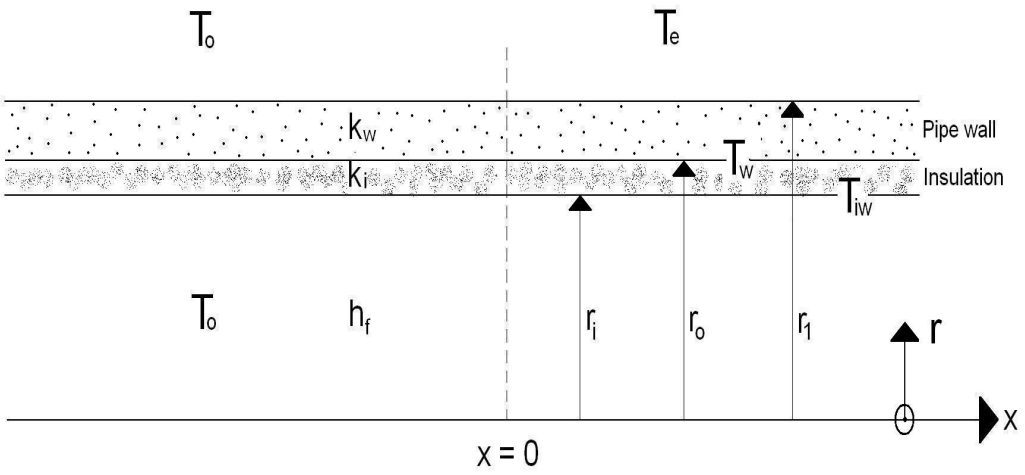

Figure 2.11: Influence of Insulation and Pipe Wall

Integration of (2.72) gives the heat transfer coefficient of the insulation :

$$U_i = \frac{k_i}{r_o \ln\left(\frac{r_o}{r_i}\right)} \tag{2.73}$$

It is now possible to derive the overall heat transfer coefficient for laminar and turbulent flow by combining the already given heat transfer coefficients of fluids and of insulation with

(2.71). The temperatures are already given by the equations, (2.64)-(2.65) or (2.67)-(2.68). Remember to replace r_o with r_i (see Figure 2.11) when using the mentioned equations.

2.5 Analysis of Wax Deposition

We consider a simplified situation where the condensate is being transported and cooled through a horisontal pipe with circular cross section. The flow is considered stationary and turbulent. The condensate is further divided into three components, liquid (l), dissolved wax and wax crystals (d) and solid wax (w). The liquid is determined to be the lighter hydrocarbon components in the condensate. The dissolved wax is the same as dissolved paraffins and wax crystals, where crystals are precipitated paraffins in the bulk flow. The solid wax represent the deposit on the pipe wall. We consider a situation of only wax in the deposit; that liquid components are not involved in the deposition process. We also consider wax deposition to occur in a localized area in the pipe (see Figure 2.12) and that the wax deposit is a uniform and concentric layer of constant thickness. The balance equations for the problem is given below.

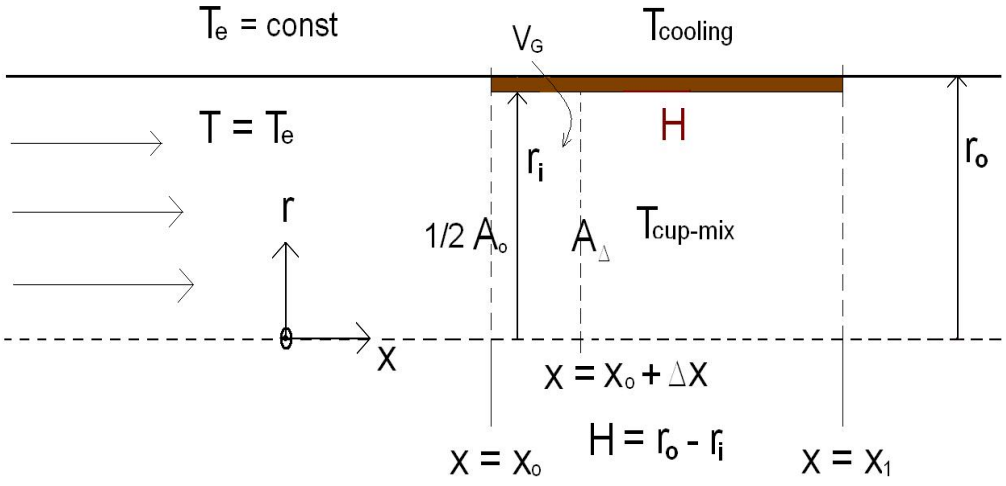

Figure 2.12: Localized deposition

2.5.1 Balance Equations

Mass Conservation

We introduce a balance equation for the fluid component (d) that contains paraffins using the control volume method (see Figure 2.12) :

$$\frac{d}{dt}\int\limits_{V_G(t)} \rho_d dV + \int\limits_{A_G(t)} \rho_d(\mathbf{v_d} - \mathbf{v_G}) \cdot d\mathbf{A} = 0 \tag{2.74}$$

Here ρ_d and $\mathbf{v_d}$ are the density $[\frac{kg}{m^3}]$ and the velocity field $[\frac{m}{s}]$ of the given phase related to the mass exchange with deposit on wall. A_G and V_G are the geometrical area $[m^2]$ and volume $[m^3]$ considered (with the inner radius) of the inside pipe. $\mathbf{v_G}$ is the velocity field related to any changes of V_G or A_G over time. We further assume time independent mass identities and use space averages as needed to rewrite (2.74) :

$$\pi(x_1 - x_o)\hat{\rho_d}\frac{d}{dt}r_i^2(t) + Q_x(x_o) - Q_x(x_1) - Q_w(r_i) = 0 \tag{2.75}$$

where $\hat{\rho_d}$ is the volume average density of the hydro-carbon components involved. Q_x and Q_w are the axial and radial mass flow rates, respectively, evaluated at locations as indicated in Figure 2.12. By definition we have :

$$Q_w(r_i) = 2\pi r_i(x_1 - x_o)\rho_w\frac{dH}{dt} \tag{2.76}$$

where we assume H to be dependent of the two parameters, time and inner wall temperature, to get :

$$\frac{dH}{dt} = \frac{\partial H(t, T_i w)}{\partial t} + \frac{\partial H(t, T_{iw})}{\partial T_{iw}}\frac{\partial T_{iw}}{\partial t} \tag{2.77}$$

By definition we also have :

$$\Gamma_w = \rho_w\frac{dH}{dt} \tag{2.78}$$

Due to lack of information (measurements) about Q_x, it is hard to simplify the mass balance equations given above.

Momentum Conservation

We assume no gravitational contributions during deposition. We also assume the wax to occupy the total surface on the inner pipe wall within the localized area.
Thus the momentum equation is (Schulkes 2006) :

$$\frac{\partial}{\partial t}(\rho_l A_l u_l) - \frac{\partial}{\partial x}(\rho_l c_l u_l^2 A_l) = \frac{\partial}{\partial x}(P_l A_l) + \frac{\partial}{\partial x}\left(\mu_l^e A_l \frac{\partial u_l}{\partial x}\right) - \frac{S_l \tau_{lw}}{A_i} \tag{2.79}$$

where P_l is the axial pressure ($[Pa]$) of the liquid, $\mu_l^e = \mu_l + \mu_T$ is the molecular and eddy viscosity ($[\frac{kg}{sm}]$), S_l is the liquid perimeter wetter ($[m]$), τ_{lw} is the wall shear stress ($[\frac{kg}{s^2 m}]$) caused by the liquid, and c_l is defined as $c_l = \frac{1}{A_l u_l^2}\int\limits_{A_l} u_n^2 dS$. We hereby declare $c_l \equiv 1$.

Energy Conservation

We assume the bulk temperature to be independent of time during deposition. An assumption that is reasonable for a finite temperature difference between the bulk flow and the cooling environment, where changes of the bulk temperature is ignorable during the transportation from $x = x_o$ to $x = x_1$. The energy equation of relevance is discussed in Sections 2.1-2.4. We therefore combine equations (2.51) and (2.47) of Section 2.2 to find :

$$\frac{\partial T_{cup-mix}}{\partial x} = -\frac{\pi k_l Nu(T_{cup-mix} - T_{cooling})}{Q_l C_{p,l}} \tag{2.80}$$

where :

$$Nu = -2r_i \frac{\left(\frac{\partial T}{\partial r}\right)_{r=r_i}}{T_{cup-mix} - T_{cooling}} \tag{2.81}$$

The rewritten inner wall temperature based on equation (2.70) of Section 2.3 is :

$$T_{iw} = T_{cup-mix} - \frac{U_{tot}}{h_l}(T_{cup-mix} - T_{cooling}) \tag{2.82}$$

2.5.2 Considerations

As will be shown in Chapter 4, deposition is a delayed process. It can be shown that a typical mass diffusion time scale (t_w) for deposition is much smaller than the time scale for mass transportation in the axial direction. Since the liquid is assumed to not influence the deposition, we further assume constant axial velocity of the oil. In addition we consider the dissolved wax to be transported with the same velocity as the liquid in the axial direction; thereby $u_l \equiv u_d = const.$ A typical time scale for molecular transportation with bulk flow in the axial direction is $t_{transp} \sim \frac{x_1 - x_o}{u_l}$. Based on typical axial velocities used in the deposition experiments in Chapter 4, an estimated time scale for this transportation is $t_{transp} \sim 2s$, while t_w is much larger.
We therefore state $t_w \gg t_{transp}$. We also assume the densities to be constant and independent of time and the wax thickness (H) to be small compared to the inner pipe radius (r_o). We therefore assume the following relation between the wax thickness and inner steel pipe radius; $\frac{H}{r_o} = \epsilon \ll 1$.

Simplifications of Impulse Conservation

Assuming steady state conditions and fully developed flow, the impulse equation can be written :

$$\frac{\partial P_l}{\partial x} = -\frac{S_l \tau_{lw}}{A_l} \tag{2.83}$$

2.5.3 Analysis of Γ_w

We analyse the mass transfer toward the wall, considering the time scale, $t \gg \frac{4r_o^2}{\nu}$. We always assume the wax thickness (H) considered to be very small compared to the inner radius of the steel pipe (r_o). To simplify the problem, we assume the inner wall temperature to be independent of time, that $\frac{\partial T_{iw}}{\partial t} = 0$. This is not unreasonable if the inner wall temperature change very little when a small layer of wax has been established on the wall. In Chapter 4, we

will find that the inner wall temperature increases fast in the initial period of each experiment and that it seems to stabilise close to the incoming oil temperature.

From these assumptions we obtain the following mass transfer rate :

$$\Gamma_w = \rho_w \frac{\partial H}{\partial t} \tag{2.84}$$

Including results from Chapter 5 where we derive correlation curves on the form $H \approx Bt^{\overline{\alpha}}$, gives :

$$\Gamma_w = B\overline{\alpha}\rho_w t^{\overline{\alpha}-1} \tag{2.85}$$

The mass transfer rate, equation (2.88) above, is decreasing for increased t since $\overline{\alpha} - 1 < 0$. This is what we expect based on the results of the calculated wax thickness that we present in Chapter 4. There we will find a clear tendency of a damped increase of the wax thickness over time.

The mass transfer (Γ_w) considering a small time scale, $t \ll \frac{4r_o^2}{\nu}$, is perhaps more complicated. Here we can not ignore the influence of the inner wall temperature. In the previous chapter we found correlation curves where the inner wall temperature where not involved. We did not find better correlations by involving the T_{iw}. We believe that the inner wall temperature has an important impact on the deposition, especially in the beginning of the wax process.

Note, we may have a singularity at $t = 0$. To evaluate this, more details is needed.

2.5.4 Conclusion

In this section, we introduced the balance equations used to evaluate the wax problem considering simplified conditions. From the considerations, the impulse conservation, equation (2.86) is the same as the hydraulic balance equation that we introduce in Chapter 4 (Section 4.2) where we establish the pressure drop method. In respect to mass balance and mass flux toward the wall, we derived the rate of deposition and information from Chapter 5 is included to derive the rate of deposition for a larger time scale, where $t \gg \frac{4r_o^2}{\nu}$. When it comes to evaluating the initial rate of deposition, more details than we have here are needed.

Chapter 3

Temperature Distributions - A Summary

The temperature equations that we found in section 2.2, 2.3 and 2.4 must be used with caution. Simplifications as area averaging and assumptions of constant fluid properties were applied. Both local (Graetz) and integral methods were used. It is of interest to compare the results obtained by the different methods in a consistent way. We expect that with turbulent flow in a pipe, the transfer of thermal energy per square unit at the wall will be more effective compared to laminar flow. This is one of the main properties that differentiate turbulent from laminar flow. When it comes to including an insulating layer or not, we expect that with insulation the decrease in temperature as the fluid is transported will be less than without insulation. Influence of the insulation clearly depends on both its thickness and its thermal conductivity. In section 2.3 we introduced the temperature distribution for stationary turbulent flow using the Petukhov Nusselt correlation. In section 2.4 the temperature distribution based on heat conduction through the fluid and the pipe wall. In section 2.5, same as in section 2.4, but in addition we included an insulating layer.

3.1 Temperature Distributions

In this chapter we always consider constant fluid properties. We base the results on unused engine oil with the given properties at 320K (Incropera & DeWitt 1996). The inner pipe radius is set to be $r_o = 50mm$, the thickness of the pipe wall to be $8mm$, and a uniform thickness of the insulation to be $0.5mm$. We further define the heat conductivity of the insulation to be two times that of oil, $k_{ins} = 2k_{oil}$, where $k_{oil} = 0.143\frac{J}{smK}$. The heat conductivity of paraffins are about two times larger than the heat conductivity of the condensate (Incropera & DeWitt 1996). That means, we can draw a parallel between the results obtained from the engine oil and the insulated pipe in this chapter, with the condensate and a small wax layer that are discussed in Chapter 4. The density of the engine oil is $\rho_{oil} = 871.8\frac{kg}{m^3}$ and the kinematic viscosity is given to be $\nu_{oil} = 1.61 \cdot 10^{-}4\frac{m^2}{s}$ Further we chose the flow rates to be $Q_{lam} = 5.0 \cdot 10^{-3}\frac{m^3}{s}$ for laminar flow and $Q_{turb} = 5.0 \cdot 10^{-1}\frac{m^3}{s}$ for turbulent flow. Main codes for numerical calculations are given in the last Section of Appendix (Maple).

3.1.1 Laminar Flow

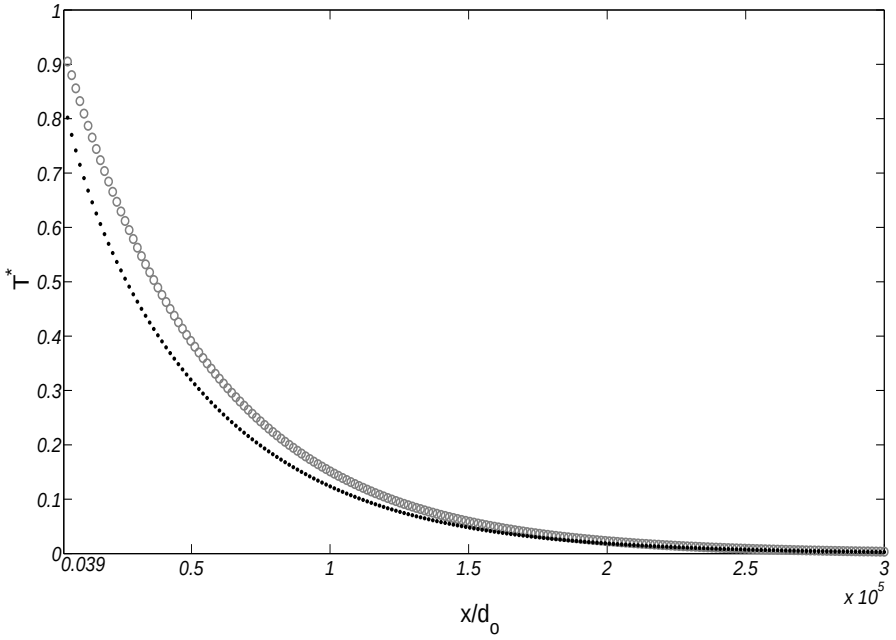

Figure 3.1: Dimensionless cup-mixing temperatures considering laminar flow

$\circ$: temperature from the integral method, equation (2.63) where $U_w = 0$
$\bullet$: temperature from Graetz problem, equation (2.39)

Figure 3.1 indicates a small difference between the profile based on laminar flow using the integral method and the resulting profile from Graetz problem. Both represent dimensionless mixing temperatures and are derived in two different ways. For a few eigenvalues we can not expect the mixing (Graetz) temperature to be representative for $x^* = 0$ due to the slow mathematical convergence of the coefficients given by (2.28). By comparing the equation (2.38) with different numbers of eigenvalues (four or more), we find that, for the dimensionless x^* defined in equation (2.5), the difference in the profiles where $x^* \geq \frac{1}{100}$ is less than 1%. For the case, we keep in mind that the dimensionless x^* defined for the solution of the Graetz problem is not the same as the scale used in this chapter. It is therefore necessary to do a transformation to the dimensionless $\frac{x}{d_o}$ used in Figures 3.1 - 3.3. The d_o is the inner pipe diameter, and we can safely compare the dimensionless (Graetz) temperature profile with others found from the integral method when $\frac{x}{d_o} \geq 3900$. The mixing temperature from the integral solution is based on constant wall temperature to make it comparable with the mixing (Graetz) temperature. It is important to mention that the Graetz profile in the figure above is valid only if $E_c P_r \simeq \frac{0.392}{T_o - T_e} \ll 1$ and $P_e \simeq 7.7 * 10^6 \cdot L \gg 1$. L represents the length of the pipe considered, and the Peclet relation is clearly true for a several meters pipe length. The Eckert-Prandtl relation holds true if the difference between the inlet and environmental temperature is hold within a restricted interval.

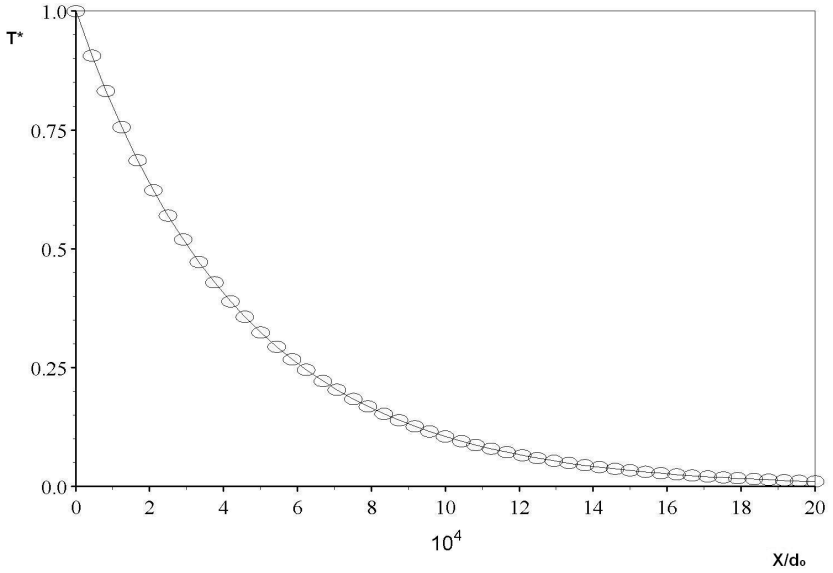

Figure 3.2: Dimensionless temperature profiles from the integral method

$\circ$: temperature distribution with (0.5mm) insulation on the inner pipe wall, equation (2.66)
$-$: temperature distribution with no insulation on the pipe wall, equation (2.66)

There is no difference in the temperature profiles in Figure 3.2, considering an insulating layer on the wall or not. We expect the insulation thickness to be larger or the heat conductivity to be much lower to achieve a clear difference. An interesting aspect is how the insulation influences the temperature drop more clearly under turbulent flow (see Figure 3.3) compared to that of laminar flow above. This is due to the strong property of heat transfer within the turbulent flow. The turbulence will try to eliminate the heat while the insulation will resist much of the thermal energy from transferring through the pipe wall. We can say that, under turbulent flow conditions, the insulation and its resistance to thermal conduction is working harder compared to when it is exposed to laminar flow, or simply, that the laminar flow better transports the thermal energy in the axial direction with less loss to the environment.

3.1.2 Turbulent Flow

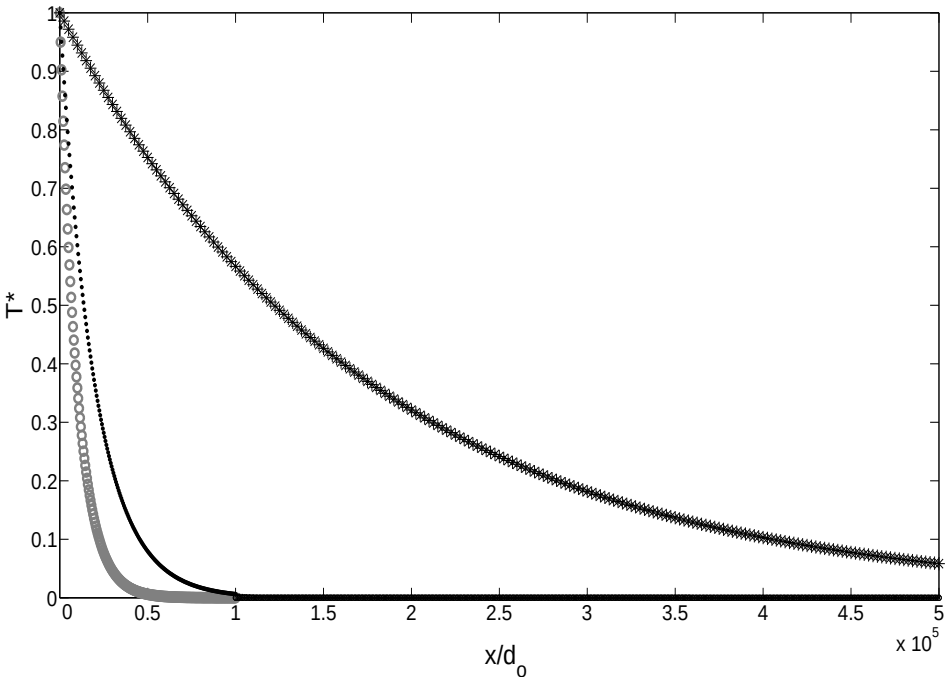

Figure 3.3: Dimensionless temperature profiles from the integral method

$*$: temp. distrib. influenced by (0.5mm) insulation on the inner pipe wall, equation(2.68)
$\bullet$: temp. distrib. based on a clean pipe (no insulation), equation (2.68)
$\circ$: temp. distrib. based on a clean pipe with constant wall temperature, equation (2.54)

From Figure 3.3, we see that the influence of a thin layer of insulation inside the pipe result in a much slower decreasing temperature as the fluid moves from a point to another in the axial direction compared to the profiles of a clean pipe. The temperature difference is small considering the profile based on a clean pipe with constant inner wall temperature ($\circ$) where $U_w = 0$, compared to the profile with a variable inner wall temperature ($\bullet$) where $U_w = U_{steel}$. We keep in mind that the occurrence of a thin layer of wax, will, as can be seen in the figure, cause the temperature in a tube under turbulent conditions to change in a pronounced way.

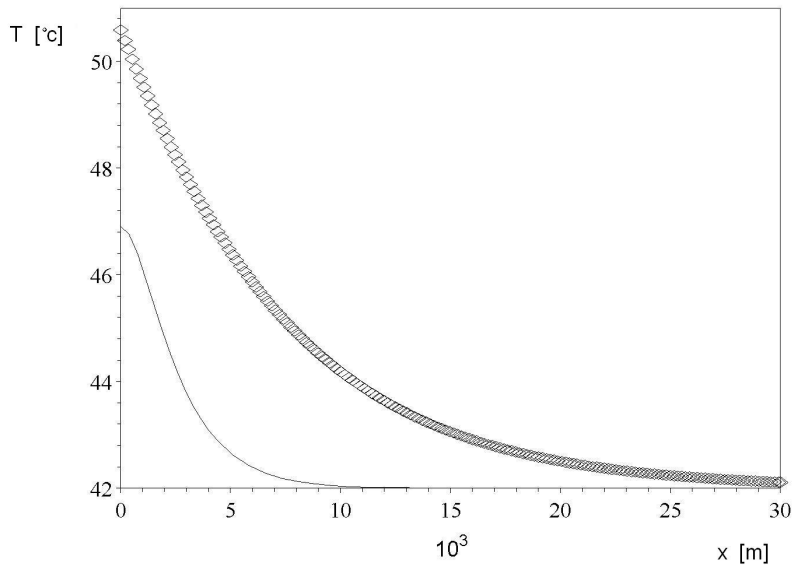

Figure 3.4: Inner wall temperatures considering turbulent flow

□ : inner wall temperature derived with a $0.5mm$ insulation (see equation (2.70)).
– : inner wall temperature derived with no insulation, (see equation (2.70))

The last figure of this chapter, Figure 3.4, depicts the inner wall temperatures of turbulent flow. The temperature distribution at the wall is of interest, especially when considering turbulent flow in an insulated pipe. As mentioned in the introduction, the precipitation of wax in crude is dependent of the temperature difference between the inside/outside pipe wall. The process where wax deposits on a cold surface will provide an insulating layer on the wall (in physical contact with the flow) causing the temperature to quickly change from lower to higher. This is due to the much lower heat transfer coefficient of wax compared to the pipe wall of steel. A prediction of the temperature along the inside wall is important to the understanding of the wax process. Figure 3.4 is based on unused engine oil at 320K, assuming an incoming constant temperature of 325K, and an outside wall temperature of 315K when the flow pass a certain axial location in the pipe. The dimensions of the pipe, insulation, and the flow rate is exactly the same as described in the beginning of this chapter. We still assume the constant properties of the oil given at 320K (Incropera & DeWitt 1996). Note that we have calculated the inner wall temperature with or without an insulation of 0.5mm compared to a much larger inner radius of the steel pipe (50mm). By the inlet of the incoming fluid we have a temperature difference about 3.8 °C, which must be considered a significant difference despite the small insulation thickness.

3.2 Conclusion

Considering laminar flow, the temperature derived from the integral method is very much the same as the result derived from Graetz problem. We have discussed two separate ways of solving the energy equation (2.2) and found that deriving a mathematical solution to the Graetz problem is much more time-consuming. We have solved the Graetz problem by mathematical analysis and we have found that a simplified model from the integral method seems to be in good agreement with our result. From numerical analysis the average difference between the two graphs are 2.8% for the plotted interval in Figure 3.1. The difference seems to be largest for the first part of the interval and the analysis give an average difference of 7.1% within $3900m < x < 10^5 m$. We will on the basis of these results expect good agreement for turbulent flow related to the Graetz problem. We explain this from the expectation of a (Graetz) temperature distribution for turbulent flow that is similar to the one found for laminar flow, with the exception of a larger damping of the temperature as a function of the mass flow in axial direction.

Finally, an important result of this chapter, is the significant difference of the inner wall temperature with or without a small insulating layer on the inner pipe wall under turbulent flow conditions. This is an interesting aspect of the study of how the inner wall temperature change in the occurrence of a small wax layer, and how this change of temperature will influence the physics related to the further deposition process.

Chapter 4

Experiments

In this chapter wax deposition measurements from pipe flow experiments carried out at StatoilHydro's Research Department in Porsgrunn are analyzed and discussed. The results of the analysis indicate that the deposited wax has a pronounced influence on the wall boundary layer temperature of the flowing oil. Eight deposition experiments are performed with constant flow rates and constant incoming temperatures of the fluids. Among these, only six are representative; those with the highest flow rates. The reasons will be discussed in the analysis below. We use the pressure drop method to calculate the thickness of wax deposits. Prior to each wax experiment, we assume constant inner wall temperature and introduce temperature variations in the pipe wall. We will find that the inner wall temperature seems to change much in the beginning of each experiment. First, we choose to neglect the influence of the roughness of the wall. Finally, we discuss the influence of a small roughness.

Figure 4.1: Wax surface
This picture illustrates a smooth surface of the wax layer from the condensate used. The picture is taken by StatoilHydro.

We introduce a picture of the test rig in Figure 4.2 below. The picture show the facility used to perform the experiments discussed in this chapter.

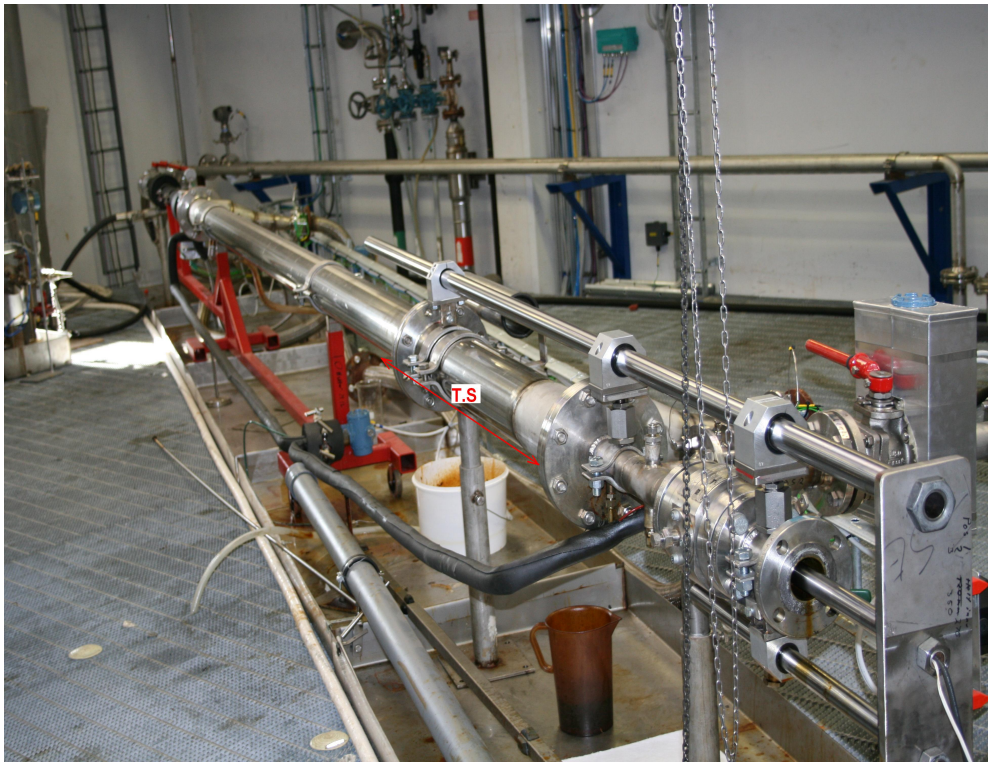

Figure 4.2: Picture of the facility

The line marked T.S. is the test section and the visible outer pipe is the water jacket enclosing the test pipe of oil. The test section is removable by disconnecting the flanges on each side. The picture is taken by StatoilHydro.

4.1 Facility Description

A sketch of the pipe flow facility used in the experiments is shown in Figure 4.3 where the main components of the facility are indicated. Two pumps generate the pressure levels needed to obtain the appropriate flow rates of the test fluid and the coolant, respectively. The test pipe is a 5.55m long steel pipe with an inner diameter of 0.0526m, and a wall thickness corresponding to 0.0039 cm. The test pipe is enclosed by a cooling jacket with an inner diameter of 0.1397m. Fully developed turbulent flow of the condensate is assumed. Temperatures of both the condensate and the coolant water were measured at the inlet and the outlet of the test section. The pressure at both inlet and outlet of the test pipe was also measured and the pressure drop is used to calculate the wax thickness. The accuracy of the pressure measurements is therefore crucial for the reliability of the wax thickness calculations. The density has also been measured during the experiments performed.

4.1.1 Properties of Condensate Used in Wax Deposition Experiments

The density measured during wax deposition experiments are typically :
$\rho_{oil} = 824 \frac{kg}{m^3}$ at $T_{oil} = 15^oC$
$\rho_{oil} = 819 \frac{kg}{m^3}$ at $T_{oil} = 20^oC$
$\rho_{oil} = 813 \frac{kg}{m^3}$ at $T_{oil} = 30^oC$
$\rho_{oil} = 806 \frac{kg}{m^3}$ at $T_{oil} = 40^oC$

The molecular viscosity is derived from interpolation of the following (rheometer) data :
$T_{oil} = [12.4658, 20.2073, 30.0067, 39.7039, 49.4686, 59.2560]^oC$
$\mu_{oil} = 10^{-3} \cdot [3.8, 2.8, 2.2, 1.8, 1.5, 1.3] \frac{kg}{sm}$

The thermal conductivity: $k_{oil} = 0.1344 \frac{J}{smK}$

The heat capacity of the oil: $Cp_{oil} = 1950 \frac{J}{kgK}$

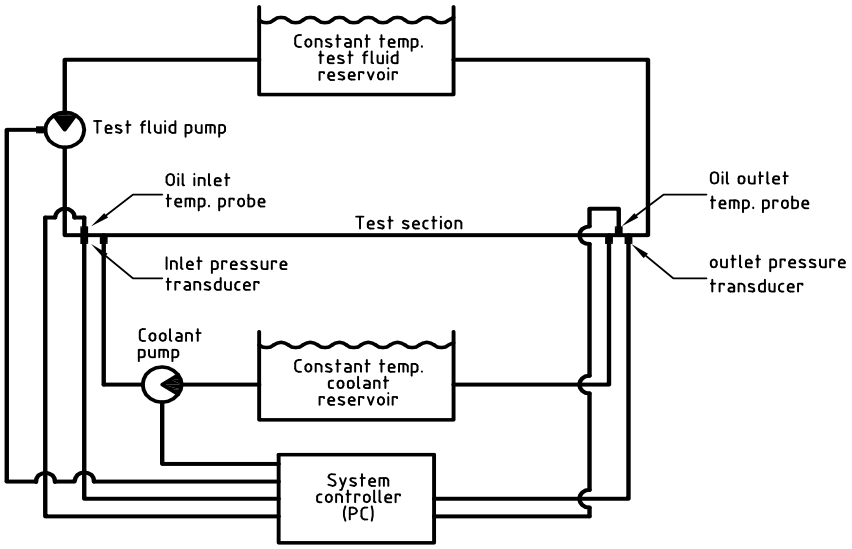

Figure 4.3: Sketch of the facility
The figure shows a sketch of the pipe flow facility used in the experiments. The main components are indicated in the figure.

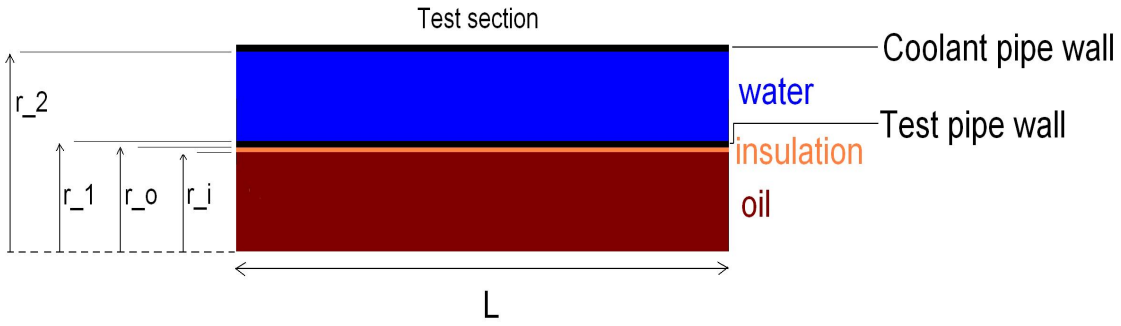

Figure 4.4: Details of the test section

r_i : inner pipe radius available for flow of oil
r_o : inner steel pipe (test pipe) radius
r_1 : outer steel pipe/test pipe radius
r_2 : inner pipe radius of water jacket
L : length of test section

4.2 Pressure Drop and Wax Thickness

A formula relating the wax thickness to the pressure drop will now be established. When wax deposits on the pipe wall, the cross section will decrease and cause an increase in the pressure drop for constant flow rates. If we assume the condensate to be incompressible and ignore the gravitational and accelerational pressure gradients, we get the following result from hydraulic force balance (see Figure 4.5) :

$$(P(x) - P(x+L))\,\pi r_i^2 - 2\pi r_i L \tau_{wall} = 0 \tag{4.1}$$

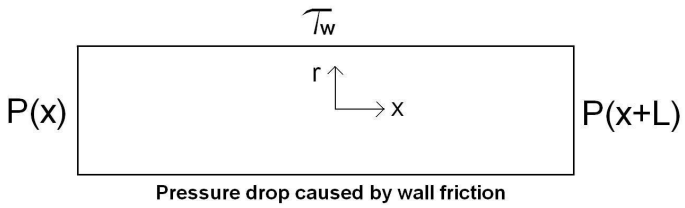

Figure 4.5: Hydraulic stresses

Thus :

$$\frac{dP}{dx} L\pi r_i^2 - 2\pi r_i L \tau_{wall} \tag{4.2}$$

where a connection between the shear stress and the Darcy friction factor is (Schulkes 2006) :

$$\tau_{wall} = \frac{1}{8}\rho_{oil}\left(\frac{Q_{oil}}{\pi r_i^2}\right)^2 f_D \tag{4.3}$$

Thus :

$$\frac{dP}{dx} = -\frac{\rho_{oil} Q_{oil}^2}{4\pi^2 r_i^5} f_D \tag{4.4}$$

We derive the wax thickness from the following equation by replacing Darcy friction factor with the best fit friction factor derived for non-isothermal flow :

$$\frac{dP}{dx} = \frac{\rho_{oil} Q_{oil}^2}{4\pi^2 r_i^5} f_{BF} \tag{4.5}$$

where :

$$r_i = r_o - H \tag{4.6}$$

H is the wax thickness and f_{BF} is the best fit friction factor formula subject to the flow condition in the experiments reported here. The procedures used to obtain the f_{BF}-formulas are discussed in section 4.4.

4.3 Inner Wall Temperature and Wax Thickness

When paraffins start to deposit and a wax layer is established on the wall, the thermal resistance in the wall increases. A growing and insulating deposit will increase the inner wall temperature and cause a decrease in the temperature difference across the thermal boundary layer. Temperature variations across the pipe give rise to changes of the molecular viscosity and will thereby influence the friction factor. It is therefore important to evaluate the inner wall temperature during a wax experiment. From equation (2.70) we derived the inner wall temperature given that the thermal conductivities and the radius available for the flow are known. The inner radius is always evaluated from the pressure drop method, and we have a closed system by putting this together with the measured oil temperatures. We introduce the tools to derive the inner wall temperature and start with the heat transfer coefficient based on the Pethukov Nusselt model (see section 2.2) :

$$h_{oil} = \frac{k_{oil} Nu}{2r_i} = \frac{k_{oil} \frac{(\frac{f_{BF}}{8}) RePr}{1{,}07+12{,}7(\frac{f_{BF}}{8})^{\frac{1}{2}}(Pr^{\frac{2}{3}}-1)}}{2r_i} \tag{4.7}$$

that is adapted to the Reynolds and Prandtl number within the intervals :

$$3 \cdot 10^3 < Re < 5 \cdot 10^6 \qquad 0.5 < Pr < 2,000 \tag{4.8}$$

From the experiments we have typically $P_r = [20, 50]$ and $R_e > 10,000$. The test pipe length L must also be much larger than its inner diameter D, i.e. $\frac{L}{D} \geq 10$, which is satisfied in our case. From the energy equation (2.63) we have the following expression for the overall heat transfer coefficient U_{tot} :

$$U_{tot} = \frac{Q_{m,oil} C_{p,oil}}{2\pi r_i (T_{water} - T_{cup-mix})} \frac{\partial T_{cup-mix}}{\partial x} \tag{4.9}$$

We define the measured oil temperature drop :

$$\Delta T_{oil,measured} = T_{oil,in} - T_{oil,out} \tag{4.10}$$

Integration of (4.9) combined with (4.10) gives :

$$U_{tot} = \frac{Q_{m,oil} C_{p,oil}}{2\pi r_i (T_{water} - T_{oil})} \frac{\Delta T_{oil,measured}}{L} \tag{4.11}$$

where the average oil and water temperature is :

$$T_{oil} = \frac{T_{oil,in} + T_{oil,out}}{2} \quad , \quad T_{water} = \frac{T_{water,in} + T_{water,out}}{2} \tag{4.12}$$

We derive the inner wall temperature based on equation (4.7), (4.11) and (4.12) from the use of equation (2.70) :

$$T_{iw} = T_{oil} - \frac{U_{tot}}{h_{oil}} (T_{oil} - T_{water}) \tag{4.13}$$

(4.11) is an acceptable approach to (4.9) by assuming that the measured oil temperatures represent the mixing temperatures well at a given location. With small temperature variations over the test pipe length (about 1%), we anticipate a linear temperature distribution over its length.

4.4 Friction Factor Formulas

Before we start analysing the wax data, we estimate the precision of the pressure measurements. The inner diameter of the pipe is given as $D_o = 0.0525 \pm 0.0003m$. It is difficult to measure the inner diameter and it is even more challenging to measure the roughness in a pipe. It is often a good approximation to ignore roughness considering a technical smooth pipe, but in this study we assume it to be within the interval $0 \leq \varepsilon \leq 5 \cdot 10^{-5}m$. We also assume a pressure offset among the measuring data, and that the real pressure drop can be expressed as $\Delta P = \Delta P_{measured} \pm p_{offset}$. For turbulent flow conditions we choose Haaland's formula to model the friction factor. Before the analysis of the wax deposition, we introduce a corrected friction factor. The Haaland factor is based on constant temperatures; an *isothermal* system. If the environmental temperature deviates from the bulk flow temperature and cause heat exchange within the system; we have a *non-isothermal* system.

4.4.1 Isothermal Experiments : No Deposition

We consider experimental data obtained in a clean and smooth pipe with variable flow rates (of oil) to test the agreement between the Haaland (4.14) and the Darcy (4.15) friction factors. We have the same inlet temperature of water and oil; thereby an isothermal system. All the flow rates considered involve turbulent flow conditions.
The Haaland friction factor is :

$$f_H = \left(1.8 \log\left(\frac{6.9}{\mathrm{Re}_{oil}} + \left(\frac{\varepsilon_{steel}}{3.7 D_o}\right)^{1.11}\right)\right)^{-2} \tag{4.14}$$

and the Darcy friction factor from hydraulic force balance is :

$$f_D = -\frac{4\pi^2 r_i^5}{\rho_{oil} Q_{oil}^2} \frac{dp}{dx} \tag{4.15}$$

We define the measured pressure drop :

$$\Delta P_{measured} = P_{in} - P_{out} \tag{4.16}$$

The calculated pressure based on the Haaland friction factor is :

$$\Delta P_{calculated} = \frac{\rho_{oil} Q_{oil}^2 L}{4\pi^2 r_i^5} f_H \tag{4.17}$$

We define the error in the calculated pressure drop via :

$$e_{relative} = \frac{\Delta P_{measured} - \Delta P_{calculated}}{\Delta P_{measured}} \tag{4.18}$$

Finally, the average of the absolute values of $e_{relative}$:

$$E_{relative} = \frac{1}{N} \sum_{i=1}^{N} |e_{relative}| \tag{4.19}$$

Integration of (4.15) combined with (4.16) gives the equation we use to calculate the Darcy friction factor. We always assume fully developed and turbulent flow conditions, and we

compare the Darcy with the Haaland friction factor through the equation (4.18). The Haaland factor depends on both roughness and inner diameter of the pipe. Based on Tables C.1 and C.2 (in Appendix) we calculate the optimal roughness, inner diameter, and pressure offset by varying their values within restricted intervals (in a three dimensional parameter space) using nonlinear optimalization to minimize $E_{relative}$. The best fit is given when $\varepsilon_{steel} = 0m$ and $D_o = 0.0526m$, where we ignore the pressure offset by setting $p_{offset} = 0\ Pa$. In Figure 4.6 the error in the calculated pressure drop is less than 4.5% for all isothermal data. We thereby have good agreement between the measured Darcy and the Haaland friction factors for the given diameter and roughness.

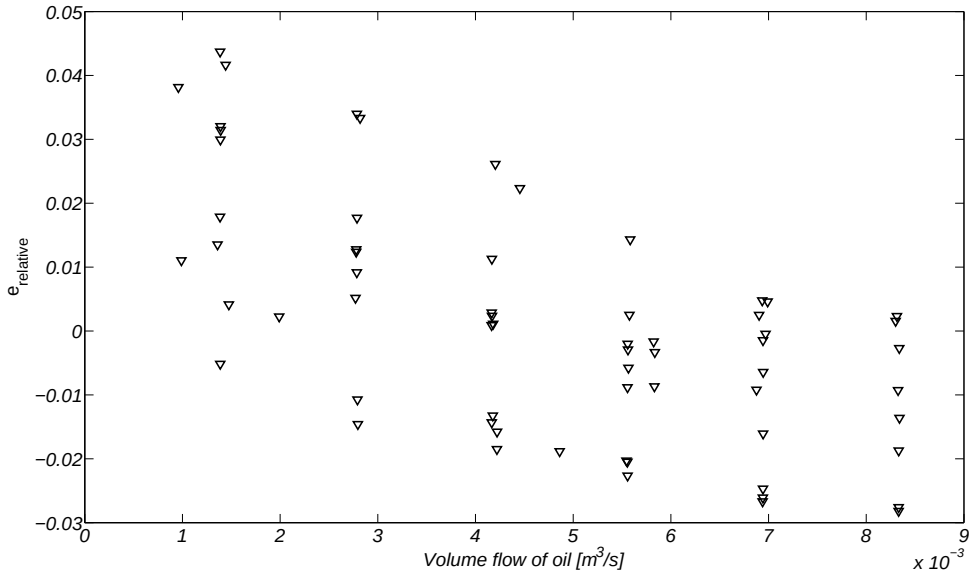

Figure 4.6: Error in the calculated pressure drop for isothermal flow, Tables C.1 and C.2 (see Appendix)

4.4.2 Non-Isothermal Experiments : No Deposition

Radial temperature variations will occur when the flowing fluid is being cooled by heat losses through the pipe wall. The molecular viscosity will thereby vary across the flow, and these variations must be taken into account when the best friction factor model is evaluated. In our evaluation of the experiments, we use the molecular viscosity measured in a rheometer (StatoilHydro 2007) with a reasonable accuracy (±4%). In general the molecular viscosity decreases rapidly with temperature (White 2006). We will therefore expect a higher oil viscosity at the inner wall compared to that of the bulk flow and this again increases the friction of the wall. For non-isothermal flow a correction factor has been introduced
(Perry & Chilton 1973) :

$$f = f_{BF} = f_H \cdot \alpha_{correction} \tag{4.20}$$

where :

$$\alpha_{correction} = \left(\frac{\mu_{wall}}{\mu_{bulk}}\right)^n \tag{4.21}$$

and $n = 0.11$ or $n = 0.17$ in the case of cooling or heating. This correlation was developed (Sieder & Tite 1936) based on three different oils. The intention was to study the effect of a radial temperature gradient on the distribution of the axial and radial components of velocity. Sieder and Tite proclaimed that this was not taken into consideration by (Graetz 1885) or (Lévêque 1928). We consider a situation where the oil is being cooled and use the given exponent. We have derived the error in the calculated pressure drop using both the Haaland and the corrected friction factor (see Figure 4.7) on basis of non-isothermal data in Table C.3 (see Appendix). Figure 4.7 indicate a smaller error in the calculated pressure drop when using the corrected friction factor, but not sufficient small. We require that the error in the calculated pressure drops are less than 0.05 (or 5%) for the case. In Figure 4.7 we expect an optimal error in the calculated pressure drop for n in the interval 0 to 0.11, and from numerical calculations using all the non-isothermal data, we find the minimum $E_{relative}$ when $n = 0.05$
(see Figure 4.8).

4.4.3 Discussion of the Isothermal and Non-Isothermal Data

The accuracy of the measuring instruments are very important, especially for the lowest flow rates and pressure drops. From the graphs in Figures 4.6 and 4.7 it is clear that the $\Delta P_{measured}$ are larger than the $\Delta P_{calculated}$ for the lowest flow rates and opposite for several of the highest rates. It also appears to be a linear connection between the error in the calculated pressure drop and the flow rate in both Figures, and it is important to note the fact that any such relation should not occur. We therefore carry out a linear regression analysis based on these two parameters for both isothermal and non-isothermal data. From the results we can not reject the hypothesis of a linear relation. In addition, the results based on isothermal data seem to have a significant auto correlation, which means that we might have a connection between the measurements performed within each experiment. We carefully conclude that we observe larger uncertainties among the lowest flow rates, and a systematic relation can not be excluded.

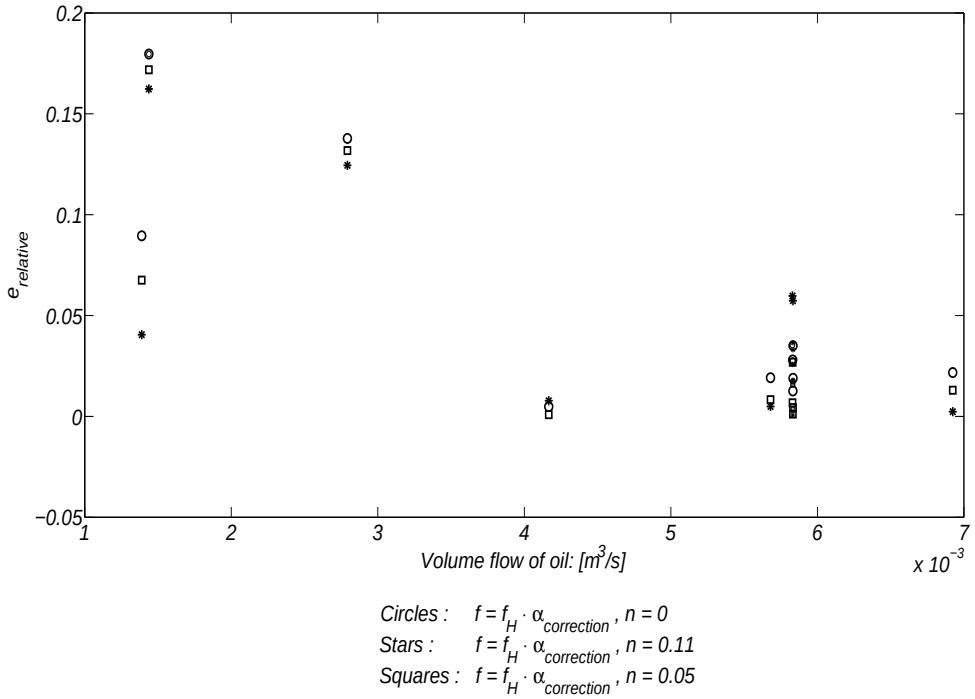

Figure 4.7: Error in calculated pressure drop for non-isothermal flow, Table C.3 (see Appendix)
$\circ$: Pressure drop using the Haaland friction factor
$\star$: Pressure drop based on non-isothermal Sieder & Tite friction factor
$\square$: Pressure drop using the best fit (non-isothermal) friction factor.

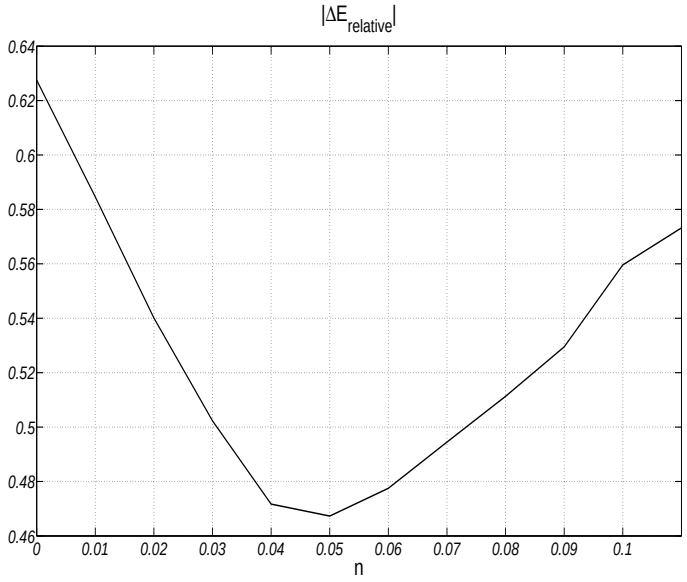

Figure 4.8: Minimum value of $|\Delta E_{relative}|$
By considering a precision of only two decimals, we find the minimum value of $|\Delta E_{relative}|$ for n = 0.05. The optimal pressure drop is based on non-isothermal data.

4.5 Experimental Results

We have eight wax experiments performed by StatoilHydro available to study. Unfortunately, we can not include all in further work using the adapted friction factor. The initial large error in the calculated pressure drop among two of the wax experiments with flow rates equal to 5 m^3/h and 10 m^3/h can not be ignored. In Figure C.1 (see Appendix) we have marked the two experiments showing a $e_{relative}$ of 0.172 and 0.132. The adapted friction factor is therefore an inaccurate approximation to these. In the continuation we will focus on the other six where the $e_{relative}$ is less than 0.4 (see Figure C.1 in Appendix). Let us first introduce the six experiments involved. The experiments are named through the general matrix $T_{oil,in} - T_{water,in} - Q_{oil}$, where $T_{oil,in}$ and $T_{water,in}$ are the measured incoming oil and water temperatures in °C and Q_{oil} is the volume flux in $\frac{m^3}{s}$.

4.5.1 Observed Pressure Drop With Comments

The measured pressure drops $\Delta P_{measured}$ (4.16) are presented in Figures 4.9 - 4.11. The pressure drops in all experiments increase with elapsed time, indicating that a growing wax layer is formed on the inside of the test pipe. We notice the most rapid growth of the pressure drop early in the experiments. The reduced growth rate with time is attributed to the temperature development in the wall boundary layers of the flowing test fluid. A wax layer on the inside of the test pipe increases the thermal resistance across the pipe wall and causes an increase in the boundary layer temperature as discussed in section 4.5.2.
The observed pressure drops are fluctuating for some reason. The typical fluctuation level may be estimated as an average deviation from a linear growth curve in a representative time interval. In general, we have a series of N measurements in each experiment with the given time interval $t_o, t_1, .., t_n, .., t_N$. Evaluation of a typical fluctuation level is based on the measured pressure drops within the fixed time interval $t \in [t_m, t_M]$, where $m = 0.65 \cdot N$ and $M = 0.85 \cdot N$. In Figure C.2 (see Appendix) $\Delta P_{measured}$ are considered linear in time, and from regression analysis we derive the linear graph D to each interval. We evaluate the typical fluctuation level of $\Delta P_{measured}$ by assuming D to represent the "fluctuation-free" pressure drop for fully developed turbulent and stationary flow conditions. The fluctuation level is determined from the following expression :

$$F_{pressure} = 100\% \frac{1}{M-m} \sum_{q=m}^{M} \left| \frac{\Delta P_{measured,q} - D_q}{\Delta P_{measured,q}} \right| \tag{4.22}$$

The results are shown in Table 4.1 below.

Table 4.1: Fluctuation level of the measured pressure drop

Experiment $T_{oil,in} - T_{water,in} - Q_{oil}$	A typical fluctuation level in percent	Standard deviation (Pa)
$15 - 10 - 21$	$\Delta P_{measured} \pm 0.06\%$	6.41
$20 - 10 - 15$	$\Delta P_{measured} \pm 0.05\%$	2.75
$20 - 10 - 21$	$\Delta P_{measured} \pm 0.14\%$	13.22
$20 - 10 - 25$	$\Delta P_{measured} \pm 0.05\%$	6.98
$30 - 10 - 21$	$\Delta P_{measured} \pm 0.11\%$	10.02
$40 - 10 - 21$	$\Delta P_{measured} \pm 0.32\%$	28.85

In table 4.1 the fluctuation level of the measured pressure drops seem to be small in all experiments. It should be mentioned that the pressure drops related to the experiment $40 - 10 - 21$ indicate a statistical weak linearity compared to the other experiments for the given interval. We conclude that the pressure transducers seem to give sufficient accuracy during the experiments.

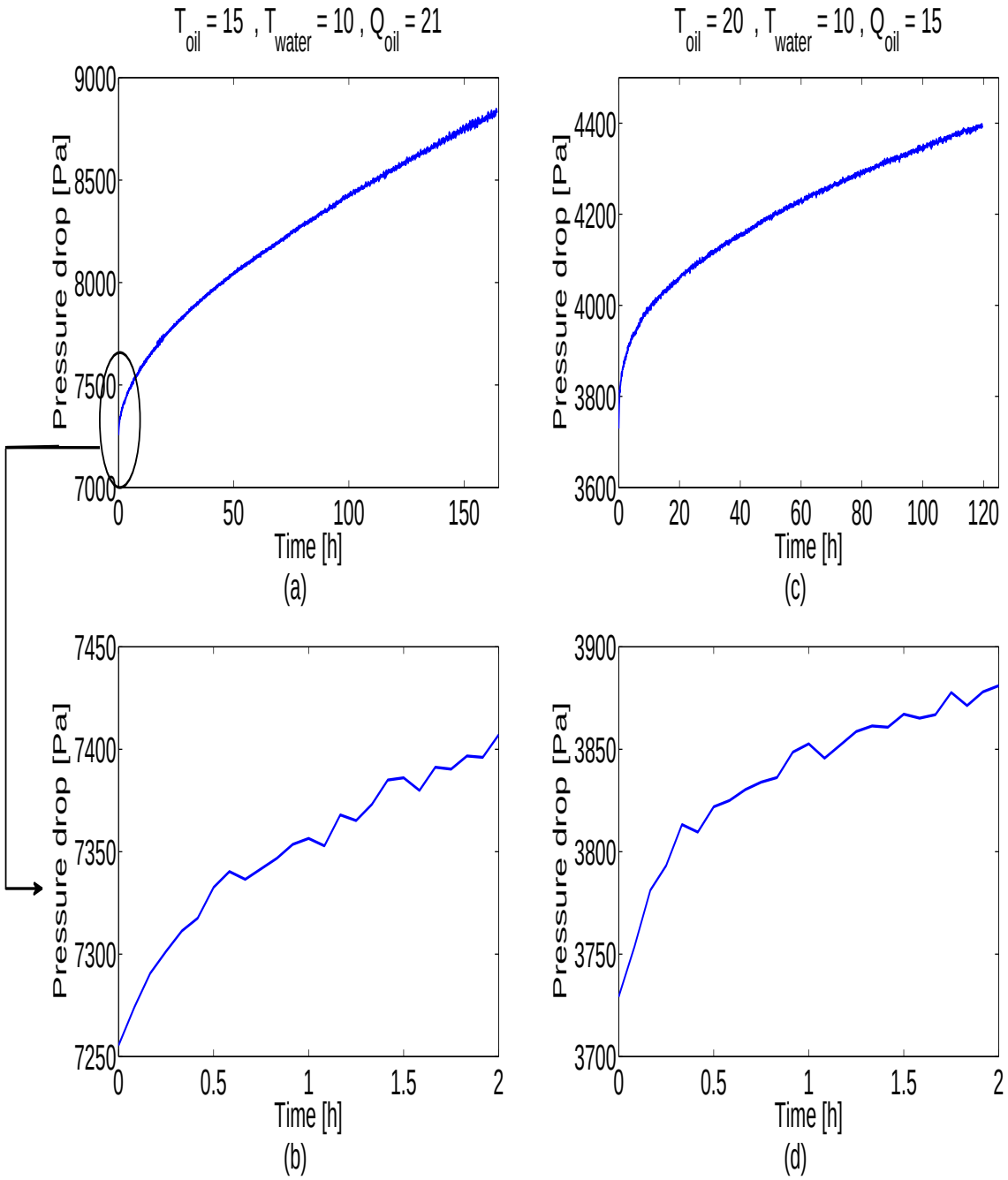

Figure 4.9: Measured pressure drop during wax deposition

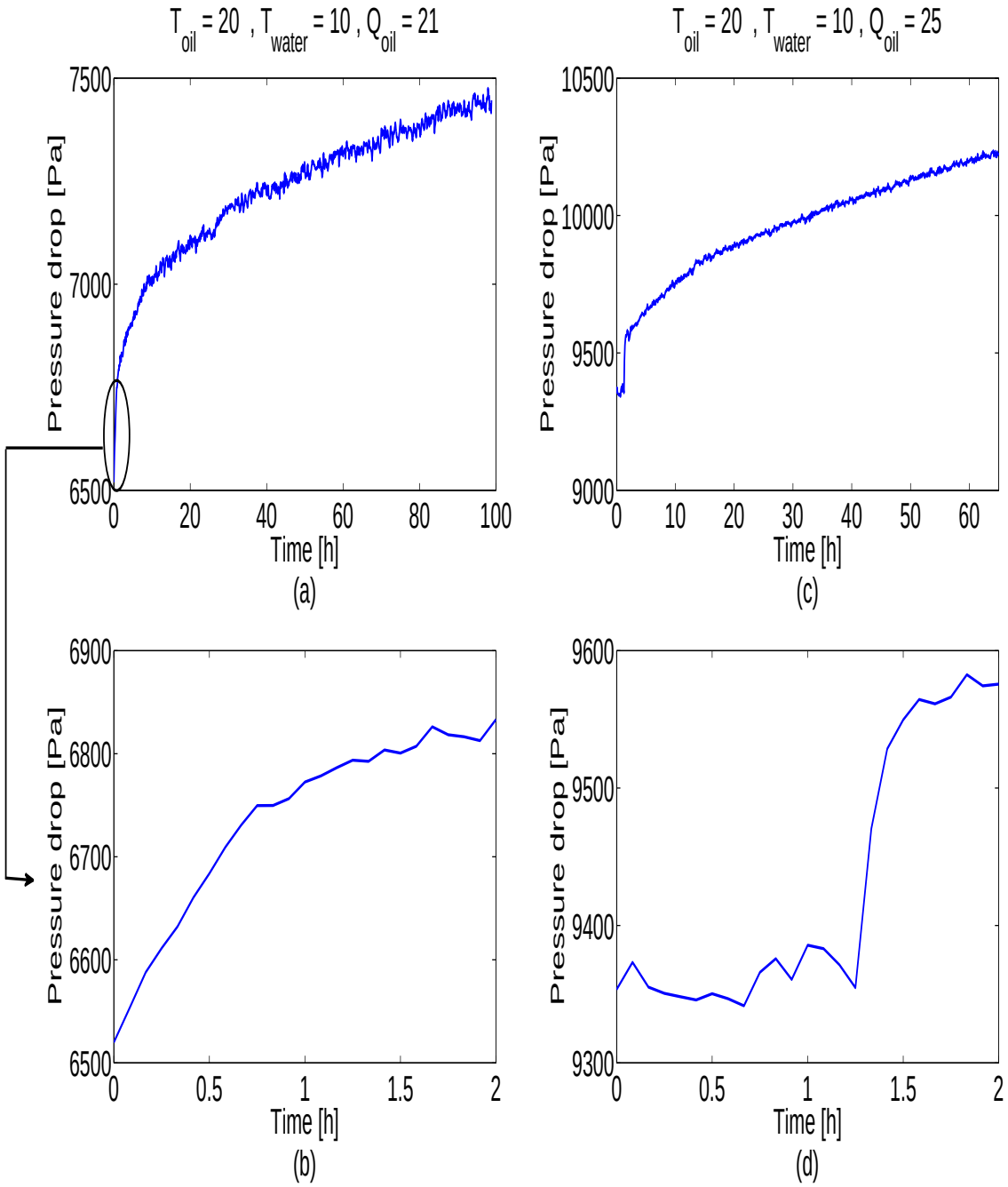

Figure 4.10: Measured pressure drop during wax deposition

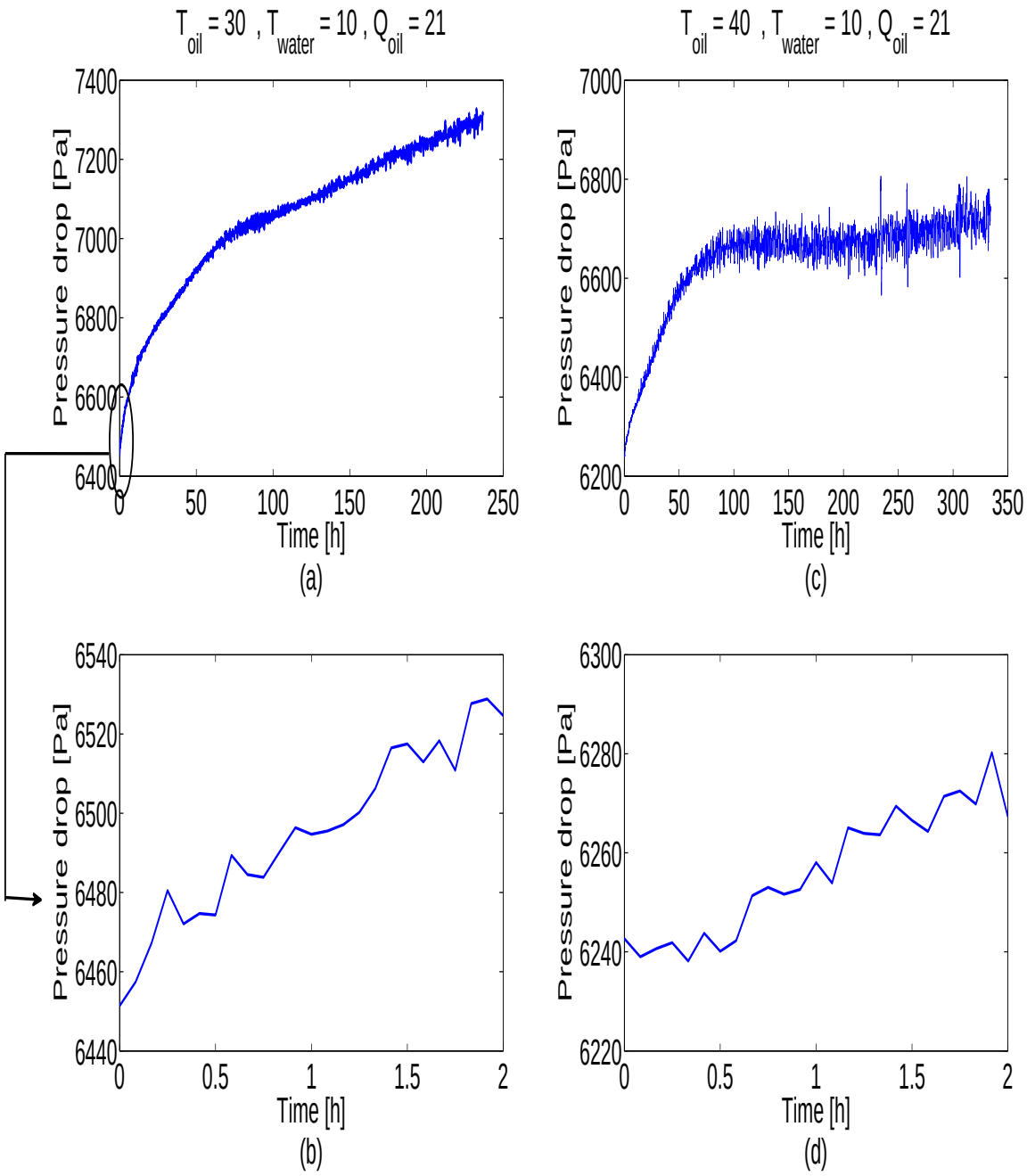

Figure 4.11: Measured pressure drop during wax deposition

Note that in experiment 40-10-21 the $\Delta P_{measured}$ seems to stabilise after 100h while in experiment $30-10-21$ the $\Delta P_{measured}$ continues to increase.

4.5.2 Observed Temperature Drop and Derived Inner Wall Temperature

The measured oil temperature drops $\Delta T_{oil,measured}$ (4.10) are presented In Figures 4.12 and 4.13. A fast decrease of the temperature drop in the beginning of each experiment indicate that thermal energy are prevented from transferring through the pipe wall as soon as paraffins deposit on the wall. This phenomenon is a very important observation in our study and in section 3.2 we found that a small insulating layer will influence the inner wall temperature significantly. This is exactly what we find by introducing the inner wall temperature given in section 4.3, and the results are presented in Figures 4.14 and 4.15. It is clear that the inner wall temperature changes quickly in the beginning of each wax experiment, and there is no doubt that during the first hour or even the first minutes, it changes much compared to the inner wall temperature before deposition occurs. Large temperature differences between inlet oil and water seem to give larger and faster changes of the inner wall temperature during the first minutes (see Figure 4.15 (c) and (e)). The temperature graphs based on experiment $20-10-15$ (see Figure 4.12 (c) and 4.14 (c)) indicate an increase of the temperature drop and a decrease of the inner wall temperature during the first minutes. This is not expected to occur during wax deposition, and we consider it to be an initial condition of inaccuracies in the measured oil temperatures. We further use the same procedure as in subsection 4.5.1 to estimate a typical fluctuation level of the temperature transducers. We redefine the time intervals with $m = 0.45 \cdot N$ and $M = 0.65 \cdot N$. There are temperature fluctuations in every experiment, and we assume the temperature distribution to be approximately linear within the given intervals (see C.3) for the case of no fluctuations. It should be mentioned that this is only an approximation we do to estimate the typical fluctuation level :

$$F_{temperature} = 100\% \frac{1}{M-m} \sum_{q=m}^{M} \left| \frac{\Delta T_{measured,q} - D_q}{\Delta P_{measured,q}} \right| \tag{4.23}$$

The results are shown in the table 4.2 under.

Table 4.2: Fluctuation level of the measured temperature drop

Experiment $T_{oil,in} - T_{water,in} - Q_{oil}$	A typical fluctuation level in percent	Standard deviation (^oC)
$15-10-21$	$\Delta T_{measured} \pm 4.19\%$	0.0035
$20-10-15$	$\Delta T_{measured} \pm 1.05\%$	0.0032
$20-10-21$	$\Delta T_{measured} \pm 1.22\%$	0.0032
$20-10-25$	$\Delta T_{measured} \pm 1.13\%$	0.0025
$30-10-21$	$\Delta T_{measured} \pm 0.61\%$	0.0040
$40-10-21$	$\Delta T_{measured} \pm 0.25\%$	0.0050

The typical fluctuation of the temperature measurements in the $20-10-15$ experiment is about 1.05%. An adjustment of the initial measured incoming oil temperature with less than 0.7% is needed to give an increase of the inner wall temperature and a decrease of the temperature drop during the first period. The inaccuracy can therefore explain the unexpected initial temperature drop and inner wall temperature related to this particular experiment. In general we have small fluctuations in the oil temperature measurements.

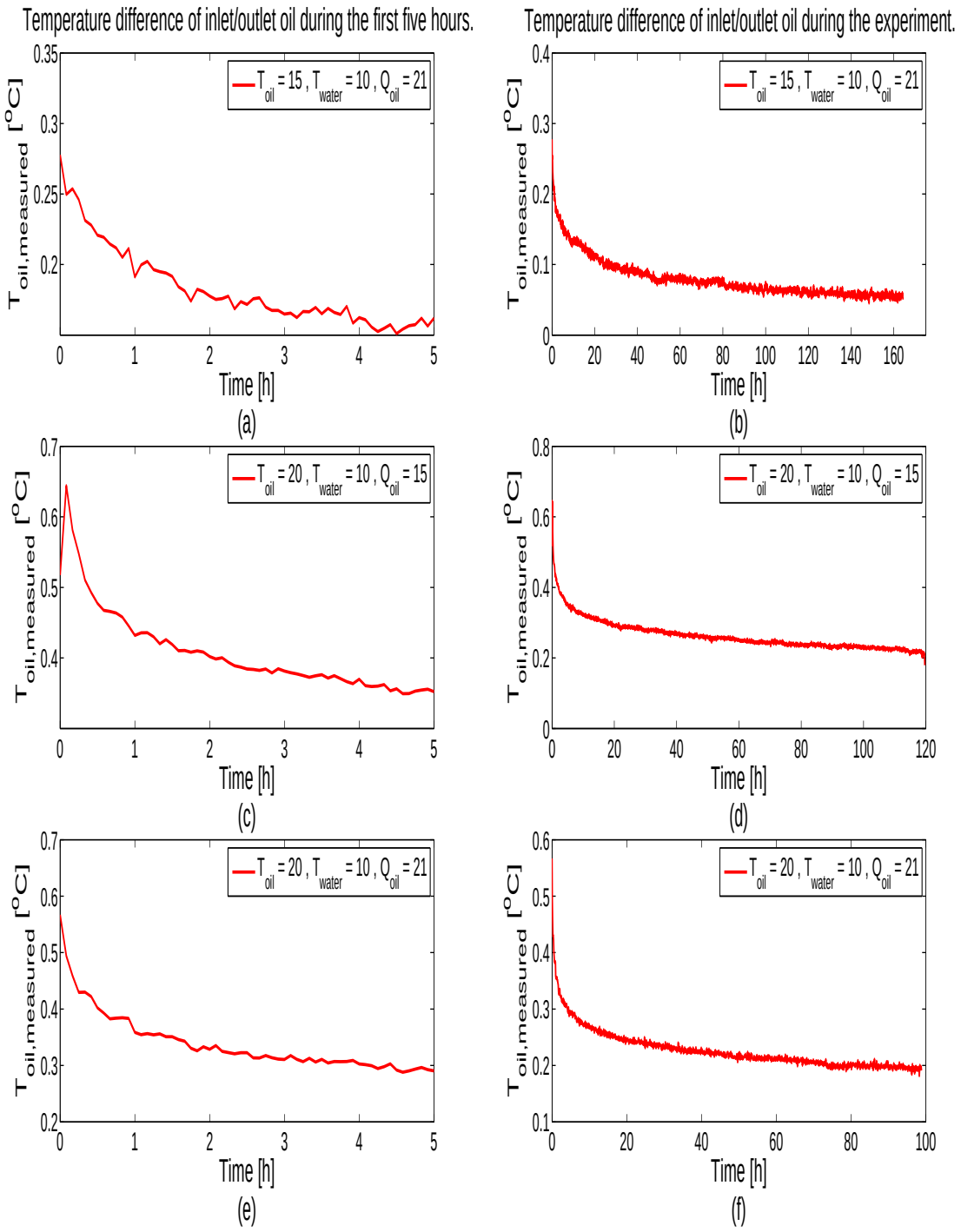

Figure 4.12: Measured temperature drop during wax deposition
Note that in figure (c) the temperature drop is first increasing.

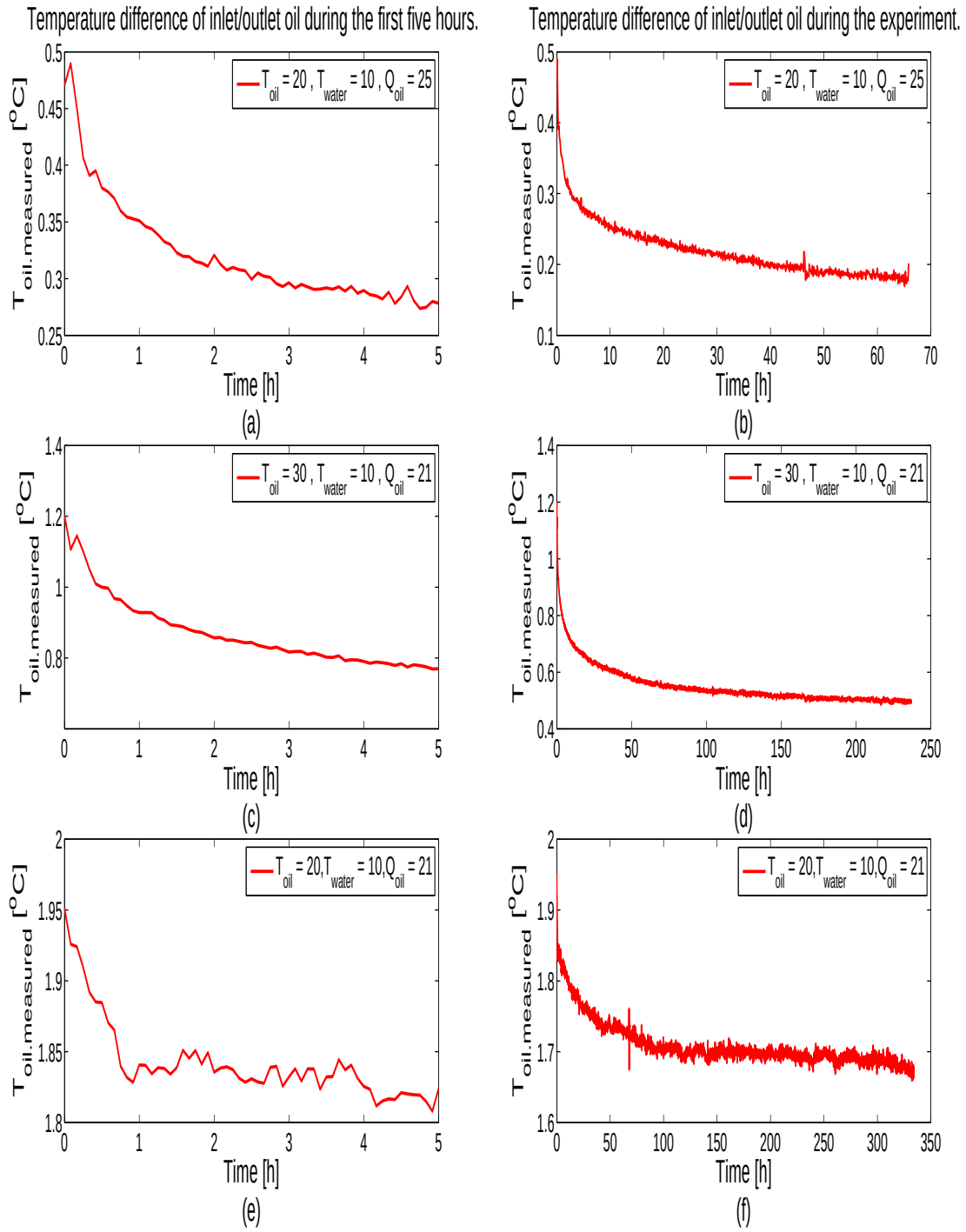

Figure 4.13: Measured temperature drop during wax deposition

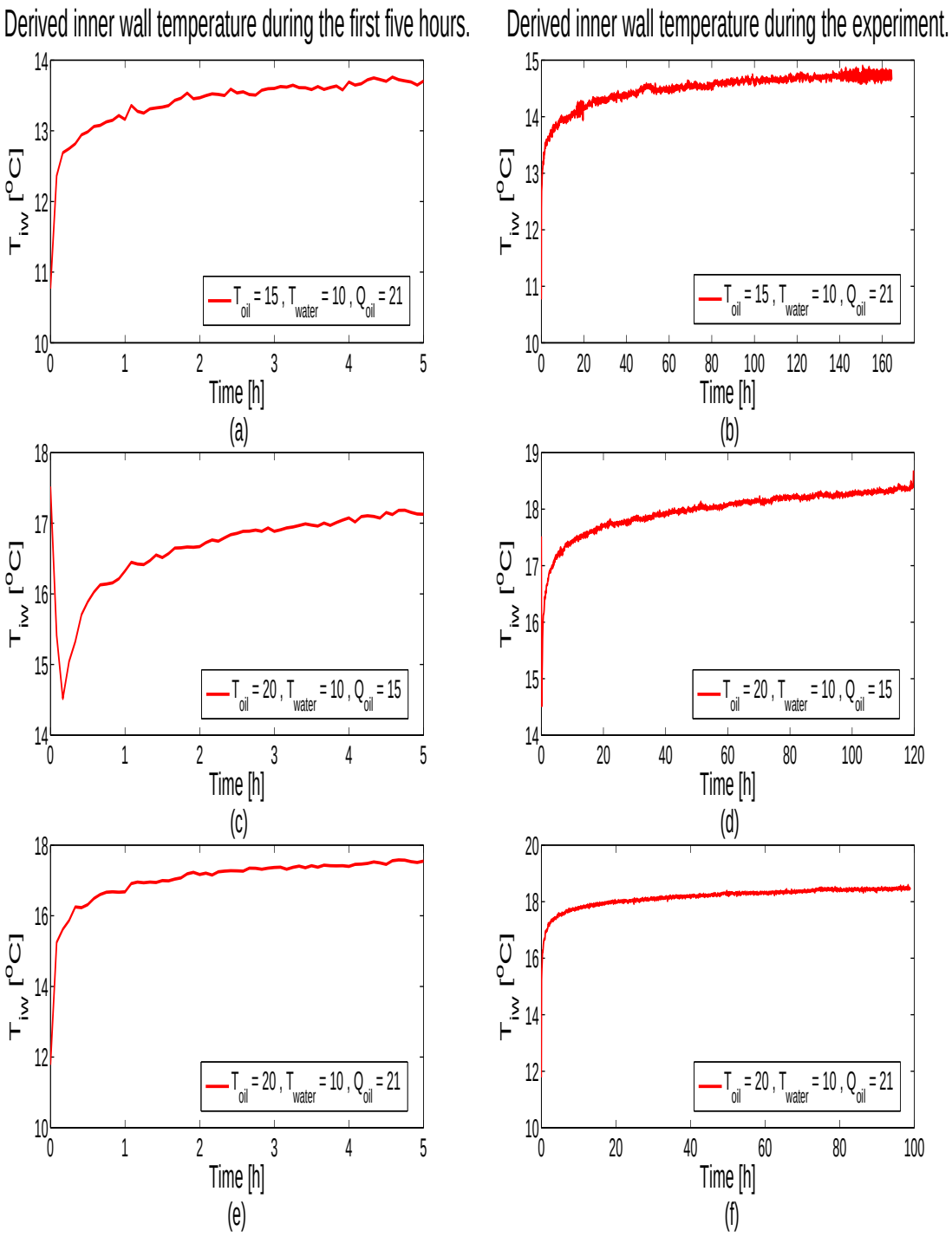

Figure 4.14: Inner wall temperature
Inner wall temperature derived from the measured pressure drop and temperature drop in the test pipe.
Note that in figure (c) the inner wall temperature is first decreasing.

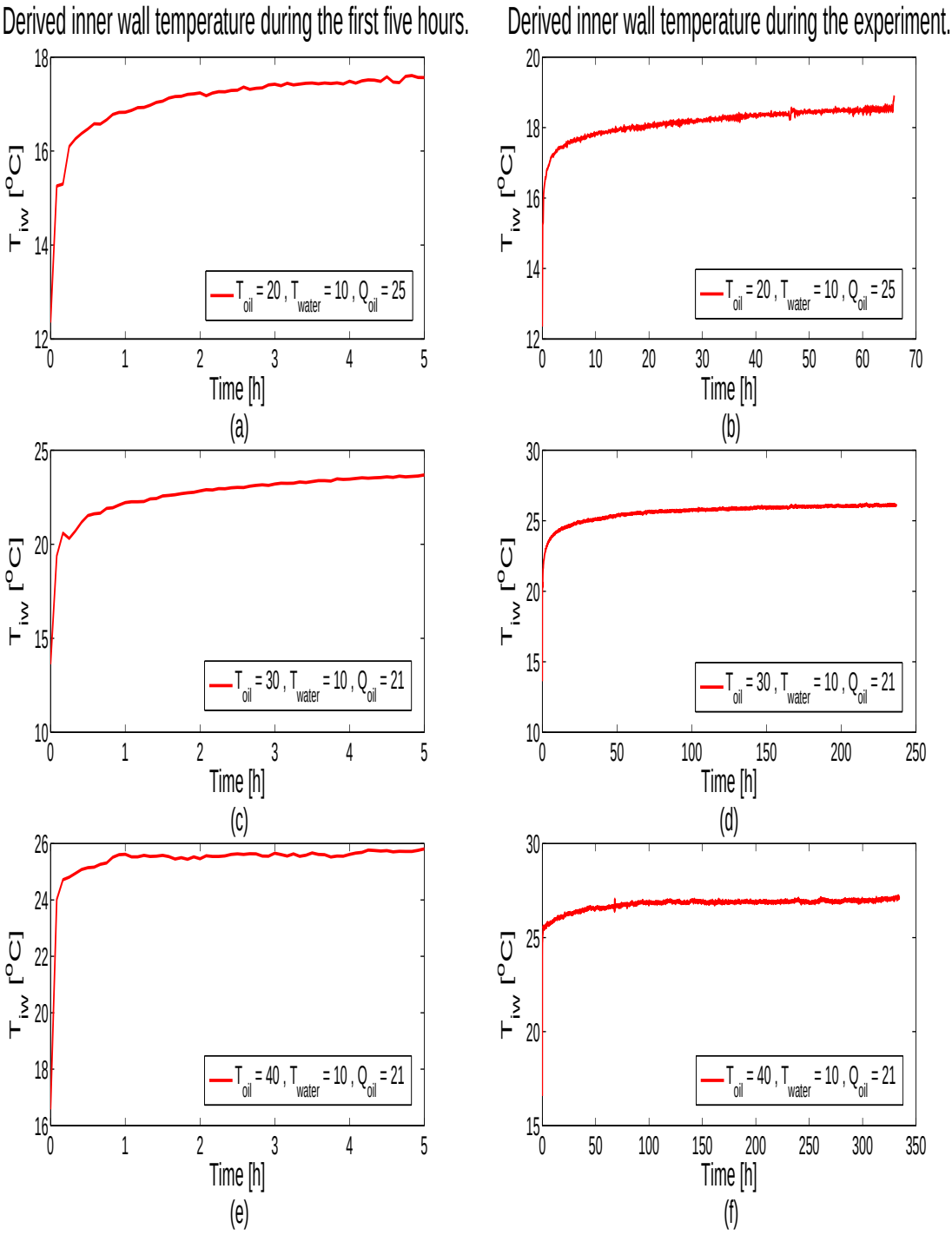

Figure 4.15: Inner wall temperature
Inner wall temperature derived from the measured pressure drop and temperature drop in the test pipe.

4.5.3 Wax Thickness Calculations

The wax thickness H is derived from integration of (4.5) combined with (4.16), (4.20)-(4.21), (4.7) and (4.9)-(4.13) :

$$H = r_o - \left(\frac{\rho_{oil} Q_{oil}^2 L}{4\pi^2 \Delta P_{measured}} f_H \left(\frac{\mu_{oil}(T_{iw})}{\mu_{oil}(T_{cup-mix})} \right)^{0.05} \right)^{\frac{1}{5}} \tag{4.24}$$

The wax thickness are calculated in two ways. One, assuming the initial inner wall temperature of the test pipe to equal the average water temperature in the cooling jacket ($T_{iw}(t_o) = T_{water}$), or two, computing the initial inner wall temperature from (4.13). In both cases we assume no initial wax on the pipe wall. The first (way) is reasonable since the thermal conductivity of steel is much higher than that of oil. The results are presented in Figures 4.16 and 4.17 ((a), (c) and (e)), where we note an initial negative wax thickness among four of the graphs. Next, we calculate the initial inner wall temperature to study its effect on the initial wax thickness calculation. The results are introduced in Figures 4.16 and 4.17 ((b), (d) and (f)), where we note an improvement of the results, reducing the number of negative wax thicknesses from four to two. All the graphs show a positive wax thickness with the exception of experiments $20 - 10 - 15$ and $30 - 10 - 21$. This is considered as an important observation of the fact that the inner wall temperature is of importance when deriving the wax thickness, especially in the beginning of a deposition process. It is also of interest to relate the negative wax thickness to the error in the measurements. We have already found a typical fluctuation level among the pressure and temperature transducers, indicating a minimum error related to the measurements. In the wax thickness calculations, the fluctuations related to the pressure drops will be further diminished by the small exponent $\frac{1}{5}$ as indicated in the wax thickness equation above. The negative wax thickness can therefore not be explained from a minimum error corresponding to a typical fluctuation level in the wax calculations. We expect the error to be larger than a typical fluctuation level, but the accuracy among the measurements is not easy to determine from the information we have. In Figures 4.18 and 4.19 calculations based on wax experiments during the whole time interval are presented. Finally, all the results are shown in Figure 4.20. We note among experiments $20 - 10 - Q_{oil}$ (where $Q_{oil} = 15, 21, 25$) in 4.20, that a higher flow rate gives a lower deposition thickness over time. This could connect the results achieved to the Reynolds number and will be discussed in the coming chapter. We also note that a higher incoming oil temperature gives a smaller wax thickness over time. This is an interesting observation that can be connected to the quickly isolating effect of the wax layer during the experiments. This will also be considered in the coming chapter.

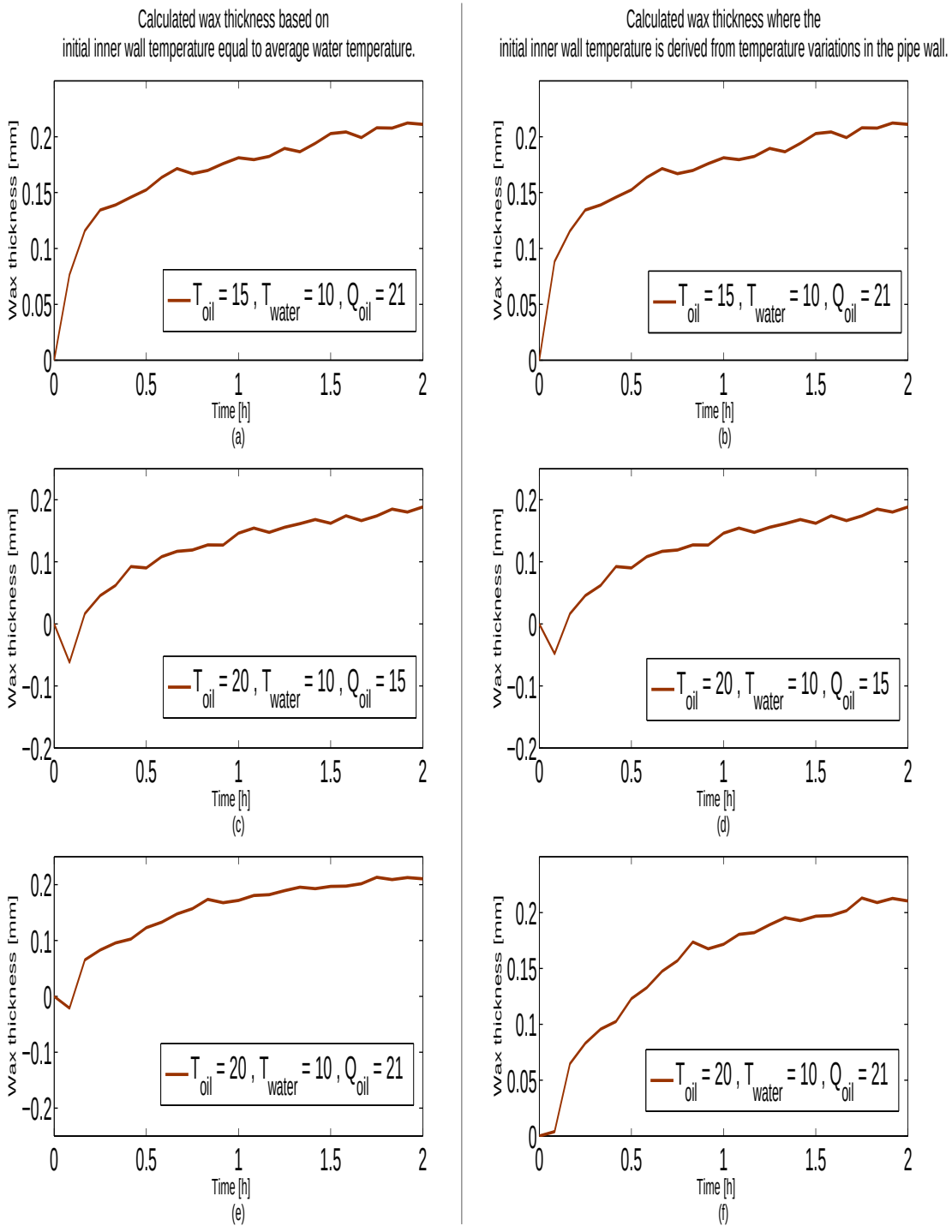

Figure 4.16: Calculated thickness of wax deposit

The difference in the initial wax thickness is shown. Note that experiment (d) give a negative wax thickness during the first minutes even though the estimated inner wall temperature was included. The vertical scales in the Figures (e) and (f) are not equal, but we confirm that the graphs are just the same except for the initial wax thickness values.

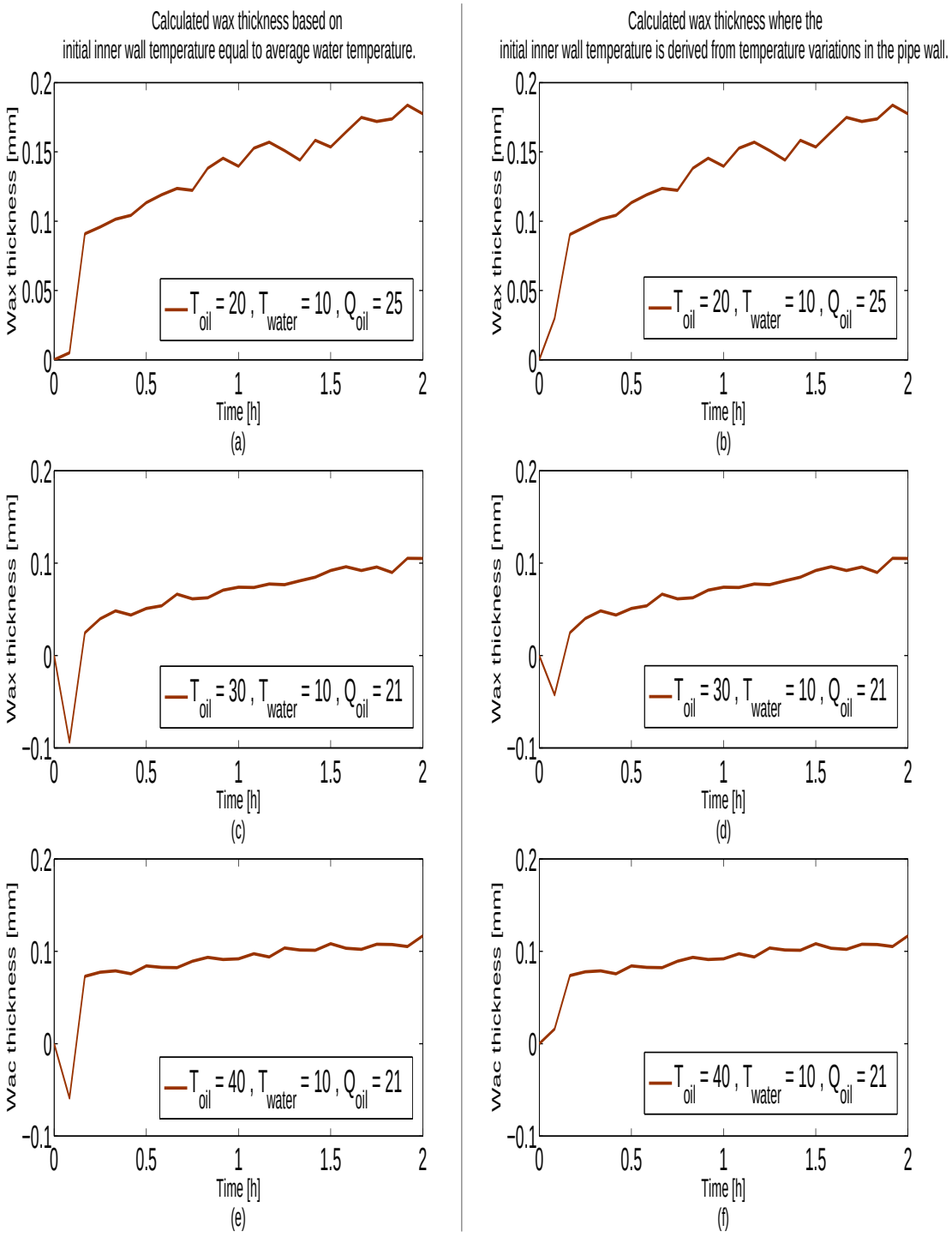

Figure 4.17: Calculated thickness of wax deposit

The difference in the initial wax thickness is shown. Note that experiment (d) give a negative wax thickness during the first minutes even though the estimated inner wall temperature was included.

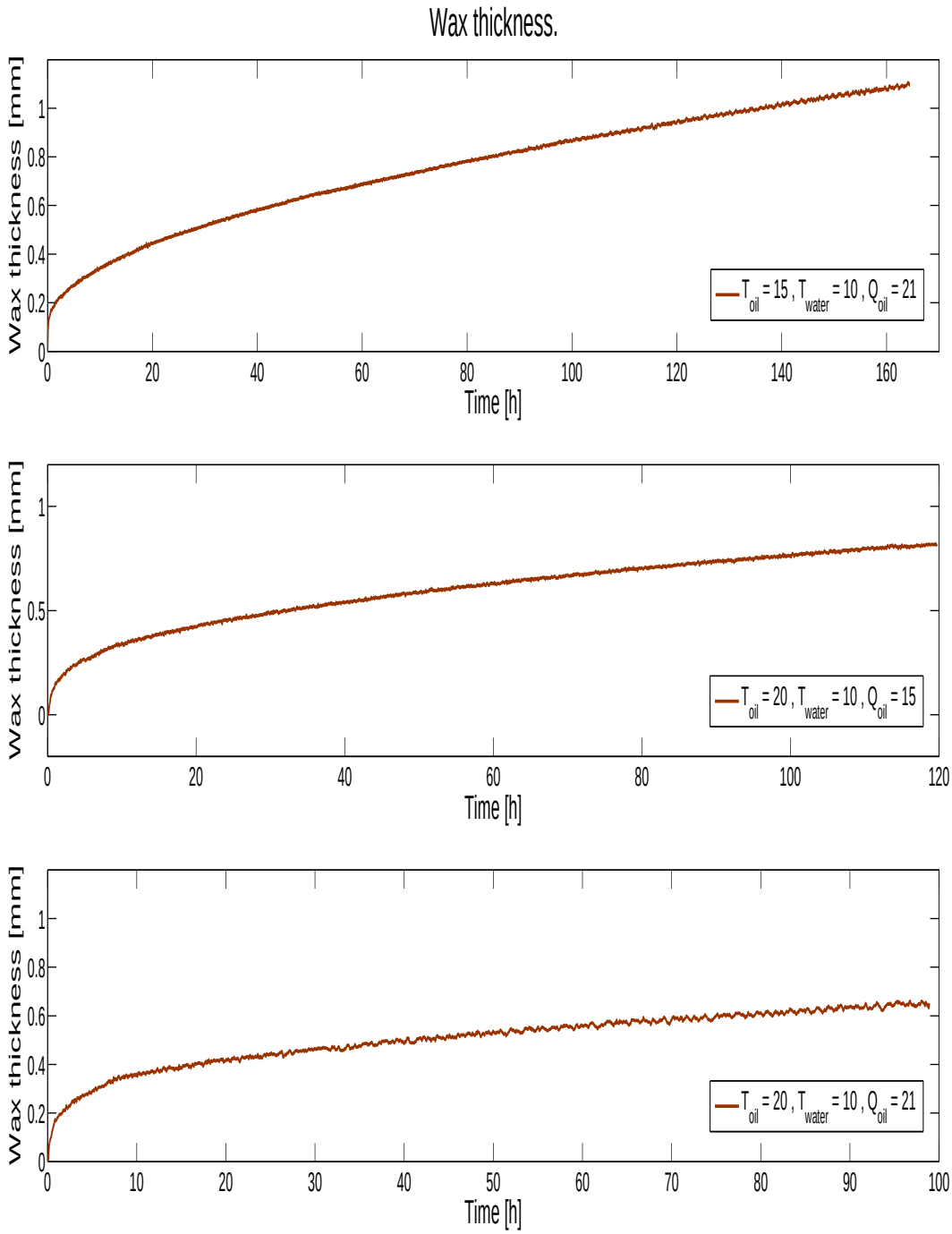

Figure 4.18: Calculated thickness of wax deposit

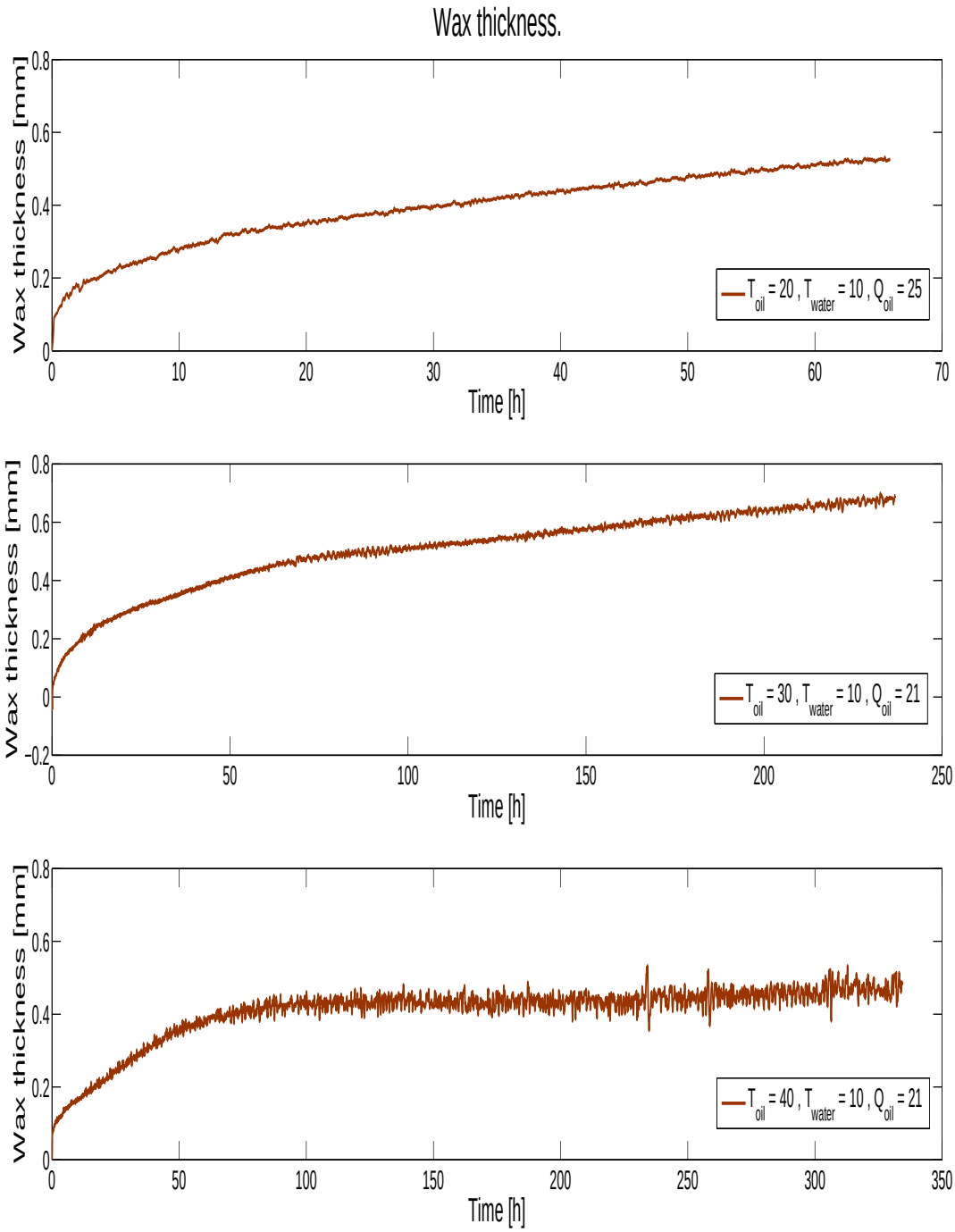

Figure 4.19: Calculated thickness of wax deposit

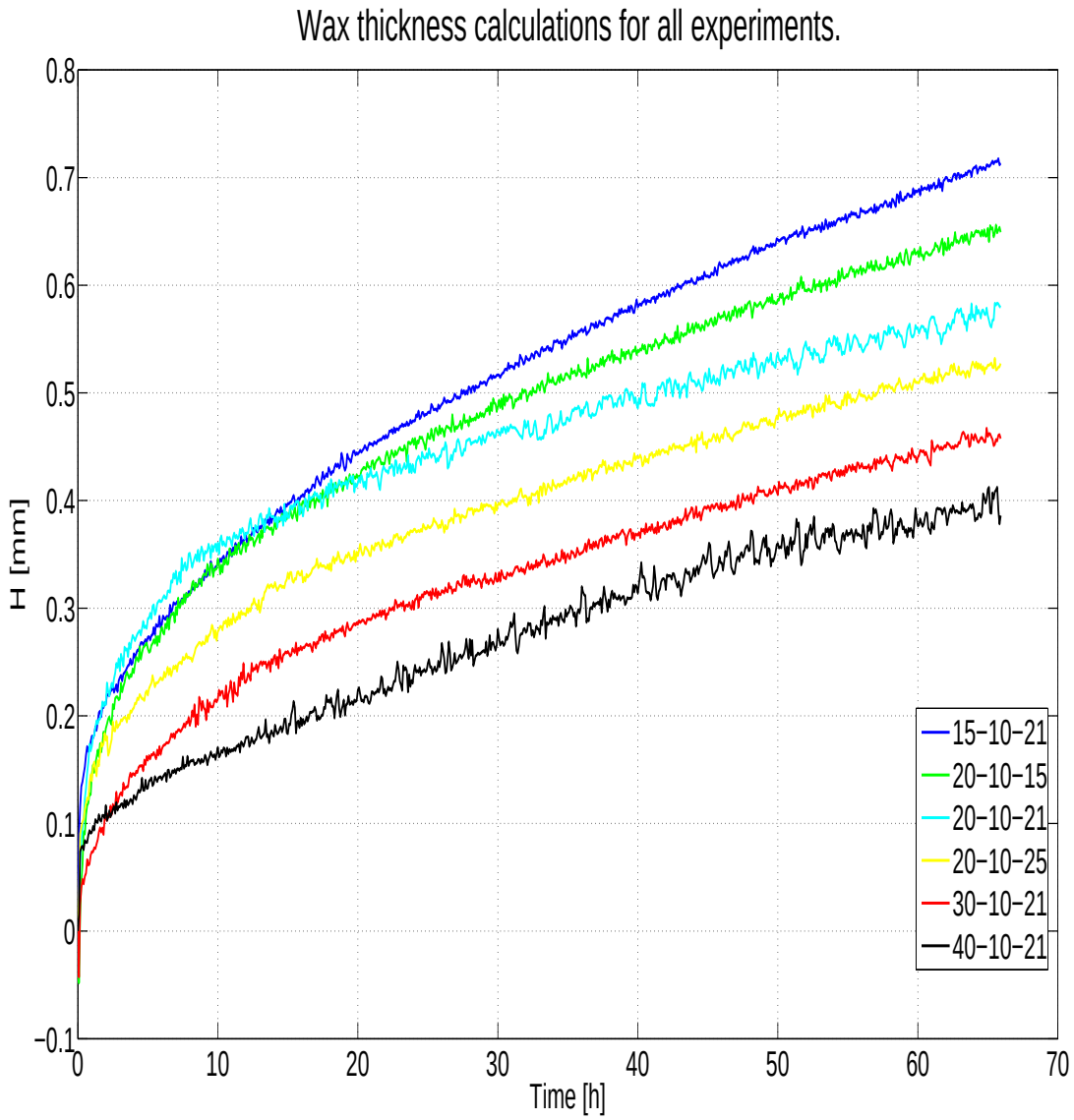

Figure 4.20: All wax thickness calculations

There is no obvious connection between the plotted results and the flow rate. We notice the lowest flow rates among the $20 - 10 - Q_{oil}$ experiments indicating a larger deposition thickness after 6o hours than with the highest flow rates.

4.5.4 Discussion of the Wax Thickness Calculations

Prior to each experiment, StatoilHydro has a run-in period from 10 to 15 minutes stabilising the incoming temperatures. We assume no wax deposition during this period. As already indicated, we found an improvement of the calculated wax thickness by not assuming the inner wall temperature to equal the average water temperature before deposition occurs. If we go back to the results in chapter 3 where we compared the inner wall temperature of turbulent flow with and without an insulating layer (see Figure 3.4), we found that a small layer on the wall will influence the inner wall temperature significantly. This indication should make us aware of a possible change in the inner wall temperature during the run-in period. It is therefore important that we do not ignore any possible initial layer at the wall in each experiment, even though it is extremely thin compared to the test pipe radius. From least-squares regression calculations a linear rate of the deposition thickness has been derived for experiment $20-10-15$ (see Figure C.4 in Appendix). We assume the gradient of the line to represent the early wax thickness as a function of time. In that case a deposit layer could increase from 0mm to 0.027mm during five minutes. Turbulent pipe flow with and without a uniform wax layer of 0.027mm, and a heat conductivity of wax that are two times to that of oil, change the inner wall temperature from 13.39 to 14.03 °C. This means that the inner wall temperature in practice can be a little higher than what we have calculated by including the small deposit in the beginning of the experiment. From calculations, we find that the thickness must be 0.31mm to reach the initial inner wall temperature giving a non-negative wax thickness. This is not possible during the short stabilising period. Calculations based on experiment $30-10-21$ give an initial wax thickness of 0.068mm when avoiding a non-negative thickness. We can not expected a layer of the given thickness to establish during the run-in period either, but we keep in mind that a deposit thickness of 0.068mm is still extremely small compared to the inner pipe radius of 26.3mm. The inner wall temperature with such a small thickness is expected to give a temperature about 4°C higher than without the wax deposit when assuming the thermal conductivity of the deposit to be two times larger than oil.

To show how important a thin wax layer can be for the inner wall temperature, we define two normalized functions for further qualitative analysis. The relative inner wall temperature :

$$\epsilon_T = \left| \frac{T_{water}}{T_{water} - T_{oil}} \right| \left| \frac{T_{wo} - T_w}{T_{wo}} \right| \tag{4.25}$$

where $T_{wo} = T_{iw}(t, r_o, ..)$ and $T_w = T_{iw}(t, r_i, ..)$.
The relative wax thickness :

$$\epsilon_r = \frac{H}{r_o} \tag{4.26}$$

ϵ_T and ϵ_r as defined here, fulfill the identities $\epsilon_T \leq 1$ and $\epsilon_r \leq 1$. Note that when $t = 0$, $\epsilon_T = 0 = \epsilon_r$. Since the inner wall temperature in the beginning of each wax experiment change much faster than the wax deposition (see Figure 4.21), we establish the following general relation for our case :

$$\frac{\epsilon_r}{\epsilon_T} \ll 1 \tag{4.27}$$

This relationship holds true for all wax experiments involving a short period of time right after wax deposition happens. A few minutes is enough. It is therefore shown that the wax thickness in the beginning of each wax experiment has a large impact on the inner wall temperature.

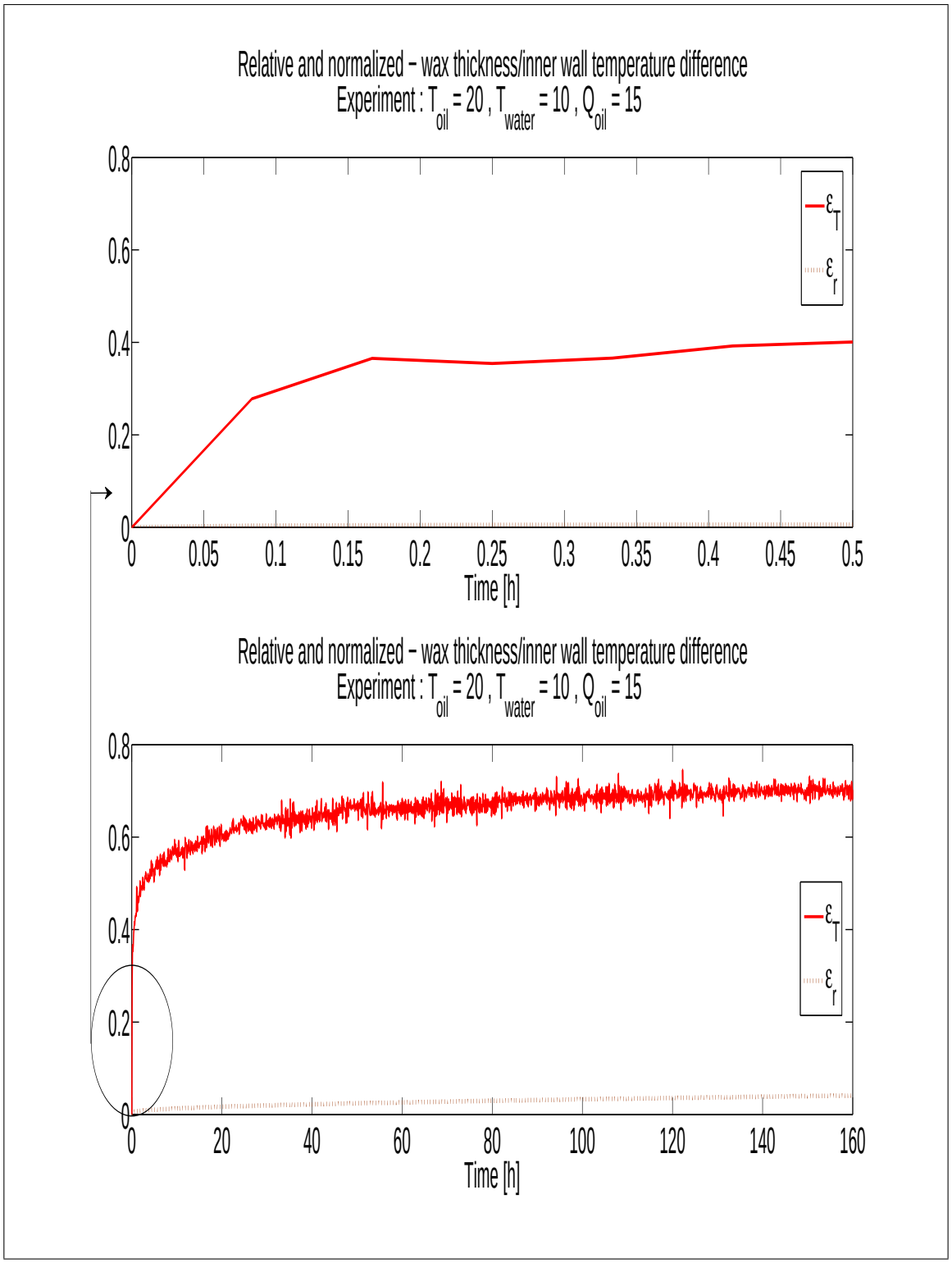

Figure 4.21: Relative inner wall temperature and relative thickness

Note the clear difference between the relative inner wall temperature compared to the relative wax thickness.

4.5.5 Influence of Roughness On Wax Deposition

Until now the wax thickness has been derived from the assumption of zero roughness of the pipe wall during the experiments. This is a bold assumption even though we obtain seemingly smooth and uniform layers on the pipe wall (see Figure 4.1). It is reasonable to believe that the roughness will increase during the wax experiments, since wax crystals that form on the surface probably make the wall less smooth to a certain level. The roughness depends on the deposit's composition, and from two oils we normally have two different compositions of wax deposits. Each deposit has its own identity through different fractions of hydrocarbon components etc. In our case the wax layer has a visible smooth surface and an approximate uniform thickness. We therefore believe that the roughness stays small during the deposition process. Considering the instance where roughness changes immediately to a constant different from zero when waxes first stick to the wall. This is only reasonable if the roughness change very little during the deposition process. We must require that the pipe is hydraulically smooth during each wax experiment. If not, there is an important question about how well our analysis so far reflects the physics inside the test pipe. From a mathematical perspective we evaluate the roughness through the dimensionless roughness height ${k_s}^+$:

$$k_s^+ = \frac{u_\tau k_s}{\nu} \tag{4.28}$$

where $k_s^+ < 5$ for a hydraulically smooth surface (see Wilcox (2006)) and u_τ is the friction velocity close to the surface given by $u_\tau \equiv \frac{\tau_{wall}}{\rho_{oil}}$.

For our analysis we require that $k_s < 5.0 \cdot 10^{-5} m$ when considering the potentially highest inner wall temperature associated with the kinematic viscosity in (4.24), and assuming $u_\tau = \overline{V}\sqrt{\frac{f_{BF}}{8}}$. (where $\overline{V}$ is the area-averaged velocity from equation (2.42)). We have therefore considered three different constant roughness heights, $k_s = 10^{-6} m$, $k_s = 5.5 \cdot 10^{-6} m$ and $k_s = 10^{-5} m$. The results are shown for three of the experiments in Figures 4.22 - 4.24. We notice a decrease in the wax thickness with increased roughness, and an initially negative thickness within the first stages of the experiments. The more we increase the roughness, the more negative wax thickness appears during the early deposition. This observation is important. In the previous work we derived the deposition thickness by setting $k_s = 0m$. We have here found that small changes of k_s predict a clear negative deposition thickness. We have therefore strong indications that k_s must be very small during the first period of deposition in a smooth pipe and that ignoring roughness is probably a good approximation to this period in reality. At the same time, the roughness could be very small in the beginning of each experiment and then change after a while.

It is therefore of interest to test the following hypothetical roughness height function :

$$k_s = A(1 - exp(-bt)) \tag{4.29}$$

where A is a constant representing an asymptotic value of the roughness height, b is a constant decided on the basis of how fast the roughness height will achieve an "equilibrium state", and the variable t represent the time in hours. We emphasize that we do not have strong reasons for this hypothetic variation of roughness, but it is still interesting to see what happens if we compare the result where $k_s = 0m$ with the function $k_s = 10^{-5}(1 - exp(-bt))m$ on

experiment $20 - 10 - 25$. In Figure 4.24 we have a clear negative thickness during the first hours when $k_s = 10^{-5}m$, but from the assumption of an exponential growth toward this value, we avoid a negative thickness. We decide the constant b from a visible evaluation of the original graph ($k_s = 0m$) where the deposition rate is almost constant after 15 to 20 hours (see 4.24). We therefore set $b = \frac{ln(20)}{15}$ as an approximation. The results are shown in Figure 4.25. It is interesting to see that if the roughness increases exponentially in the beginning of each experiment, then we see a trend of a linear growth of the deposition instead of an exponentially growth during the first period of time. For large time scales (several days) there are small variations of the thickness when considering a little or no roughness as illustrated in Figure 4.24.

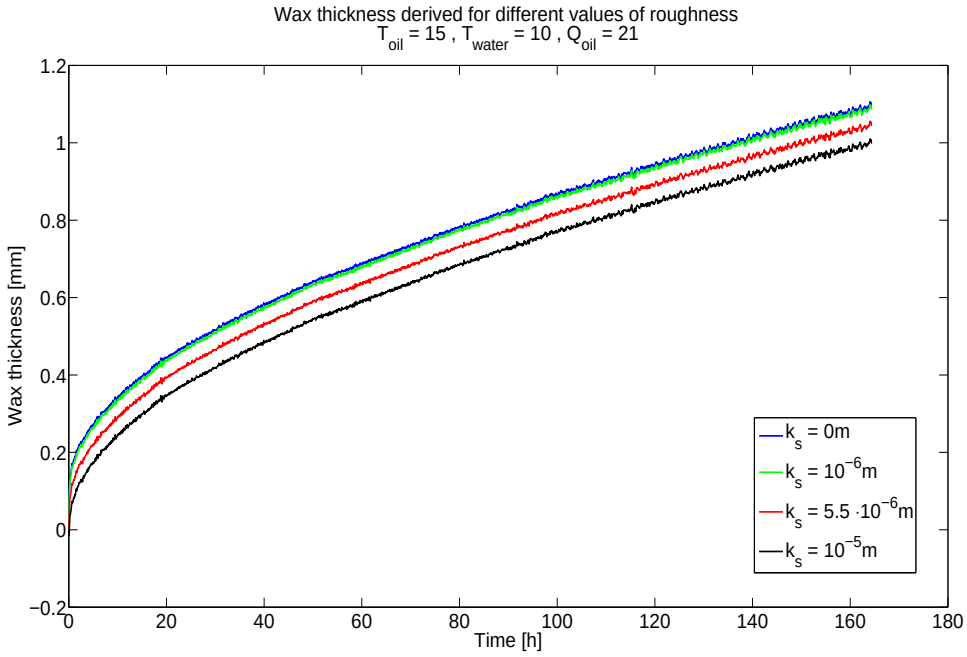

Figure 4.22: Wax thickness derived with constant roughness

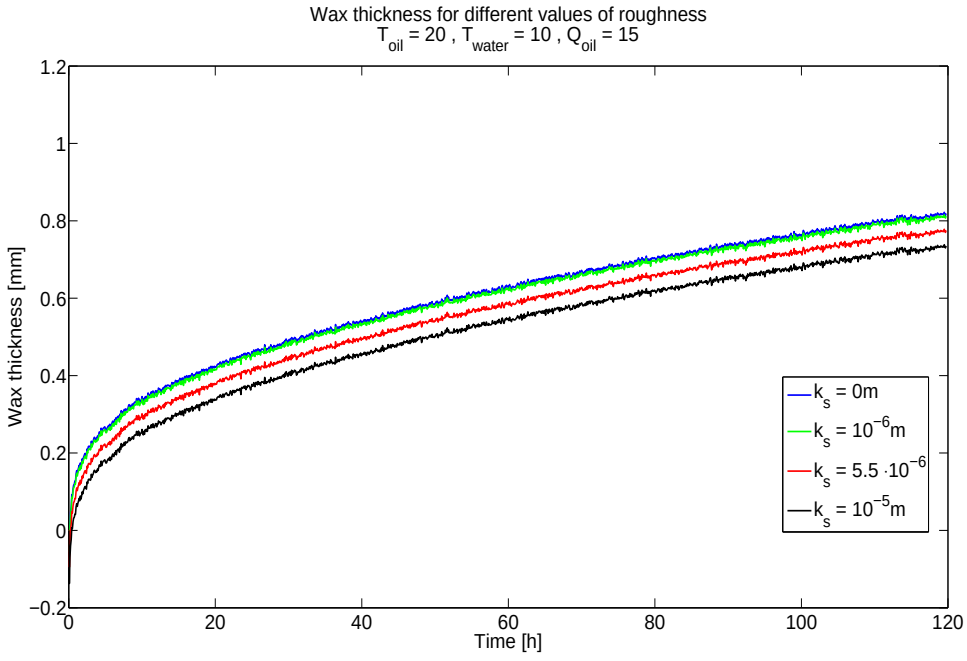

Figure 4.23: Wax thickness derived with constant roughness

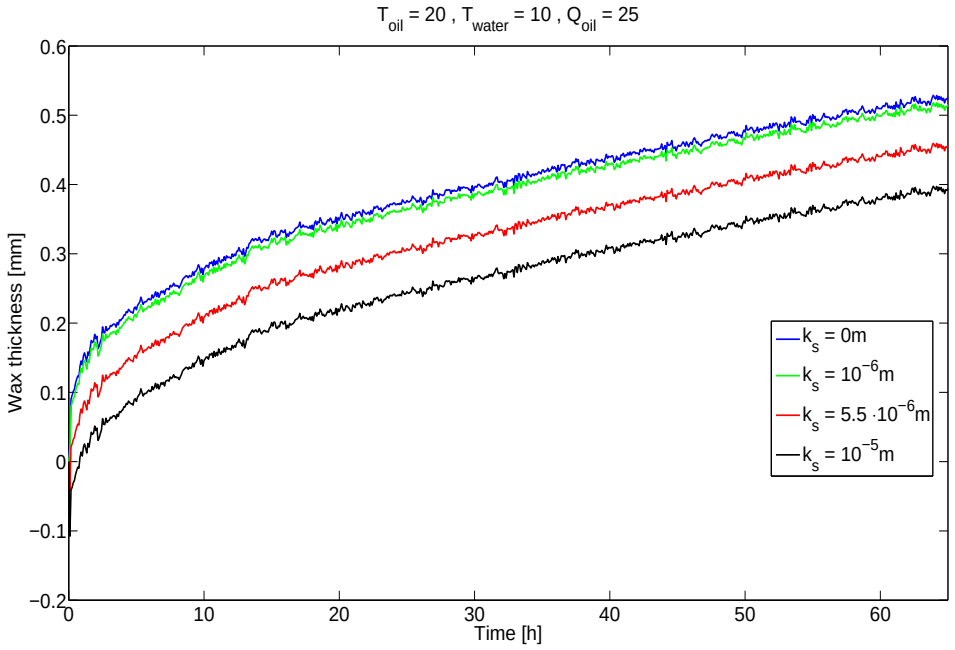

Figure 4.24: Wax thickness derived with constant roughness.

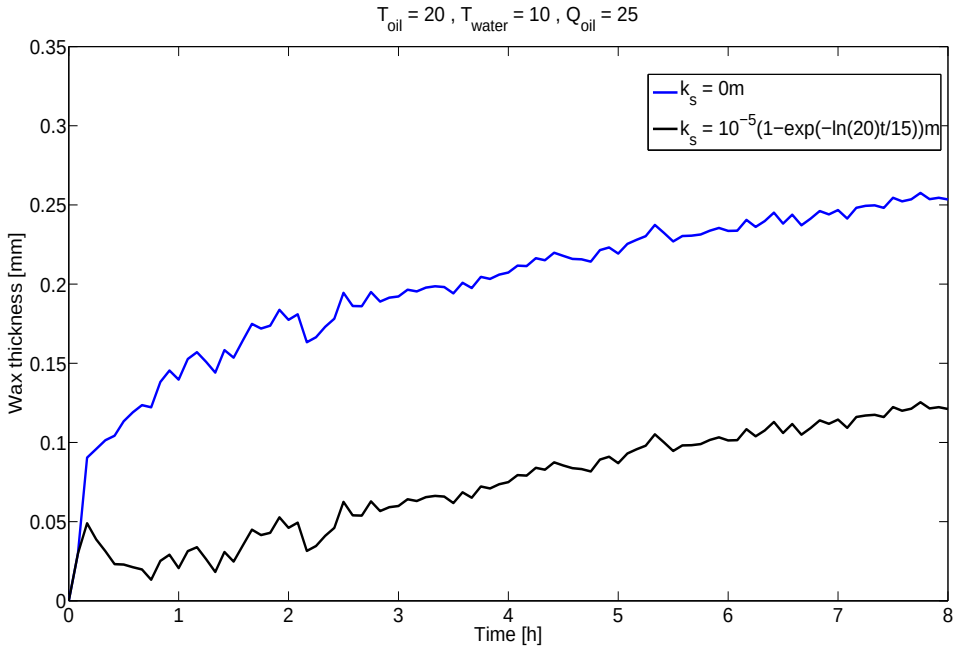

Figure 4.25: Wax thickness derived with variable roughness

4.5.6 The Relative Thermal Conductivity of the Wall Insulated by Wax

In the Chapter 2 equation (2.71), we introduced the overall heat transfer coefficient U_{tot} on the basis of a system consisting of an insulated pipe with a flowing fluid inside. Consider the deposit as the insulating layer. We have calculated U_{tot} and the wax thickness H as functions of time. It is therefore only one unknown left in (2.71), the thermal conductivity of the wax deposit. From the assumption of constant thermal conductivities, we derived a general expression for the overall heat transfer coefficient of a pipe system with concentric layers (see section B.1, Appendix). Within each layer we assumed the temperature to be constant for a fixed radius. We therefore derived U_{tot} on the basis of a constant heat flux through every point within the layer of the given radius, a condition that is probably not satisfactory for the deposit in the beginning of each experiment. When wax starts to form on the pipe wall, it will take some time before the deposit can be considered a uniform and concentric layer. The thermal conductivity of paraffins is a given property whether we have a deposit or not. We can not reject the uncertainty related to the composition of the layer that sticks to the wall. In the wax experiments StatoilHydro study wax deposition in a localized area in the pipe; the test pipe. It will probably take time before the deposition layer covers the whole inner pipe surface during deposition when crystals stick to the wall. It is therefore better to introduce a relative thermal conductivity of the wall-layers (steel and deposit) and subsequently calculate how it develops during the wax experiments.
We define k_{rel} as :

$$k_{rel} = \frac{k_{wax} k_{wall} \ln\left(\frac{r_1}{r_i}\right)}{k_{wax} \ln\left(\frac{r_1}{r_o}\right) + k_{wall} \ln\left(\frac{r_o}{r_i}\right)} \tag{4.30}$$

where k_{rel} is derived from (2.71) by defining $\frac{1}{U_{rel}} = \frac{1}{U_i} + \frac{1}{U_w}$ (see section B.1, Appendix).

Here $k_{rel}(t = 0) = k_{steel}$, and we expect k_{rel} to decrease with time since the increased deposit thickness increases the resistance from heat transfer through the pipe wall. In Figure 4.26, k_{rel} seems to stabilise after a few hours in each experiment. A wax thickness that increases slowly after a few hours and a thermal conductivity that appears to stabilise within one hour, could indicate that the deposit layer after a while better fulfill the assumptions of constant thermal conductivity (section B.1, Appendix). We have therefore plotted the fraction of $k_{deposit}$ over k_{oil} within the time interval from 50 to 60 hours in Figure 4.27. In the Figure we observe an interesting trend among the experiments. The experiments with the largest temperature difference between the inlet of water and oil appear to have deposits with a larger thermal conductivity. Let us introduce an expression for the thermal conductivity of the wax deposit. The Maxwell correlation used by Singh (2000), give the following expression for the thermal heat conductivity of the wax deposit :

$$k_{deposit} = \frac{2k_{wax} + k_{oil} + (k_{wax} - k_{oil})F_w}{2k_{wax} + k_{oil} - 2(k_{wax} - k_{oil})F_w} k_{oil} \tag{4.31}$$

F_w represents the wax fraction of the deposit. The correlation gives $k_{deposit} \approx k_{oil}$ when the wax fraction is small, and $k_{deposit} \approx k_{wax}$ when the wax fraction is large. In our thermal analysis (section 4.5.4) we assumed $k_{deposit} = k_{wax} \simeq 2k_{oil}$. We expected the wax fraction of the deposit to be large, an assumption that turns out to be inaccurate if we accept the indications we have in Figure 4.27. Here the predicted wax deposits show a high content of lighter hydrocarbons. This is common to all the experiments except from that with the largest

temperature difference between oil and water, experiment $(40 - 10 - 21)$. According to StatoilHydro, measurements of the deposits gave a wax content between 35% and 65% depending on the experiment. Further, we have a fundamental problem related to the calculated thermal conductivity among several deposits. It is not consistent with equation (4.31) that some of the deposits have a thermal conductivity less than the oil. This gives us reasons to believe that our calculations are not sufficient for the case. Pressure and temperature measurements are included in the calculations of the thermal conductivity. In Figure 4.27, we note that the experiments associated with a $k_{deposit} < k_{oil}$, are those with the lowest temperature difference between the oil and water. We have already mentioned (in section 4.3) that the temperature changes about 1 % (or less) during the deposition. It is therefore important that the temperature measurements give an accuracy much smaller than one percent during the experiments. The source of error among the temperature measurements are therefore considered as crucial for the case.

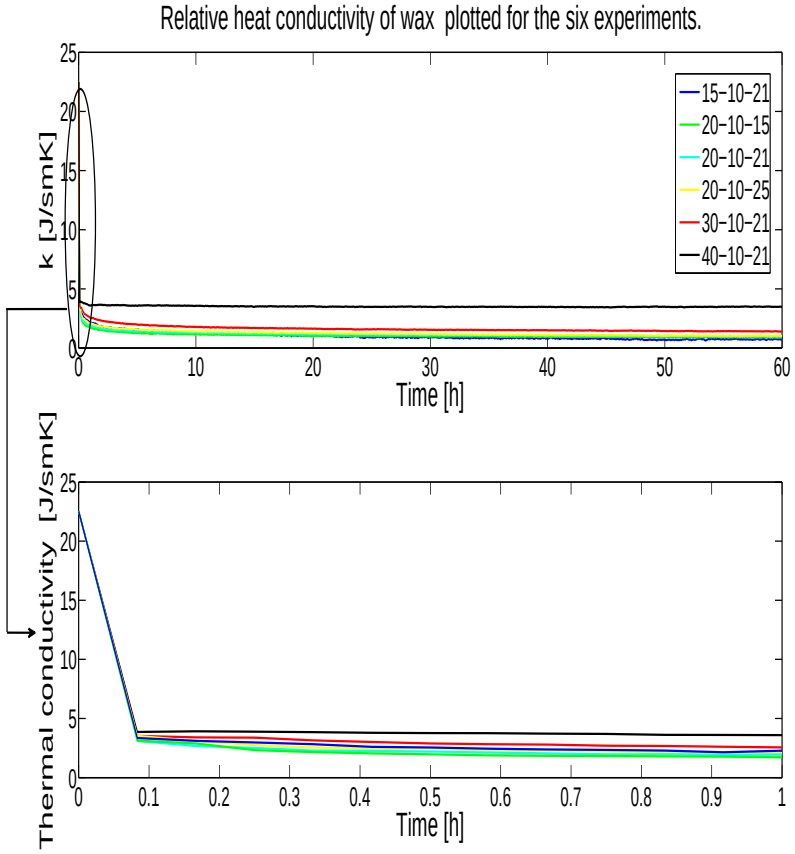

Figure 4.26: The relative heat conductivity given by (4.30)

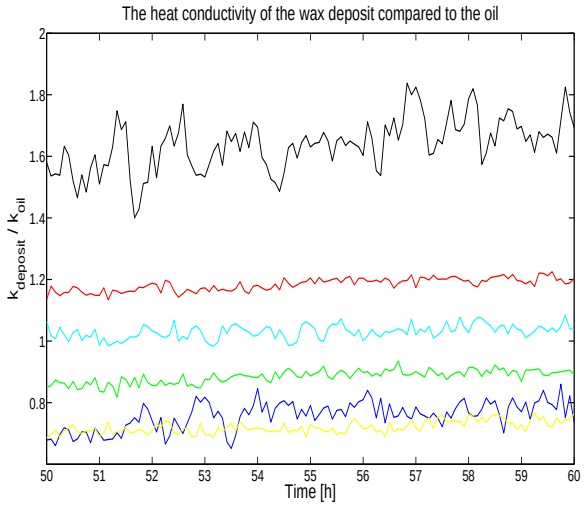

Figure 4.27: The relative heat conductivity of wax deposit compared to oil
The color codes are the same as in the figure above.

4.6 Correlation Curves for Wax Thickness

Based on the calculated wax thickness (H) we derive a best fit curve related to each experiment. The calculated wax thickness seems to have the general property $H \sim t^{\alpha}$, where $0 < \alpha < 1$. We therefore introduce the following expression for the correlation curves :

$$H_{correlation} = At^{\alpha} \tag{4.32}$$

where A and α are constant to be determined, and the correlation are based on the measured time in hours (h) (see Table 4.3 below). It is of interest to try a log-log analysis of the

Table 4.3: Correlation parameters

Experiment	A	α
$15-10-21$	$10^{-3.92}$	0.427
$20-10-15$	$10^{-3.85}$	0.365
$20-10-21$	$10^{-3.73}$	0.271
$20-10-25$	$10^{-3.89}$	0.332
$30-10-21$	$10^{-3.98}$	0.342

calculations to see if the results show a strong or weak linearity between $log(H)$ and $log(t)$. The results based on five experiments are presented in Figure 4.28.
The $40-10-21$ is not representative in this case since the log-log analysis give a weak linearity compared to the others. We therefore based on these find the best fit line to each of the five wax thickness calculations. Finally, we derive $H_{correlation}$, and the results are shown in Figures 4.29 - 4.31. The curves seem to agree well with the wax thickness calculations, especially those associated with experiments $20-10-21$ and $20-10-25$ in Figure 4.30.

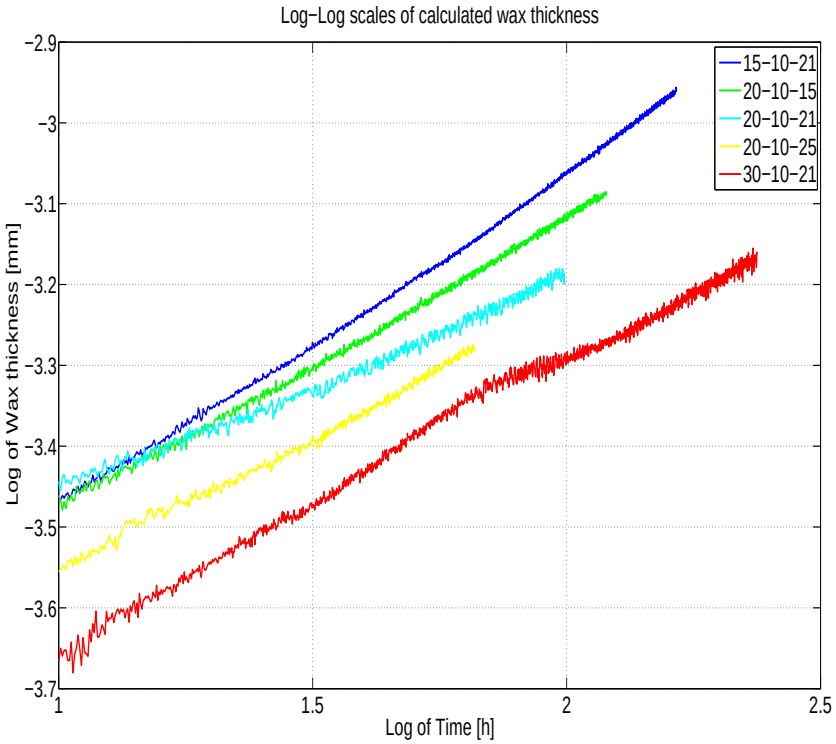

Figure 4.28: Log-log-scales of the calculated wax thickness

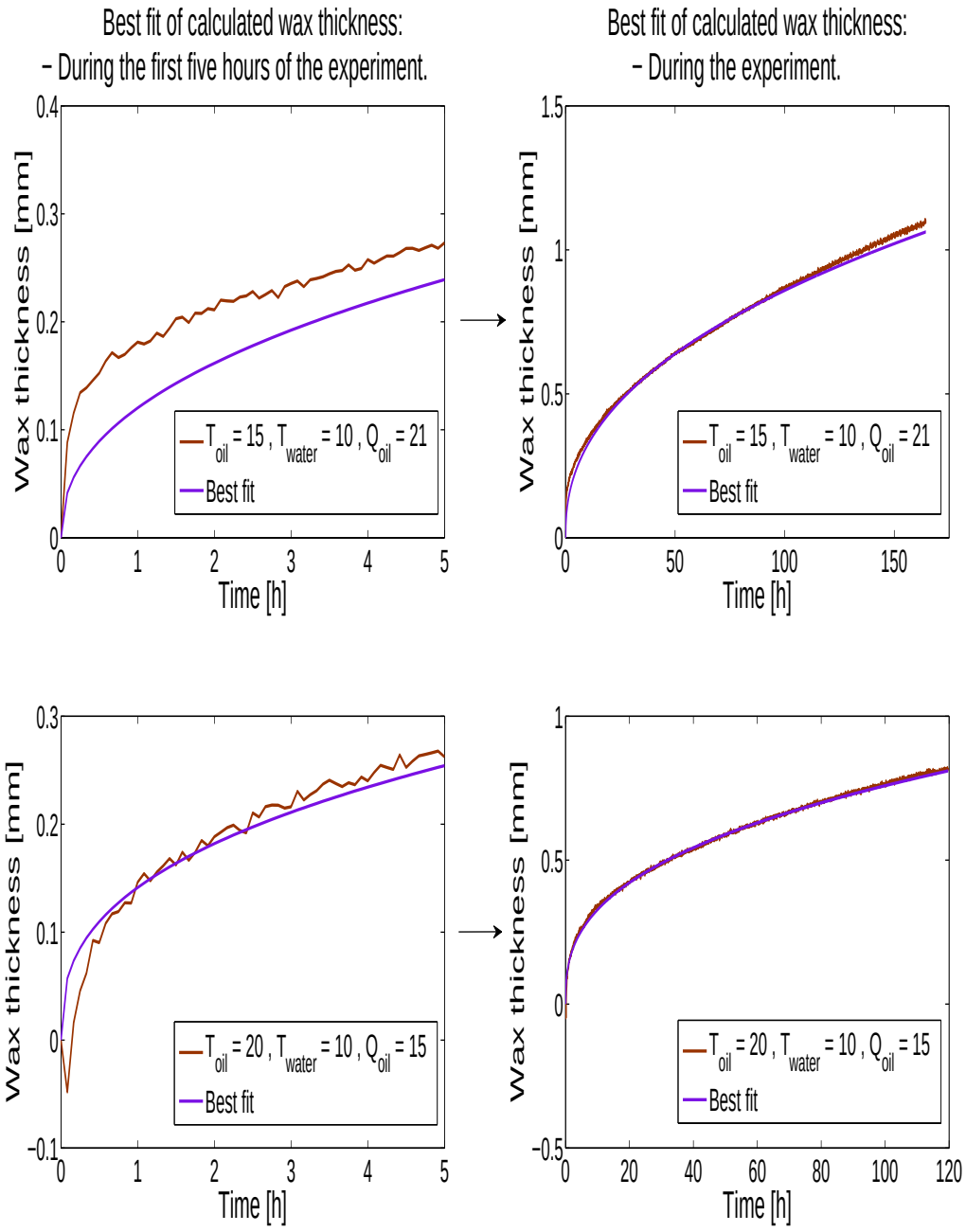

Figure 4.29: Best fit of calculated wax thickness based on log-log analysis

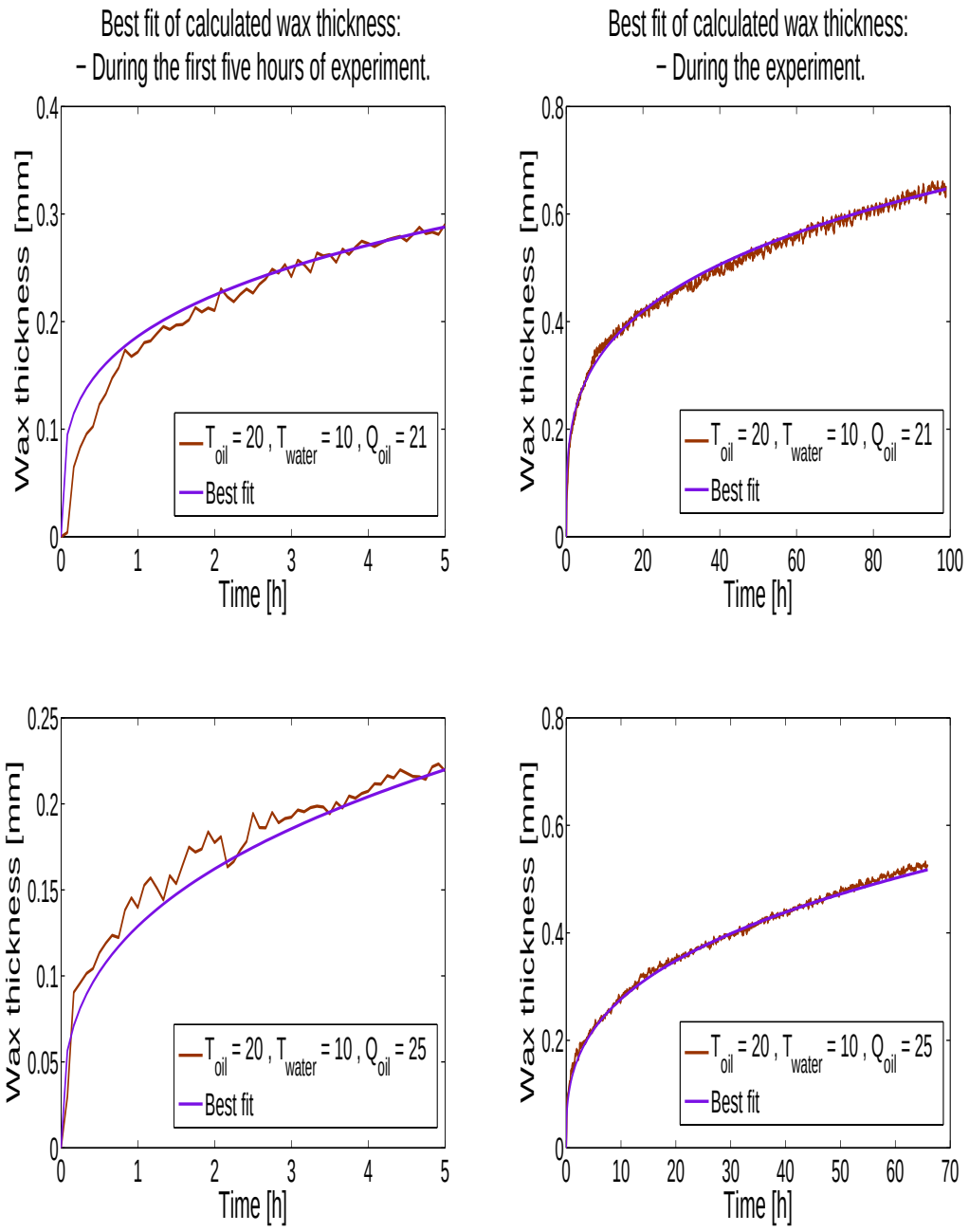

Figure 4.30: Best fit of calculated wax thickness based on log-log analysis.

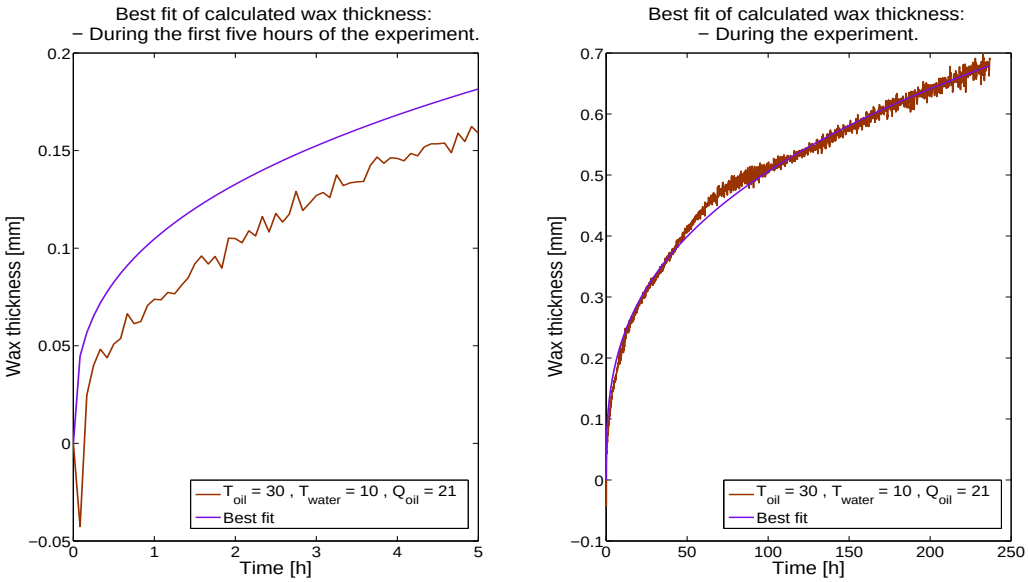

Figure 4.31: Best fit of calculated wax thickness based on log-log analysis

4.7 Experimental Results - A Summary

Based on a clean pipe and isothermal flow we found the optimal inner pipe diameter and roughness. With the optimal parameters, the error in the calculated pressure drops for isothermal flow experiments confirmed good agreement between the calculated and the modeling friction factor. For isothermal flow we used the Haaland friction factor model. Considering a clean pipe and non-isothermal flow we needed to correct the Haaland friction factor which is adapted to isothermal flow. A temperature gradient over the cross section gives a different viscosity at the wall compared to the viscosity in the bulk flow. This was taken into consideration by a friction factor correlation developed by Sieder and Tite in 1936, but due to large error in the calculated pressure drops compared to those derived for isothermal flow, we tried to find a better correlation by further adjustment of the friction factor correlation. Finally, we found a better correlation, but at the expense of larger discrepancies among the error in the calculated pressure drops achieved for the lowest flow rates. We could therefore not use the corrected friction factor to predict wax thickness for the flow rates of $5m^3/h$ and $10m^3/h$. Further we utilised the new friction factor in the prediction of the deposit thickness during the wax experiments. A growing wax layer diminishes the inner pipe radius and increases the pressure drop along test pipe for a constant flow. Several wax thickness calculations based on an initial wall temperature equal to the cooling water predicted a negative thickness during the beginning of the wax experiments. By including temperature variations in the pipe wall we obtained more consistent results of the deposit thickness. The inner wall temperature seemed to be very sensitive to small variations of the wax thickness when the first layers were established on the wall. Each experiment were allowed a period from 10 to 15 minutes to stabilise the incoming temperatures of oil and water. During this time a small scale deposition could occur since the inner wall temperature is lower than the WAT. We assumed an initially clean pipe in each wax experiment; that is any possible layer is ignorable at the moment the experiment is declared started. In the wax calculations we also calculated the inner wall temperature of the test pipe. Through our analysis, we have seen that small changes of the wax thickness have a large impact on the inner wall temperature during the first minutes or hours of the wax experiments. When it comes to roughness, we always considered a hydraulic smooth pipe. We found that after a long time (several hours), the roughness had a little impact on the wax thickness. Further, the analysis of the thermal conductivity of the wax deposit was expected to have an average value between k_{oil} and k_{wax}. Among three experiments we calculated a $k_{deposit}$ lower than k_{oil} that was found to be incorrect. The accuracy among the temperature measurements are of large importance for the case. If the accuracy of the temperature transducers are not small enough, this would also influence the inner wall temperature derived earlier. In the final section of this chapter we derived fitted curves based on the calculated wax thickness, which show good approximations to the calculated deposit thickness.

Chapter 5

Dimensional Analysis

From log-log analysis in the previous chapter we found correlation curves for the calculated wax thickness as given by equation (4.32). Further, let us consider which physical parameters that probably influence wax thickness during deposition. We therefore go back to Figure 4.20 where the wax thickness results are gathered. We believe that the averaged axial velocity ($\overline{V}$) influence the deposition thickness (H), an assumption that is based on the wax thickness calculations of the three experiments with constant inlet temperature of oil and water (equal to 20 °C and 10 °C). They show an increase of wax thickness for a decrease in velocity. It is therefore interesting to note that the largest thickness is related to experiment $15-10-21$ instead of experiment $20-10-15$, even though the last has the lowest flow rate and thereby a lower velocity. This could indicate that the incoming oil temperature ($T_{oil,in}$) is of importance. Based on the wax thickness calculations, it is possible that a low incoming oil temperature gives a larger thickness than a higher incoming oil temperature during a constant flow rate operation when the water temperature is held fixed. Based on the experiments studied, we therefore believe that a connection between deposited wax layer thickness, T_{WAT} and $T_{oil,in}$ could be considered. As already mentioned, the precipitation of paraffins will only occur when the fluid reaches temperatures below the WAT. In the previous chapter we found that the inner wall temperature change quickly in the beginning of each wax experiment; increasing fast toward the incoming oil temperature. It is therefore reasons to consider the incoming oil temperature as important here. Finally, we expect parameters as the inner diameter (D_o), the kinematic oil viscosity (ν), and the time (t) to be associated with the deposition process. We therefore first assume a relationship among the quantities through a physical law given by :

$$F(\overline{V}, D_o, \nu, T_{oil,in}, T_{WAT}, t, H) = 0 \tag{5.1}$$

The Pi theorem (Logan 2006) states that there is an equivalent physical law between the independent dimensionless quantities that can be formed from $\overline{V}$, D_o, ν, $T_{oil,in}$, T_{WAT} and t. The parameters involve three independent dimensions (length, time and temperature), and the function F involve 7 parameters and 3 independent dimensions. According to the Pi theorem it is then guaranteed that a physical law as (5.1) is equivalent to a physical law involving only (7-3) 4 dimensionless quantities in this case.

Expressed as :

$$G(\Pi_1, \Pi_2, \Pi_3, \Pi_4) = 0 \tag{5.2}$$

where we define the dimensionless quantities as :

$$\Pi_1 = \frac{D_o \overline{V}}{\nu} = Re \quad , \quad \Pi_2 = \frac{T_{WAT}}{T_{oil,in}} = \widehat{T} \quad , \quad \Pi_3 = \frac{\nu}{D_o^2} t = \widehat{t} \;\; and \;\; \Pi_4 = H/D_o \tag{5.3}$$

We thereby express the wax thickness function as :

$$H = D_o \cdot \Phi(Re, \widehat{T}, \widehat{t}) \tag{5.4}$$

and in the following we assume the dimensionless function Φ on the form :

$$\Phi = \cdot Re^{\beta} \cdot \widehat{T}^{\gamma} \cdot \widehat{t}^{\eta} \tag{5.5}$$

where β, γ and η are constants to be determined.
The wax thickness is therefore assumed to be on the form :

$$H = D_o \cdot Re^{\beta} \cdot \widehat{T}^{\gamma} \cdot \widehat{t}^{\eta} \approx B t^{\overline{\alpha}} \tag{5.6}$$

and B is determined as :

$$B = D_o \cdot \left(\frac{\nu}{3600 D_o^2} \right)^{\overline{\alpha}} \cdot Re^{\beta} \cdot \left(\frac{T_{WAT}}{T_{oil,in}} \right)^{\gamma} \tag{5.7}$$

where $\eta = \overline{\alpha}$ and $\overline{\alpha}$ is the average of the α-values given in Table 4.3. B is the amplitude found from best fit analysis related to the calculated wax thickness with the given $\overline{\alpha}$, through the assumption $H \approx B t^{\overline{\alpha}}$. The results are presented in table 5.1 below. Note, in equation (5.7) we transformed the correlation curves based on the measured time in hours to seconds.

Table 5.1: Correlation parameters from dimensional analysis

Experiment	B	$\overline{\alpha}$
$15-10-21$	$10^{-3.76}$	0.347
$20-10-15$	$10^{-3.82}$	0.347
$20-10-21$	$10^{-3.87}$	0.347
$20-10-25$	$10^{-3.91}$	0.347
$30-10-21$	$10^{-3.99}$	0.347

We derive the kinematic viscosity based on the incoming oil temperature. The three wax experiments where $T_{oil,in} = 20^oC$ give a system of three equations with two unknowns; β and γ. From calculations we find a negative β and a positive γ. The equations based on $20-10-15$ and $20-10-21$ give $\beta = -0.313$, while the equations based on $20-10-21$ and $20-10-25$ give $\beta = -0.521$. We derive the average value and determine $\beta = -0.4$. Determination of γ is more challenging and we will not obtain a sufficient approximation to the calculated wax thickness for the five experiments with a fixed γ in this case. We will therefore not search for correlations with the given $\widehat{T}$ in power of a constant γ. Instead, we try to find a better alternative for $\widehat{T}$. Several combinations have been tried and the best
alternative found for a fixed γ requires that we include the incoming water temperature $T_{water,in}$.

We therefore redefine $\widehat{T}$ to the following :

$$\widehat{T} = \frac{\sqrt{(T_{WAT} - T_{oil,in})T_{oil,in}}}{T_{water,in}} \tag{5.8}$$

The best correlation curves with the new $\widehat{T}$ above is found for a best fit γ, where $\gamma_{BF} = \gamma = 4.2$. The results are presented in the Figures 5.1 and 5.2. We note that the correlation curves correspond seemingly well with the calculated wax thickness.

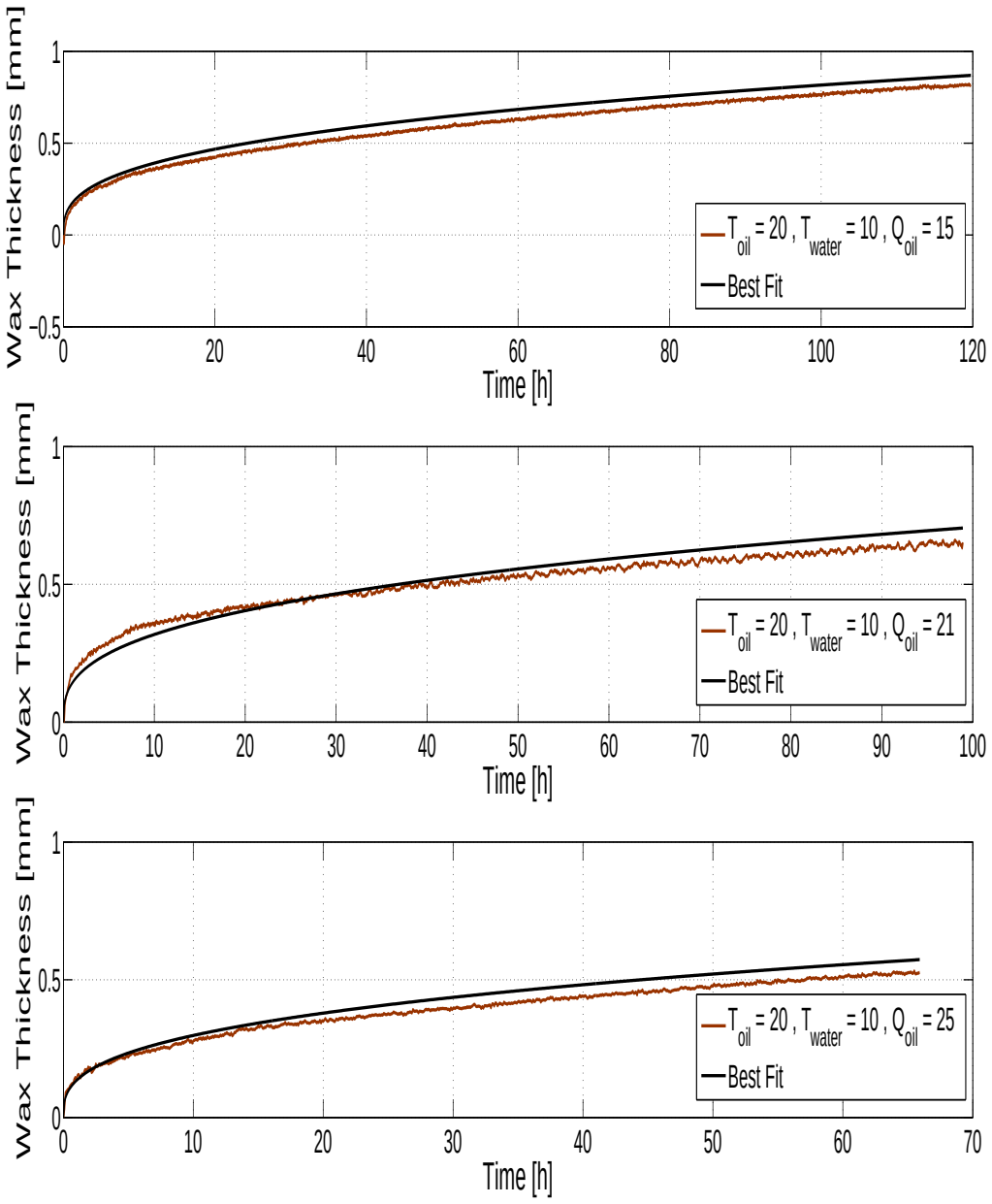

Figure 5.1: Best fit of calculated wax thickness based on dimensional analysis.

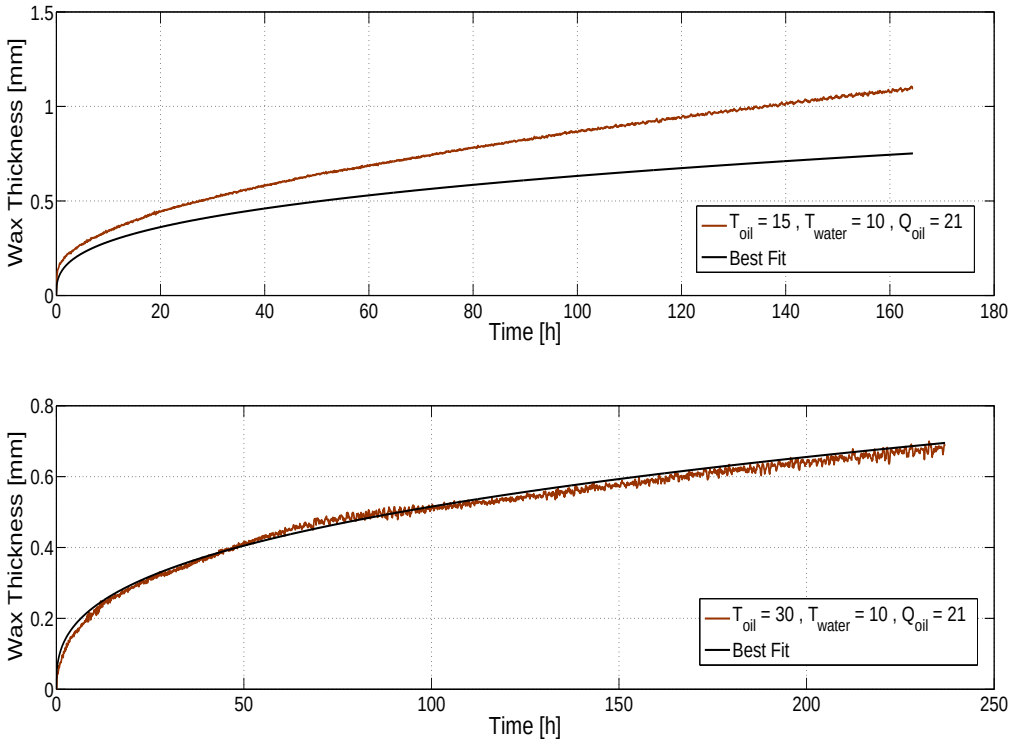

Figure 5.2: Best fit of calculated wax thickness based on dimensional analysis

5.1 Conclusion

The correlation curves based on dimensional analysis correspond well with the calculated wax thickness for three of the four experiments. The curves are derived involving important physical parameters. We assumed the temperature to have impact on the deposition process. Based on results of the wax thickness calculations, we chose the WAT and the incoming oil temperature to be most relevant when doing dimensional analysis. We could included the cooling water temperature right from the start. From the temperature analysis in the previous chapter, we found that the inner wall temperature increases very fast in the beginning of each wax experiment. We further found that the inner wall temperature approaches the incoming oil temperature after a short period in each wax experiment. Due to the isolating effect of a thin wax layer on the pipe wall, we ignored the influence of the cooling water temperature, when considering turbulent flow conditions. We therefore assumed the WAT and the bulk flow temperature as fundamental to the understanding of the calculated wax thickness for most of the time during the experiments. Since we did not find satisfactory correlation curves with the first given dimensionless temperature, we redefined it and included the incoming water temperature.

A correlation model on the form of equation (5.4) with the dimensionless temperature as defined in equation (5.3) is controversial and should therefore be discussed. In the previous chapter we found that the inner wall temperature has a large impact on the wax thickness. It is also important to keep in mind that the cooling effect of the water is one of the "driving mechanisms" that causes the paraffins to deposit on the wall. It is therefore not sure that we can ignore the effect of the inner wall temperature and the water temperature as we first did when settling a physical law for the problem of wax deposition. The main reason why we ignored the water temperature is based on the assumption that even though the water temperature is considerably lower than the oil temperature, the inner wall temperature will quickly increase toward the oil temperature. The assumption is clearly based on the condition $T_{water,in} < T_{oil,in} < T_{WAT}$, which is always satisfied among the experiments analyzed here. From the wax thickness calculations, we found that the experiment $15 - 10 - 21$ gave the largest wax thickness. From calculations of the inner wall temperature of this experiment, we also found that the temperature on the wax surface after a few hours will be much closer to the incoming oil temperature then that of the water. We will therefore expect from the analysis of this experiment, that the wax deposition after a few hours will occur as a consequence of a small temperature gradient in the thermal boundary layer close to the wall. We must therefore except that the inner wall temperature is still of large importance even though it is very close to the incoming oil temperature. Ignoring the inner wall temperature in the dimensional analysis is therefore a risky approach to the problem considered and we therefore accept that our correlation model is controversial. For the case, we should also keep in mind that the inner wall temperature itself is difficult to determine exactly, especially since it is based on a very small (measured) temperature difference between inlet and outlet of the test pipe. More accurate temperature measurements are therefore requested.

Chapter 6

Results and Conclusions

In Chapter 2, Graetz problem was studied and we established the cup-mixing temperatures defined for the flowing fluid, giving axial temperature distribution inside a pipe of laminar or turbulent flow. A summary of the results were given in Chapter 3. Considering laminar flows, the analytical temperature distributions compared well with temperature profiles obtained using integral methods.

The temperature field in a fluid flowing in a steel pipe covered with a wax layer on the inside, was also studied. It was found that a wax layer much thinner than the steel wall, affected the inside wall temperature appreciably and further influenced the wall boundary condition of the temperature of the flowing fluid.

The StatoilHydro wax deposition experiments were analyzed in Chapter 4. The analysis revealed that the wax layer thickness increased most rapidly during the first minutes or hours of all experiments and ended after typically 100 hours with a very slow growth rate compared to the first minutes. The accuracy of the measured pressures and temperatures are of importance when it comes to analysis of the calculated wax thickness. The friction number is also of importance and especially during the initial wax deposition. A better understanding of the initial deposition process requires very accurate measurements. As already indicated, the thermal boundary layer seems to diminish quickly during the first minutes in each wax experiment. We can therefore not ignore alterations of the boundary conditions for the flowing fluid, owing to the growing wax layer.

From the results obtained, we believe that there is a strong connection between the wax thickness and the inner wall temperature. The inner wall temperature has clearly an impact on the wax thickness. It would therefore been interesting if StatoilHydro had measured the inner wall temperature during the wax deposition. In this way we could have tested the calculated inner wall temperature. Another consideration that we can also relate to the inner wall temperature, is the initial deposition process. Whether the first layer has a high or low content of lighter hydrocarbons and how long it takes before the whole inner wall of the test section is covered with a thin waxy layer. All this together has an impact on the initial inner wall temperature.

Appendix A

Graetz Problem

The complete energy equation :

$$u\frac{\partial T}{\partial x} = \frac{k_f}{\rho C_p}\frac{1}{r}\frac{\partial}{\partial r}\left(r\frac{\partial T}{\partial r}\right) + \frac{k_f}{\rho C_p}\frac{\partial^2 T}{\partial x^2} + \frac{\nu}{C_p}\left(\frac{\partial u}{\partial r}\right)^2 \tag{A.1}$$

Using the dimensionless variables defined in (2.5) together with $x^* = \frac{x}{L}$ (in (A.1)) where L represent a characteristic (axial) length for modification of the thermal energy , we have :

$$\frac{u_o}{L}u^*(T_o - T_w)\frac{\partial T^*}{\partial x^*} = \frac{k_f}{\rho C_p}\frac{(T_o - T_w)}{r_o^2}r^*\frac{\partial}{\partial r^*}\left(r^*\frac{\partial T^*}{\partial r^*}\right) + \frac{k_f}{\rho C_p}\frac{(T_o - T_w)}{L^2}\frac{\partial^2 T^*}{\partial x^{*2}} + \frac{\nu}{C_p}\left(\frac{u_o}{r_o}\right)^2\left(\frac{\partial u^*}{\partial r^*}\right)^2 \tag{A.2}$$

Comparing radial diffusion with dissipation by dimensional analysis :

$$\frac{k_f}{\rho C_p}\frac{1}{r}\frac{\partial}{\partial r}\left(r\frac{\partial T}{\partial r}\right) \sim \frac{\nu}{C_p}\left(\frac{\partial u}{\partial r}\right)^2 \tag{A.3}$$

Gives :

$$\frac{k_f}{\rho C_p}\frac{\Delta T}{r_o^2} \sim \frac{\nu}{C_p}\frac{u_o^2}{r_o^2} \tag{A.4}$$

Finally :

$$\frac{1}{P_r} \sim E_c \tag{A.5}$$

where the Prandtl number is $P_r = \frac{\rho C_p \nu}{k_f}$, the Eckert number is $E_c = \frac{u_o^2}{C_p \Delta T}$, and $P_r E_c \ll 1$ must be fulfilled for the fluid considered.

Comparing axial advection with axial diffusion :

$$u\frac{\partial T}{\partial x} \sim \frac{k_f}{\rho C_p}\frac{\partial^2 T}{\partial^2 x} \tag{A.6}$$

Gives :

$$u_o\frac{\Delta T}{L} \sim \frac{k_f}{\rho C_p}\frac{\Delta T}{L^2} \tag{A.7}$$

Finally :

$$P_e \sim 1 \tag{A.8}$$

where the Peclet number is defined as $P_e = \frac{u_o L \rho C_p}{k_f}$ and $P_e \gg 1$ must be met for the fluid considered.

A.1 Coefficients

In general the coefficients are determined from :

$$A_n = \frac{\int_0^1 r_*(1-r_*^2)\exp\left(\frac{-\lambda_n r_*^2}{2}\right)\left(1+\sum_{k=1}^{K}\frac{(a_n)_k}{(k!)^2}\lambda_n^k r_*^{2k}\right)dr_*}{\int_0^1 r_*(1-r_*^2)\exp\left(-\lambda_n r_*^2\right)\left(1+\sum_{k=1}^{K}\frac{(a_n)_k}{(k!)^2}\lambda_n^k r_*^{2k}\right)^2 dr_*} \tag{A.9}$$

Including many Eigen values give :

$$N = \sum_{k=1}^{K}\frac{(a_n)_k}{(k!)^2}\lambda_n^k \to \pm\infty \tag{A.10}$$

and we find that $|A_n| \to 0$ when $n \to \infty$. We thereby expect that a restricted number of coefficients are sufficient to determine the solution of Graetz problem.

A.2 Analysis of the Coefficient Terms

We introduce the analytical expressions needed to determine A_n. Based on (A.9) we consider the general expression :

$$I = \int_0^1 R^m \exp\left(-\beta_n R^2\right) dR \tag{A.11}$$

where $\beta_n = \frac{\lambda_n}{2}$ and $m > 0$. Integration by parts of (A.11) gives :

$$I = \sum_{i=0}^{S} I_i = \sum_{i=0}^{S}\frac{(2\beta_n)^i \exp\left(-\beta_n\right)}{\prod_{j=0}^{i}(m+2j+1)} + \frac{(2\beta_n)^{(S+1)}}{\prod_{j=0}^{i}(m+2j+1)}\int_0^1 R^{2(S+1)}\exp\left(-\beta_n R^2\right) dR \tag{A.12}$$

and we ignore the integral term in (A.12) letting $s \to \infty$. It is therefore of interest to define :

$$\Delta = \frac{(2\beta_n)^{(S+1)}}{\prod_{j=0}^{i}(m+2j+1)}\int_0^1 R^{2(S+1)}\exp\left(-\beta_n R^2\right) dR \tag{A.13}$$

requiring :

$$\frac{\Delta}{\sum_{i=0}^{S}\frac{(2\beta_n)^i \exp(-\beta_n)}{\prod_{j=0}^{i}(m+2j+1)}} \ll 1 \tag{A.14}$$

Taylor expansion of the exponential term in the integral expression of (A.12) gives :

$$\int_0^1 R^{2(S+1)} \exp\left(-\beta_n R^2\right) dR = \int_0^1 R^{2(S+1)} \left(1 - \beta_n R^2 + O(R^4)\right) dR < \frac{1}{2S+3} \tag{A.15}$$

and estimation of a minimum value of S are determined through :

$$\frac{exp(-\beta_n)}{m+1} \gg \frac{(2\beta_n)^{(S+1)}}{(2S+3)\prod_{j=0}^{i}(m+2j+1)} \tag{A.16}$$

where we already know from (2.29)-(2.30) that $m \geq 3$.
S depends on number of Eigen values included in the solution, increasing with increased n. We set $S = 40$ for the five first Eigen values $(\lambda_0..\lambda_4)$ where the term on left side of (A.16) is about 10^9 times larger than the term on the right side. For the next five Eigen values $(\lambda_5..\lambda_9)$ we set $S = 75$ in the same matter. In accordance with the restrictions on S, we find it is sufficient to state :

$$\int_0^1 R^{2(S+1)} \exp\left(-\beta_n R^2\right) dR \cong \sum_{i=0}^{S} \frac{(2\beta_n)^i \exp\left(-\beta_n\right)}{\prod_{j=0}^{i}(m+2j+1)} \tag{A.17}$$

Based on (2.29)-(2.30) it is further of interest to evaluate the general expression given by :

$$\int_0^1 \sum_{k=1}^{K} \hat{A}_{n,k} R^{ak+c} \exp\left(-\beta_n R^2\right) dR \tag{A.18}$$

where a and c are constants to be determined, and $\hat{A}_{n,k}$ is defined :

$$\hat{A}_{n,k} = \frac{(a_n)_k}{(k!)^2} \lambda_n^k \tag{A.19}$$

Integration by parts of (A.18) give the following expression :

$$\int_0^1 \sum_{k=1}^{K} \hat{A}_{n,k} R^{\tilde{a}k+c} \exp\left(-\beta_n R^2\right) dR \cong \sum_{i=0}^{S} (2\beta_n)^i \sum_{k=1}^{K} \hat{A}_{n,k} \frac{\exp\left(-\beta_n\right)}{\prod_{j=0}^{i}(\tilde{a}_k + c + 1 + 2j)} \tag{A.20}$$

Finally we evaluate an expression for the general definition :

$$\int_0^1 \sum_{a=1}^{K} \sum_{b=1}^{K} \hat{A}_{n,a} \hat{A}_{n,b} R^{2(a+b)+c} \exp\left(-2\beta_n R^2\right) dR \tag{A.21}$$

where a, b and c are constants to be determined.
Integration by parts gives :

$$\int_0^1 \sum_{a=1}^{K}\sum_{b=1}^{K} \hat{A}_{n,a}\hat{A}_{n,b} R^{2(a+b)+c} \exp\left(-2\beta_n R^2\right) dR \cong$$

$$\exp\left(-2\beta_n\right) \sum_{i=0}^{S} \left(4\beta_n\right)^i \sum_{a=1}^{K}\sum_{b=1}^{K} \hat{A}_{n,a}\hat{A}_{n,b} \frac{1}{\prod_{j=0}^{i} \left(2j+2a+2b+c+1\right)} \tag{A.22}$$

A.3 Numerator

The numerator (2.29) are then determined from the following expressions :

$$\int_0^1 r_* \exp\left(-\beta_n r_*^2\right) dr_* = \frac{1}{2\beta_n}\left(1-\exp\left(-\beta_n\right)\right) \tag{A.23}$$

$$\int_0^1 r_*^3 \exp\left(-\beta_n r_*^2\right) dr_* \cong \exp\left(-\beta_n\right) \sum_{i=0}^{S} \frac{\left(2\beta_n\right)^i}{\prod_{j=0}^{i}\left(4+2j\right)} \tag{A.24}$$

$$\int_0^1 \sum_{k=1}^{K} \frac{\left(a_n\right)_k}{\left(k!\right)^2} \lambda_n^k r_*^{2k+1} \exp\left(-\beta_n r_*^2\right) dr_* \cong$$

$$\exp\left(-\beta_n\right) \sum_{i=0}^{S} \left(2\beta_n\right)^i \sum_{k=1}^{K} \frac{\left(a_n\right)_k}{\left(k!\right)^2} \lambda_n^k \frac{1}{\prod_{j=0}^{i}\left(2j+2k+2\right)} \tag{A.25}$$

$$\int_0^1 \sum_{k=1}^{K} \frac{\left(a_n\right)_k}{\left(k!\right)^2} \lambda_n^k r_*^{2k+3} \exp\left(-\beta_n r_*^2\right) dr_* \cong$$

$$\exp\left(-\beta_n\right) \sum_{i=0}^{S} \left(2\beta_n\right)^i \sum_{k=1}^{K} \frac{\left(a_n\right)_k}{\left(k!\right)^2} \lambda_n^k \frac{1}{\prod_{j=0}^{i}\left(2j+2k+4\right)} \tag{A.26}$$

A.4 Denominator

The denominator (2.30) are determined from :

$$\int_0^1 r_* \exp\left(-2\beta_n r_*^2\right) dr_* = \frac{1}{4\beta_n}\left(1-\exp\left(-2\beta_n\right)\right) \tag{A.27}$$

$$\int_0^1 r_*^3 \exp\left(-2\beta_n r_*^2\right) dr_* \cong \exp\left(-2\beta_n\right) \sum_{i=0}^{S} \frac{(4\beta_n)^i}{\prod_{j=0}^{i} (4+2j)} \tag{A.28}$$

$$2\int_0^1 \sum_{k=1}^{K} \frac{(a_n)_k}{(k!)^2} \lambda_n^k r_*^{2k+1} \exp\left(-2\beta_n r_*^2\right) dr_* \cong$$

$$2\exp\left(-2\beta_n\right) \sum_{i=0}^{S} (4\beta_n)^i \sum_{k=1}^{K} \frac{(a_n)_k}{(k!)^2} \lambda_n^k \frac{1}{\prod_{j=0}^{i} (2j+2k+2)} \tag{A.29}$$

$$2\int_0^1 \sum_{k=1}^{K} \frac{(a_n)_k}{(k!)^2} \lambda_n^k r_*^{2k+3} \exp\left(-2\beta_n r_*^2\right) dr_* \cong$$

$$2\exp\left(-2\beta_n\right) \sum_{i=0}^{S} (4\beta_n)^i \sum_{k=1}^{K} \frac{(a_n)_k}{(k!)^2} \lambda_n^k \frac{1}{\prod_{j=0}^{i} (2j+2k+4)} \tag{A.30}$$

$$\int_0^1 \sum_{k=1}^{K} \left(\frac{(a_n)_k}{(k!)^2} \lambda_n^k r_*^{2k+\frac{1}{2}}\right)^2 \exp\left(-2\beta_n r_*^2\right) dr_* \cong$$

$$\exp\left(-2\beta_n\right) \sum_{i=0}^{S} (4\beta_n)^i \sum_{k=1}^{K} \sum_{b=1}^{K} \frac{(a_n)_k}{(k!)^2} \lambda_n^k \frac{(a_n)_b}{(b!)^2} \lambda_n^b \frac{1}{\prod_{j=0}^{i} (2j+2k+2b+2)} \tag{A.31}$$

$$\int_0^1 \sum_{k=1}^{K} \left(\frac{(a_n)_k}{(k!)^2} \lambda_n^k r_*^{2k+\frac{3}{2}}\right)^2 \exp\left(-2\beta_n r_*^2\right) dr_* \cong$$

$$\exp\left(-2\beta_n\right) \sum_{i=0}^{S} (4\beta_n)^i \sum_{k=1}^{K} \sum_{b=1}^{K} \frac{(a_n)_k}{(k!)^2} \lambda_n^k \frac{(a_n)_b}{(b!)^2} \lambda_n^b \frac{1}{\prod_{j=0}^{i} (2j+2k+2b+4)} \tag{A.32}$$

A.5 Cup Mixing Temperature

The cup mixing temperature for incompressible flow is :

$$T_{cup-mix} = \frac{\int\limits_A uTdA}{\int\limits_A udA} \tag{A.33}$$

Considering laminar flow, we replace u with the Poiseuille profile given by (2.1), deriving :

$$T_{cup-mix} = \frac{4}{r_o^4} \int\limits_0^{r_o} r\left(r_o^2 - r^2\right) Tdr \tag{A.34}$$

Transforming (A.34) on dimensionless form, and introducing the dimensionless variables (see (2.5) and (2.53) as well) :

$$r^* = \frac{r}{r_o} \quad T^* = \frac{T_w - T}{T_w - T_o} \quad and \quad T^*_{cup-mix} = \frac{T_w - T_{cup-mix}}{T_w - T_o} \tag{A.35}$$

Note for the instance that r^* are used instead of r_*; only a difference of notation. The cup-mixing temperature on dimensionless form is then :

$$T^*_{cup-mix} = 4 \int\limits_0^1 r^*\left(1 - r^{*2}\right) T^* dr^* \tag{A.36}$$

Replacing T^* with the dimensionless temperature solution of Graetz problem T^*_{Graetz} (2.38) gives :

$$\begin{aligned} T^*_{Graetz-cup-mix} = {} & 4 \int\limits_0^1 \sum_{n=0}^{\infty} A_n \exp\left(-\lambda_n^2 x^*\right) r^* \exp\left(-\beta_n r_*^2\right) dr_* + \\ & 4 \int\limits_0^1 \sum_{n=0}^{\infty} A_n \exp\left(-\lambda_n^2 x^*\right) \sum_{k=1}^{K} \frac{(a_n)_k}{(k!)^2} \lambda_n^k r^{*2k+1} \exp\left(-\beta_n r_*^2\right) dr_* - \\ & 4 \int\limits_0^1 \sum_{n=0}^{\infty} A_n \exp\left(-\lambda_n^2 x^*\right) r^{*3} \exp\left(-\beta_n r_*^2\right) dr_* - \\ & 4 \int\limits_0^1 \sum_{n=0}^{\infty} A_n \exp\left(-\lambda_n^2 x^*\right) \sum_{k=1}^{K} \frac{(a_n)_k}{(k!)^2} \lambda_n^k r^{*2k+3} \exp\left(-\beta_n r_*^2\right) dr_* \end{aligned} \tag{A.37}$$

We evaluate the four terms of the dimensionless cup mixing temperature (A.37) in the same matter as we did for the terms of the coefficients A_n.

The result is :

$$
\begin{aligned}
T^*_{Graetz-cup-mix} \quad = \quad & 4\sum_{n=0}^{\infty} A_n \exp(-\lambda_n^2 x)\frac{(1-\exp(-\beta_n))}{2\beta_n} \\
& + 4\sum_{n=0}^{\infty} A_n \exp(-\lambda_n^2)\sum_{i=1}^{S}(2\beta_n)^i \sum_{k=1}^{K}\frac{(a_n)_k}{(k!)^2}\lambda_n^k \frac{\exp(-\beta_n)}{\prod_{j=0}^{i}(2k+2+2j)} \\
& - 4\sum_{n=0}^{\infty} A_n \exp(-\lambda_n^2 x)\sum_{i=0}^{S}\frac{(2\beta_n)^i \exp(-\beta_n)}{\prod_{j=0}^{i}(4+2j)} \\
& - 4\sum_{n=0}^{\infty} A_n \exp(-\lambda_n^2)\sum_{i=1}^{S}(2\beta_n)^i \sum_{k=1}^{K}\frac{(a_n)_k}{(k!)^2}\lambda_n^k \frac{\exp(-\beta_n)}{\prod_{j=0}^{i}(2k+4+2j)}
\end{aligned}
\tag{A.38}
$$

Appendix B

Turbulent Flow and Heat Transfer

The energy equation for stationary turbulent and incompressible flow in a pipe is (by ignoring dissipation and axial heat conduction) :

$$(V+v_x^{'})\frac{\partial}{\partial x}\left(T+T^{'}\right)+v_r^{'}\frac{\partial}{\partial r}\left(T+T^{'}\right)+v_\theta^{'}\frac{1}{r}\frac{\partial}{\partial \theta}\left(T+T^{'}\right)=\frac{k}{\rho C_p}\frac{1}{r}\frac{\partial}{\partial r}\left(r\frac{\partial}{\partial r}\left(T+T^{'}\right)\right) \tag{B.1}$$

Continuity :

$$\frac{1}{r}\frac{\partial}{\partial r}\left(rv_r^{'}\right)+\frac{1}{r}\frac{\partial v_\theta^{'}}{\partial \theta}+\frac{\partial v_x^{'}}{\partial x}=0 \tag{B.2}$$

The Reynolds time averaged energy equation, with typically $V \gg v_x^{'}$:

$$V\frac{\partial T}{\partial x}=\frac{k}{\rho C_p}\frac{1}{r}\left(r\frac{\partial T}{\partial r}\right)-\overline{v_x^{'}\frac{\partial T^{'}}{\partial x}}-\overline{v_r^{'}\frac{\partial T^{'}}{\partial r}}-\overline{v_\theta^{'}\frac{1}{r}\frac{\partial T^{'}}{\partial \theta}} \tag{B.3}$$

Reynolds time averaging the product of the continuity equation multiplied with the fluctuating velocity and rewriting gives :

$$\overline{\frac{\partial}{\partial r}\left(v_r^{'}T^{'}\right)}+\overline{\frac{\partial}{\partial \theta}\left(\frac{1}{r}v_\theta^{'}T^{'}\right)}+\overline{\frac{\partial}{\partial x}\left(v_x^{'}T^{'}\right)}+\frac{\overline{v_r^{'}T^{'}}}{r}-\overline{v_r^{'}\frac{\partial T^{'}}{\partial r}}-\overline{v_\theta^{'}\frac{1}{r}\frac{\partial T^{'}}{\partial \theta}}-\overline{v_x^{'}\frac{\partial T^{'}}{\partial x}}=0 \tag{B.4}$$

In (B.4) we neglect the terms $\overline{\frac{\partial}{\partial x}(...)}$ and $\overline{\frac{\partial}{\partial \theta}(...)}$ assuming fully developed flow. By combining (B.4) with (B.3) we obtain the energy equation :

$$V\frac{\partial T}{\partial x}=\frac{k}{\rho C_p}\frac{1}{r}\frac{\partial}{\partial r}\left(r\frac{\partial T}{\partial r}\right)-\frac{1}{r}\frac{\partial}{\partial r}\left(r\overline{v_r^{'}T^{'}}\right) \tag{B.5}$$

Further, we define the thermal eddy-diffusivity by modelling the fluctuating temperature transported in the radial direction :

$$-\overline{v_r^{'}T^{'}}=\kappa_t\frac{\partial T}{\partial r} \tag{B.6}$$

which, introduced into equation (B.5) give :

$$V\frac{\partial T}{\partial x}=\frac{1}{r}\frac{\partial}{\partial r}\left(r\frac{\partial}{\partial r}\left(\kappa+\kappa_t\right)\frac{\partial T}{\partial r}\right) \tag{B.7}$$

We will manipulate B.7 by using the defined cup-mixing temperature $T_{cup-mix}$ and the defined mass flux Q_m :

$$\frac{2\pi C_p \int_0^{r_o} \rho V \frac{\partial T}{\partial x} r dr}{2\pi \int_0^{r_o} \rho V r dr} = \frac{2\pi \int_0^{r_o} \frac{\partial}{\partial r}\left((k+k_t)\, r \frac{\partial T}{\partial r}\right) dr}{2\pi \int_0^{r_o} \rho V r dr} \tag{B.8}$$

Notice that k in (B.8) is the thermal conductivity while κ in (B.7) is the thermal diffusivity. By carry out the integration of (B.8) we get :

$$\frac{\partial T_{cup.mix}}{\partial x} = -\frac{2\pi r_o q_w}{C_p Q_m} \tag{B.9}$$

B.1 Heat Conduction Through Concentric Walls

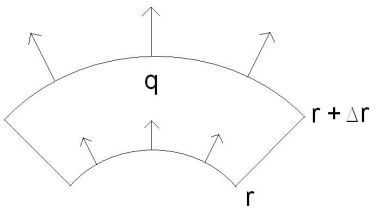

Figure B.1: Radial heat flux through a concentric element

The (radial) heat flux which streams into the element (see B.1) must equal the (radial) heat flux leaving the element :

$$q(r)A(r) - q(r+\Delta r)A(r+\Delta r) = 0 \tag{B.10}$$

Letting $\Delta r -> 0$ and rewriting (B.10), we get :

$$\frac{d}{dr}\left(rq(r)\right) = 0 \tag{B.11}$$

Integration of (B.11) gives :

$$rq(r) = r_1 q_w \tag{B.12}$$

where q_w is the heat flux found at the inner wall of radius r_1, see B.2.
Substituting Fourer's law into (B.12) gives :

$$-k_f r \frac{\partial T}{\partial r} = r_1 q_w \tag{B.13}$$

where k_f is the thermal conductivity of the fluid in the inner pipe.

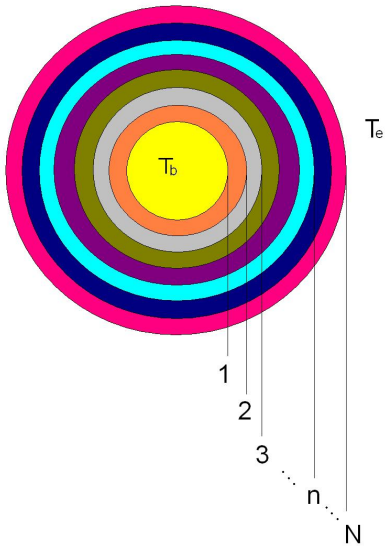

Figure B.2: Heat conduction through uniform concentric layers

Further integration between two arbitrary concentric layers (see Figure B.2) gives :

$$T_{n-1} = T_n + \frac{r_1 q_w}{k_n} ln\left(\frac{r_n}{r_{n-1}}\right) \tag{B.14}$$

Notice that we have replaced $r_n q_n$ with $r_1 q_w$ from (B.12). We use the Newton's law of cooling to evaluate the temperature difference between the inner wall and the fluid, or the outer wall and the environmental temperature. The temperature difference between the inner wall T_1 and the bulk flow T_b is (see B.2) :

$$(T_1 - T_b) = \frac{q_w}{h_f} \tag{B.15}$$

where h_f is the heat transfer coefficient of the fluid. The temperature difference between the outer wall T_N and the environmental temperature is :

$$(T_e - T_b) = \frac{1}{h_N}\frac{r_1 q_w}{r_N} \tag{B.16}$$

where we have replaced q_n with $\frac{r_1 q_w}{r_N}$ using (B.12). We can now add the temperature differences to evaluate $T_e - T_b$:

$$T_e - T_b = q_o\left(\frac{1}{h_f} + \sum_{n=2}^{N}\frac{r_1}{k_n}\ln\left(\frac{r_n}{r_{n-1}}\right) + \frac{r_1}{r_N}\frac{1}{h_N}\right) \tag{B.17}$$

If we now introduce the overall heat transfer coefficient $U_{tot} = \frac{q_w}{T_e - T_b}$ and rewrite (B.17), we get a general expression for U_{tot} :

$$U_{tot} = \left(\frac{1}{h_f} + \sum_{n=2}^{N}\frac{r_1}{k_n}\ln\left(\frac{r_n}{r_{n-1}}\right) + \frac{r_1}{r_N}\frac{1}{h_N}\right)^{-1} \tag{B.18}$$

or by defining the heat transfer coefficients related to the different concentric layers :

$$\frac{1}{U_n} = \frac{r_1}{k_n} \ln\left(\frac{r_n}{r_{n-1}}\right) \tag{B.19}$$

and rewriting the expression of U_{tot} we have :

$$U_{tot} = \left(\frac{1}{h_f} + \sum_{n=2}^{N} \frac{1}{U_n} + \frac{r_1}{r_N}\frac{1}{h_N}\right)^{-1} \tag{B.20}$$

This expression is used in both Chapter 2 and Chapter 4.

Appendix C

Experiments

C.1 Isothermal Data

Table C.1: Isothermal Experiments 2007

Month-Year	$T_{oil} = T_{water}$ $[^oC]$	Q_{oil} $[\frac{m^3}{h}]$	ΔP $[mPa]$	ρ_{oil} $[\frac{kg}{m^3}]$
Nov-2007	40	30.00	110.97	801
Nov-2007	40	24.99	79.64	801
Nov-2007	40	20.00	53.65	801
Nov-2007	40	17.50	42.46	801
Nov-2007	40	15.04	32.62	801
Nov-2007	40	9.98	16.10	801
Nov-2007	40	4.99	4.85	801
Nov-2007	40	15.00	32.44	801
Nov-2007	40	3.45	2.62	801
Nov-2007	40	4.89	4.68	801
Nov-2007	40	7.17	9.01	801
Nov-2007	40	10.06	16.09	801
Nov-2007	40	15.19	33.18	801
Nov-2007	40	19.96	53.52	801
Nov-2007	40	24.98	79.35	801
Nov-2007	40	29.99	109.89	801
Nov-2007	30	3.56	2.86	808
Nov-2007	30	5.31	5.66	808
Nov-2007	30	10.05	17.01	808
Nov-2007	30	15.19	35.05	808
Nov-2007	30	20.00	56.65	808
Nov-2007	30	24.99	83.75	808
Nov-2007	30	29.99	115.76	808

Table C.2: Isothermal Experiments 2008

Month-Year	$T_{oil} = T_{water}$ $[^oC]$	Q_{oil} $[\frac{m^3}{h}]$	ΔP $[mPa]$	ρ_{oil} $[\frac{kg}{m^3}]$
Jan-2008	60	29.88	104.3	792
Jan-2008	60	25.09	75.82	792
Jan-2008	60	20.07	51.02	792
Jan-2008	60	15.05	30.50	792
Jan-2008	60	10.15	15.68	795
Jan-2008	60	5.19	4.88	803
Jan-2008	60	24.85	74.83	792
Jan-2008	60	16.03	34.88	792
Mar-2008	40	30.02	113.39	806
Mar-2008	40	25.00	81.84	806
Mar-2008	40	20.02	55.07	806
Mar-2008	40	15.00	33.47	806
Mar-2008	40	10.00	16.37	806
Mar-2008	40	5.00	4.97	806
Mar-2008	40	20.97	59.87	806
Mar-2008	30	29.98	118.17	812
Mar-2008	30	25.00	85.78	812
Mar-2008	30	20.01	57.98	812
Mar-2008	30	15.01	35.00	812
Mar-2008	30	10.01	17.31	812
Mar-2008	30	4.99	5.31	812
Mar-2008	30	21.01	63.14	812
Feb-2008	30	21.38	64.67	811
Feb-2008	30	29.97	117.48	811
Feb-2008	30	25.01	85.29	811
Feb-2008	30	20.00	57.57	811
Feb-2008	30	15.01	34.86	811
Feb-2008	30	10.00	17.19	811
Feb-2008	30	5.00	5.23	811
Jan-2008	20	29.93	126.86	819
Jan-2008	20	25.17	93.53	819
Jan-2008	20	20.10	63.19	820
Jan-2008	20	15.13	38.81	820
Jan-2008	20	10.03	19.01	820
Jan-2008	20	5.01	5.68	823
Jan-2008	20	24.97	92.04	820
Feb-2008	20	30.03	125.15	818
Feb-2008	20	24.76	89.26	818
Feb-2008	20	20.04	61.51	818
Feb-2008	20	15.00	37.27	818
Feb-2008	20	10.03	18.48	818
Feb-2008	20	4.99	5.43	818
Mar-2008	15	25.00	97.09	824
Mar-2008	15	20.00	65.94	824
Mar-2008	15	14.99	40.09	824
Mar-2008	15	10.03	20.19	824
Mar-2008	15	5.00	6.12	824
Mar-2008	15	20.99	71.73	824

C.2 Non-Isothermal Data

Table C.3: Non-Isothermal Experiments 2008

Month-Year	T_{oil} $[^oC]$	T_{water} $[^oC]$	Q_{oil} $[\frac{m^3}{h}]$	ΔP $[mPa]$	ρ_{oil} $[\frac{kg}{m^3}]$
Mar-2007	40	10	20.99	62.38	808
Mar-2007	30	20	21.00	64.14	813
Feb-2007	30	10	21.00	64.40	812
Feb-2007	20	10	5.00	6.01	818
Mar-2007	15	10	20.99	72.55	824
Des-2007	20	12	15.00	43.86	814
Jan-2008	20	10	24.93	93.53	820
Feb-2008	30	9	21.00	64.51	812
Mar-2008	40	10	21.00	62.43	808
Mar-2008	15	10	21.00	72.55	824
Jan-2008	21	10	21.45	65.20	817
Jan-2008	21	12	10.05	19.01	816
Jan-2008	20	10	5.18	6.36	818

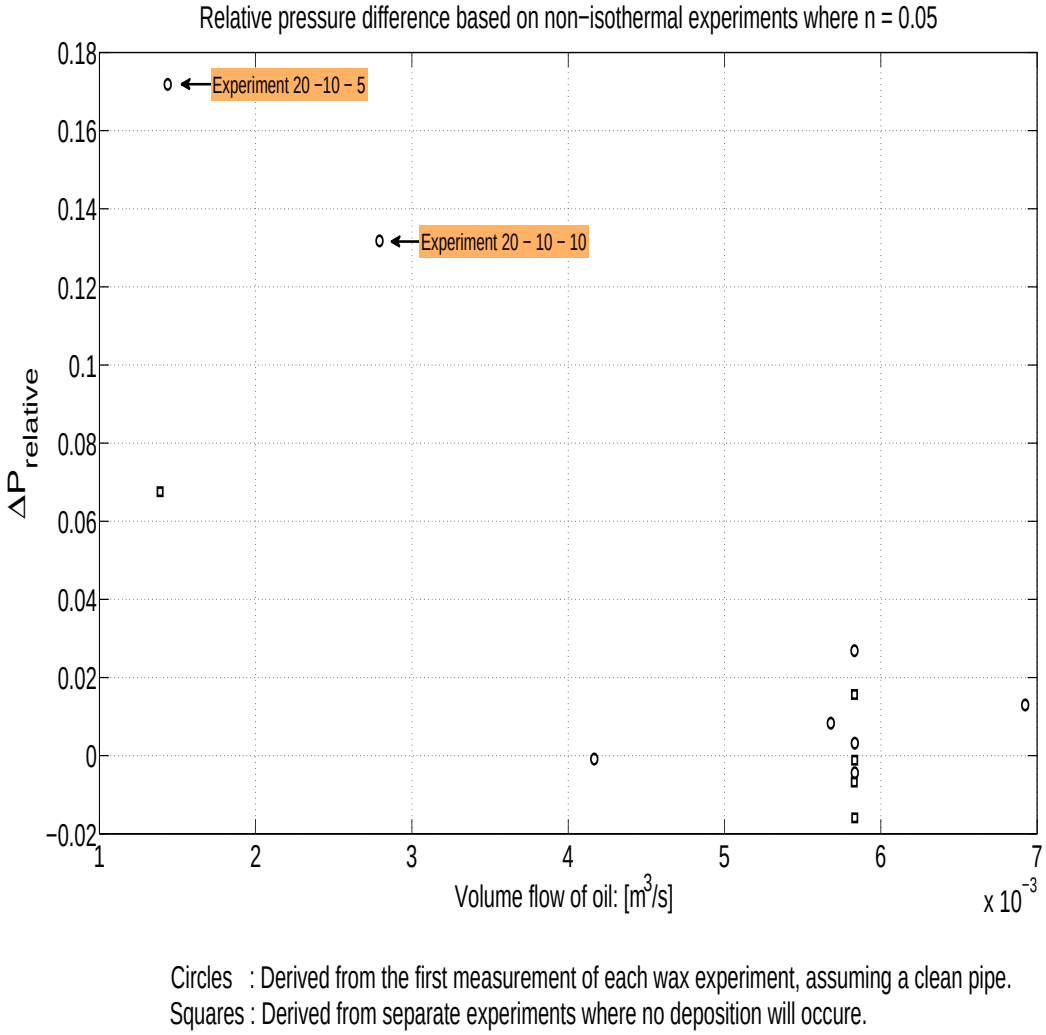

Figure C.1: Relative pressure differences for non-isothermal flow

C.3 Best fit of Measured Pressure Drops

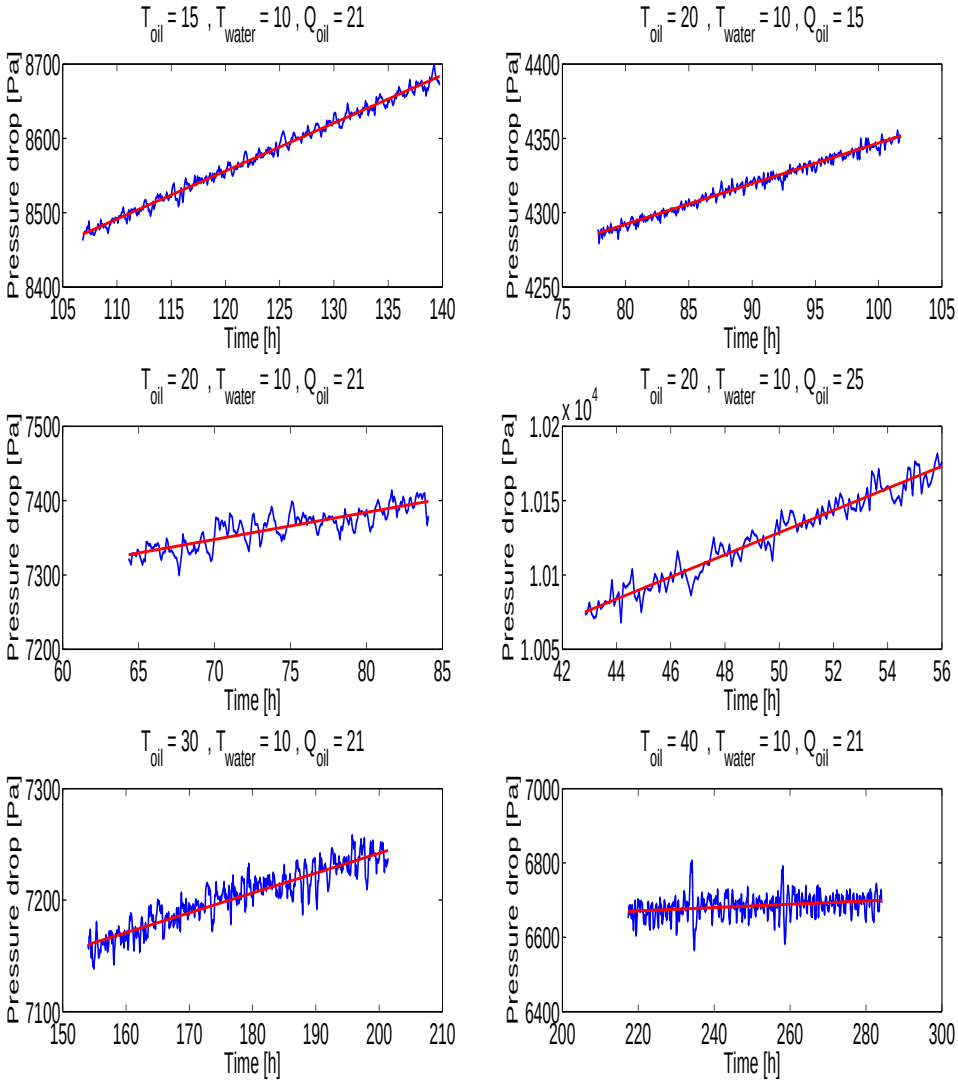

Figure C.2: Measured pressure drop and best fit curve
The red line shows the best fit line (D) from least-square analysis.

C.4 Best fit of Measured Temperature Drops

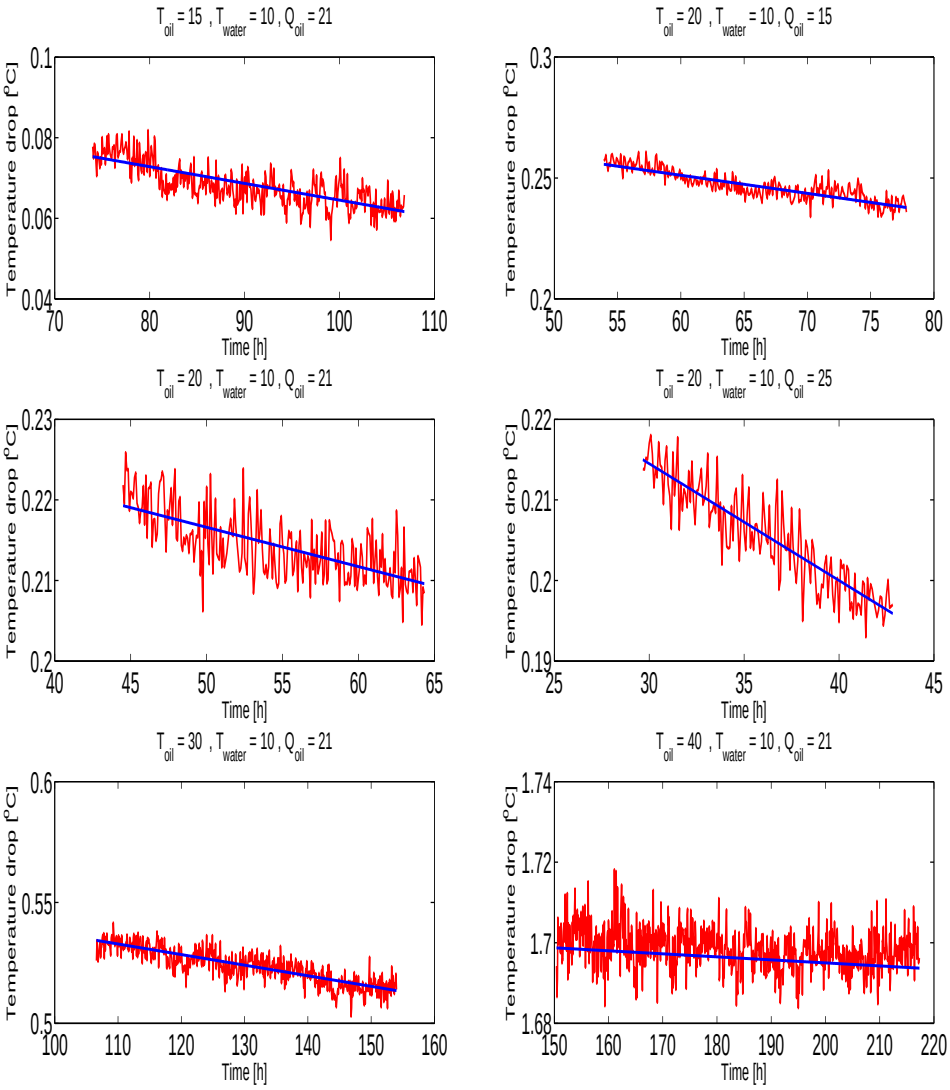

Figure C.3: Measured pressure drop and best fit curve
The blue line shows the best fit line (D) from least-square analysis.

C.5 Best Fit of Wax Thickness Calculations

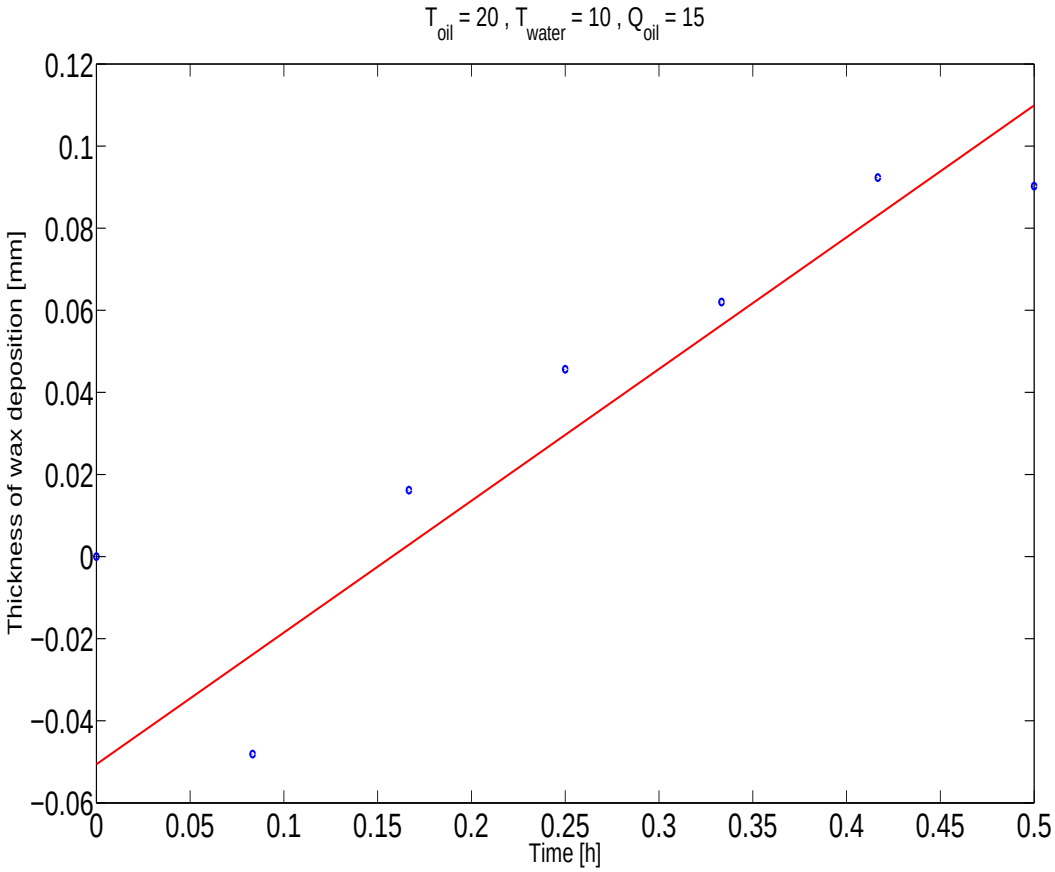

Figure C.4: Calculated wax thickness with linear approximation

The regression line is given by : $R = -0.0506 + 0.321t$
and based on the measured thickness in the interval 5min to 30 min.

Appendix D

Program Codes

D.1 Maple

```
# Codes used to derive graphs presented in Chapter 3

> reset;

> #  Intention : Comparing the analytical solution of
     Graetz problem with the profile based on the integral
     method, using unused engine oil at 320K

> #  The radius [m] on the outside (steel) wall of a smooth
     pipe:

> r_1 := 0.058;

> #  The radius on the inside steel wall:

> r_o := 0.050;

> #  The radius available for flow with inside insulation
     of 0.5mm:

> r_i := 0.0495;

> #   The area [m^2] on the inside of the smooth pipe, no
      insulation:

> A_o := evalf[5](Pi*r_o^2);

> #  Assuming the volume flux [m^3/s]( turbulent flow) to
     be a given constant:

> Q_turb := evalf[5](1/2);

> #  Volume flux (laminar flow):

> Q_lam := evalf[5](1/(2*100));

> #  The density [kg/m^3] given in the table:

> rho := 871.8;

> #  The mass flux [kg/s] (turbulent flow) is:

> F_turb := evalf[5](rho*Q_turb);
```

```
> #  The mass flux [kg/s] (laminar flow) is:

> F_lam := evalf[5](rho*Q_lam);

> #  The area averaged velocity (turbulent flow) [m/s]:

> V_turb := evalf[5](Q_turb/A_o);

> #  The area averaged velocity (laminar flow):

> V_lam := evalf[5](Q_lam/A_o);

> #  The kinematic viscosity (from table):

> nu := evalf[5](161*10^(-6));

> #  The Reynolds number is:

> R[e] := evalf[5](2*r_o*V_turb/nu);

> #  The Prandtl number is given in the table:

> Pr := 1965;

> #  The Darcy friction factor:

> f := evalf[5]((0.790*ln(R[e])-1.64)^(-2));

> #  The Pethukov Nusselt number:

> Nu_turb :=evalf[5](((f/8)*R[e]*Pr)/...
  (1.07+12.7*(f/8)^(1/2)*(Pr^(2/3)-1)));

> Nu_lam := evalf[5](3.657);

> #  The specific heat at constant pressure [J/kgK] from
     the table:

> Cp := evalf[5](1.993*10^(3));

> #  The thermal conductivity of oil [J/smK] from the
     table:

> k_f := 0.143;
```

```
> #  The viscosity given in the table:

> mu := 0.141;

> #  The thermal conductivity of the pipe wall
     (Hydro 2007):

> k_w := 22.5;

> #  The heat coefficient for laminar fluid without
     insulation:

> h_lam := evalf[5](k_f*Nu_lam/(2*r_o));

> #  The heat coefficient for turbulent flow without
     insulation:

> h_turb := k_f*Nu_turb/(2*r_o);

> #  The heat coefficient for laminar fluid with
     insulation:

> h_lam_i := evalf[5](k_f*Nu_lam/(2*r_i));

> #  The heat coefficient for turbulent flow with
     insulation:

> h_turb_i := k_f*Nu_turb/(2*r_i);

> #  The thermal conductivity of the insulation inside the
     pipe.
> #  The insulation can be associated with the wax where:

> k_i := 2*k_f;

> #  The heat transfer coefficient for the wall:

> U_w := k_w/(r_o*ln(r_1/r_o));

> #  The heat transfer coefficient for the insulation:

> U_i := k_i/(r_o*ln(r_o/r_i));
```

```
> #  The overall heat transfer coefficient for laminar
     flow, including steel wall only:

> U_lam_w := (1/h_lam)^(-1);

> #  The overall heat transfer coefficient for turbulent
     flow, including steel wall only:

> U_turb_w := (1/h_turb + 1/U_w)^(-1);

> #  The overall heat transfer coefficient for laminar
     flow, including steel wall and insulation:

> U_lam_w_i := (1/h_lam_i + 1/U_i)^(-1);

> #  The overall heat transfer coefficient for turbulent
     flow, including steel wall and insulation:

> U_turb_w_i := (1/h_turb_i + 1/U_i + 1/U_w)^(-1);

> #  The dimensionless temperature profile derived for
     turbulent flow based on the Pethukov Nusselt
     correlation:

> T_turb_a := x-> evalf[5](exp(-2*r_i*Pi*k_f*Nu_turb*x/...
    (F_turb*Cp)));

> #  The dimensionless temperature profile based on laminar
     flow (Nusselt number), including pipe wall only:

> T_lam_a := x ->  evalf[5](exp(-2*r_o*Pi*k_f*Nu_lam*x/...
  (F_lam*Cp)));

> #  The dimensionless temperature profile based on
     turbulent flow, including pipe wall only:

> T_turb_b := x -> evalf[5](exp(-4*Pi*r_i^2*U_turb_w*x/...
  (F_turb*Cp)));

> #  The dimensionless temperature profile based on
     turbulent flow, including insulation and pipe wall:

> T_turb_c := x-> evalf[5](exp(-4*Pi*r_i^2*U_turb_w_i*x/...
  (F_turb*Cp)));
```

```
> #  The dimensionless temperature profile based on laminar
     flow, including pipe wall only:

> T_lam_b := x-> evalf[5](exp(-4*Pi*r_o^2*U_lam_w*x/...
  (F_lam*Cp)));

> #  The dimensionless temperature profile based on laminar
     flow, including insulation and pipe wall:

> T_lam_c := x -> evalf[5](exp(-4*Pi*r_o^2*U_lam_w_i*x/...
  (F_lam*Cp)));

> #  Transforming the physical x to the one used in Graetz
     problem:

> a := 2*k_f/(rho*Cp*V_lam*2*r_o);

> #  The area-averaged Graetz temperature profile
     (8 first eigenvalues):

> T_Graetz := x -> 0.5811207140*exp(-7.313586808*a*x)+
                   0.1337702864*exp(-44.60946178*a*x)+
                  0.06188452782*exp(-113.9210300*a*x)+
                  0.03660743080*exp(-215.2405444*a*x)+
                  0.02457468598*exp(-348.5641168*a*x)+
                  0.01782201444*exp(-513.8900806*a*x)+
                  0.02005425268*exp(-711.2180449*a*x)-
                 0.000014443214*exp(-940.5522368*a*x)+
                 0.008814253414*exp(-1201.918059*a*x)+
                 5.5996*10^(-8)*exp(-1495.400594*a*x);

> #  The dimensionless cup-mixing temperature based on
     laminar flow and the dimensionless Graetz temperature
     (8 first eigenvalues):

     > T_m := x -> 0.8190502020*exp(-7.313586808*a*x)+
                    0.0975269400*exp(-44.60946178*a*x)+
                   0.03250393024*exp(-113.9210300*a*x)+
                   0.01544014236*exp(-215.2405444*a*x)+
                  0.008788433200*exp(-348.5641168*a*x)+
                   0.00558385500*exp(-513.8900806*a*x)+
                  0.003820188404*exp(-711.2180449*a*x)+
                   0.00275656884*exp(-940.5522368*a*x)+
                  0.002071232000*exp(-1201.918059*a*x)+
                  0.001607635356*exp(-1495.400594*a*x);
```

D.2 Matlab

```
function Wax_deposition_20_10_21_Jan_2008()

% Basic codes used to derive the graphs in Chapter 4
% Here for a fixed wax experiment (20-10-21)


% The following physical variables and parameters are used in the script:
% Volume flow (oil):                                Q_oil           [m³/s]
% Volume flow (water):                              Q_water         [m³/s]
% Pressure drop in oil pipe:                        dp              [Pa]
% Temperature incoming oil:                         T_oil_in        [°C]
% Temperature outgoing oil:                         T_oil_out       [°C]
% Temperature incoming water:                       T_water_in      [°C]
% Temperature outgoing water:                       T_water_out     [°C]
% Wax apperance temperature:                        T_WAT           [°C]
% Temperature difference:                           Temp_difference [°C]
% Inner wall temperature                            T_iw            [°C]
% Density of oil:                                   rho_oil         [kg/m³]
% Density of water:                                 rho_water       [kg/m³]
% Length of test pipe:                              dL              [m]
% Radius of oil/inner pipe:                         r_oil_i         [m]
% Thickness of oil/inner pipe:                      thickness       [m]
% Radius of inner jacket:                           r_water_i       [m]
% Radius of outer jacket:                           r_water_o       [m]
% Radius available for flow in oil pipe:            r_i             [m]
% Calculated thickness of wax:                      Wax_thickness   [m]
% Correlation curve of Wax_thickness                h               [m]
% Roughness of wall:                                eps             [m]
% Average velocity of oil:                          v_oil           [m/s]
% Molecular viscosity of oil:                       my_oil          [kg/sm]
% Molecular viscosity of water:                     my_water        [kg/sm]
% Molecular viscosity of the wall:                  my_wall         [kg/sm]
% Heat capacity of oil:                             Cp_oil          [J/kgK]
% Heat capacity of water:                           Cp_water        [J/kgK]
% Thermal conductivity of steel:                    k_steel         [J/smK]
% Thermal conductivity of oil:                      k_oil           [J/smK]
% Thermal conductivity of water:                    k_water         [J/smK]
% Thermal conductivity of deposit:                  k_wax           [J/smK]
% Reynolds number (oil):                            Re_oil          [1]
% Reynolds number (water):                          Re_water        [1]
% Prandtl number (oil):                             Pr_oil          [1]
% Prandtl number (water):                           Pr_water        [1]
% Heat transfer coefficient of oil:                 h_oil           [J/sm²K]
% Heat transfer coefficient of water:               h_water         [J/sm²K]
% Heat transfer coefficient of the wall:            U_w             [J/sm²K]
% Calculated heat transfer coefficient of deposit   U_i             [J/sm²K]
% Overall heat transfer coefficient:                U_tot           [J/sm²K]
% Pethukov friction factor:                         f_p             [1]
% Darcy friction factor:                            f_d             [1]
% Friction factor found from best fit analysis:     f               [1]
% Pethukov Nusselt correlation                      Nu              [1]




% Calling on the xls file and declaring the parameters:
% Max_row = 1193
data = xlsread('Vale_20_10_21.xls',1,'a6:p1193');
```

```
Q_oil = data(:,3)/3600;
dp = data(:,6);
T_oil_in = data(:,7);
T_oil_out = data(:,8);
% The average oil temperature
T_oil = (T_oil_in+T_oil_out)/2;
T_water_in = data(:,10);
T_water_out = data(:,11);
% The average water temperature
T_water = (T_water_in+T_water_out)/2;
% The condensate has a WAT in the interval [45,48], we therefore define :
T_WAT = (45+48)/2;
Temp_difference = -data(:,9);
rho_oil = data(:,13);
dL = 5.55;
r_oil = 0.0526/2;
Steel_thickness = 0.0039;
r_water_i = r_oil + Steel_thickness;

% Declaring further variables
r_i = zeros(1,length(Q_oil+1));
% Initial value of the inner radius
r_i(1) = r_oil;
h_oil = r_i;
T_iw = r_i;
Wax_thickness = r_i;
% Initial value of wax thickness
Wax_thickness(1) = 0;
eps = 0;
v_oil = Q_oil/(pi*r_oil^2);
% The molecular viscosity of oil is determined from a StatoilHydro function
my_oil = eta_vale(T_oil);
my_wall = r_i;

Cp_oil = 1950;
k_steel = 22.5;
k_oil = 0.1344;
Re_oil = my_wall;
Re_oil(1) = v_oil(1)*2*r_oil*rho_oil(1)/my_oil(1);
Pr_oil = Cp_oil*my_oil/k_oil;
f_p = (0.790*log(Re_oil(1))-1.64)^(-2);
Nu = ((f_p/8)*Re_oil(1)*Pr_oil(1))/(1.07+12.7*(f_p/8)^(1/2)*(Pr_oil(1)^(2/3)-
1));
h_turb = k_oil*Nu/(2*r_oil);
% The heat transfer coefficient of steel wall
U_w = k_steel/(r_oil*log(r_water_i/r_oil));
% The overall heat transfer coefficientbased on oil and steel wall
U_turb_w = (1/h_turb + 1/U_w)^(-1);
T_iw(1) = T_oil(1) - U_turb_w/h_turb*(T_oil(1)-T_water(1));
% Initialising the viscosity of the fluid at the wall
my_wall(1) = eta_vale(T_iw(1));

% Declaring lower and upper boundary
t_min = 2;
t_max = length(Q_oil) + 1;
% Declaring the time variable (hours) used in most calculations
T = zeros(1,t_max);
T(1) = 0;
```

```
% Declaring the best fit function found from log-log analysis in Chapter 4
h = T;
% Initialising
h(1) = 0;
% Declaring the correlation vector for the averaged exponential alpha-value
% given in Chapter 5
Correlation = T;
% Declaring the correlation vector based on dimensional analysis in Chapter 5
H_c = T;

%tid = zeros(1,t_max-1);
f = T;
% Defining the vector for the corrected Pethukov friction factor
f_p_corrected = T;
U_tot = T;
k_wax = T;
% Assuming no initial deposit on the wall
k_wax(1) = k_oil;
% Declaring a relative thermal conductivity of steel and wax (Chapter 4)
k_steel_wax = T;
k_steel_wax(1) = k_steel;

% Declaring the vectors used in the log-log analysis
Time = zeros(t_max-120,1);
W = zeros(t_max-120,1);
Wax = W;

%The difference-vector between h and correlation
Diff = T;

for t = t_min:t_max

        T(1,t) = 5/60*t - 5/60;


        Re_oil(t-1) = v_oil(t-1)*2*r_i(t-1)*rho_oil(t-1)/my_oil(t-1);
        f(t-1) = ((1.8*log10(6.9/Re_oil(t-1)+(eps/…
        (3.7*2*r_i(t-1)))^1.11))^(-2))*(my_wall(t-1)/my_oil(t-1))^(0.05);

        h(t) = 10^(-3.73)*T(t)^(0.271);
        Correlation(t) = 10^(-3.87)*T(t)^(0.347);
        H_c(t) = (2*r_oil*(my_oil(1)/…
        (3600*rho_oil(1)*(2*r_oil)^2))^0.347)*(Re_oil(1)^(-0.4))*…
        (((((T_WAT-T_oil_in(t-1))*T_oil_in(t-1))^(0.5))/…
        T_water_in(t-1))^(4.2))*T(t)^(0.347);


    if (T_water_in < T_oil_in)
        Wax_thickness(t) = r_oil - (rho_oil(t-1)*…
        Q_oil(t-1)^2*f(t-1)/(4*pi^2*dp(t-1)/dL))^(1/5);
        r_i(t) = r_oil - Wax_thickness(t);
        % The Pethukov friction factor corrected for non-isothermal flow
        f_p_corrected(t-1) = ((0.790*log(Re_oil(t-1))-1.64)^(-2))*…
        (my_wall(t-1)/my_oil(t-1))^(0.05);
        Nu(t-1) = ((f_p_corrected(t-1)/8)*Re_oil(t-1)*…
        Pr_oil(t-1))/(1.07+12.7*(f_p_corrected(t-1)/8)^(1/2)*…
        (Pr_oil(t-1)^(2/3)-1));
        h_oil(t-1) = k_oil*Nu(t-1)/(2*r_i(t-1));
        U_tot(t-1) = rho_oil(t-1)*v_oil(t-1)*Cp_oil*…
        (r_oil-Wax_thickness(t-1))./(2*(T_oil(t-1)-…
        T_water(t-1))).*(Temp_difference(t-1))/dL;
        T_iw(t) = T_oil(t-1) - U_tot(t-1)/h_oil(t-1)*(T_oil(t-1)-T_water(t-1));
        my_wall(t) = eta_vale(T_iw(t));
```

```
            k_wax(t) = r_oil*log(r_oil/r_i(t))/(1/U_tot(t-1) - 1/U_w - 1/h_turb);
            k_steel_wax(t) = r_oil*log(r_water_i/r_i(t))/(1/U_tot(t-1) - 1/h_turb);

        else
            Wax_thickness(t) = Wax_thickness(t-1);
            r_i(t) = r_i(t-1);
            h_oil(t-1) = k_oil*Nu(t-1)/(2*r_i(t-1));
            U_tot(t-1) = rho_oil(t-1)*v_oil(t-1)*Cp_oil*…
            (r_oil-Wax_thickness(t-1))./(2*(T_oil(t-1)-…
            T_water(t-1))).*(Temp_difference(t-1))/dL;
            T_iw(t) = T_oil(t-1) - U_tot(t-1)/h_oil(t-1)*(T_oil(t-1)-T_water(t-1));
            my_wall(t) = eta_vale(T_iw(t));
        end

    end

                for t = 1:t_max-120
                    % Defining the "Log-vectors"
                    Time(t) = log10(T(t+120));
                    W(t) = log10(Wax_thickness(t+120));
                    % The log vectors are implemented in Minitab, a statistical
                    % program deriving the linear relation given as:
                    Wax(t) = -3.73 + 0.271*Time(t);
                end
```

```
%hold on
%plot(Time,Del_Temp,'r');
%plot(Time,Wax,'b')
%hold off



%hold on
%subplot(3,1,2);
%plot(T,dp,'b');
%plot(T,1000*Wax_thickness,'c');
%plot(T,1000*Wax_thickness,'b',T,1000*h,'r');
%plot(T,1000*Wax_thickness,'b',T,1000*H_c,'r');
%plot(Time,W,'c');
%plot(Time,Wax,'r');
%plot(T,k_wax/k_oil,'r');
%plot(T,h,'r');
%xlabel('Time [h]');
%ylabel('Wax Thickness [mm]');
%title('Best fit of calculated wax thickness: - During the first five hours of
the experiment.');
%legend('T_{oil} = 20 , T_{water} = 10 , Q_{oil} = 21','Best Fit');
%hold off

%hold on
%subplot(3,2,6);
%plot(T,T_iw,'r');
%xlabel('Time [h]');
%ylabel('T_{iw} [^oC]');
%title('Inner wall temperature');
%legend('T_{oil} = 20 , T_{water} = 10 , Q_oil = 21');
%hold off

% From Dimensional Analysis
%2*r_oil*(my_oil(1)/(3600*rho_oil(1)*(2*r_oil)^2))^0.347
%Re_oil(1)
%40/T_oil_in(1)
```

List of Figures

List of Tables

Nomenclature

u :	Laminar flow velocity	$\left[\frac{m}{s}\right]$
$\overline{V}$:	Area-averaged velocity	$\left[\frac{m}{s}\right]$
μ :	Molecular viscosity	$\left[\frac{kg}{sm}\right]$
ν :	Kinematic viscosity	$\left[\frac{m^2}{s}\right]$
k :	Thermal conductivity	$\left[\frac{J}{smK}\right]$
ρ :	Density	$\left[\frac{kg}{m^3}\right]$
C_p :	Heat capacity	$\left[\frac{J}{kgK}\right]$
κ :	Thermal diffusivity	$\left[\frac{m^2}{s}\right]$
q :	Heat flux	$\left[\frac{J}{sm^2}\right]$
h :	Heat transfer coefficient of fluid	$\left[\frac{J}{sm^2K}\right]$
U :	Heat transfer coefficient	$\left[\frac{J}{sm^2K}\right]$

x :	Axial position along pipe	$[m]$
r :	Radius	$[m]$
T :	Temperature	$[K]$
P :	Pressure	$[Pa]$
τ :	Shear stress	$[Pa]$
Q :	Mass flux	$\left[\frac{kg}{s}\right]$
H :	Wax thickness	$[m]$

Appendix E

Bibliography

Abramowitz, M. and Stegun, I.A., 1964, *Handbook of Mathematical Functions*, National Bureaux of Standards.

Brown T.S., Niesen, V.G. and Erickson, D.D., 1993, "Measurement and Prediction of the Kinetics of Paraffin Deposition," *Society of Petroleum Engineers 26548.*

Elphingstone, G.M., Greenhill, K.L. and Hsu, J.J.C., 1999, "Modeling of Multiphase Wax Deposition," *Journal of Energy Resources Technology*, Vol. 121, pp. 81 - 85.

Graetz, L., 1885, *Ann. Physik*, Vol. 25, No. 337.

Hausen, H., 1959, "Neue fur die Warmeubertragung bei frir und Erzwungener Stromung," *Allg. Warmetchnik*, Vol. 9, pp. 75-79.

Incropera F.P. and DeWitt D.P., 1996, *Fundamentals of Heat and Mass Transfer, Fourth Edition*, John Wiley & Sons.

Kok, M.V. and Saracoglu, R.O., 2000, "Mathematical Modelling of Wax Deposition in Crude Oil Pipelines," *Petroleum Science and Technology*, Vol. 18, No. 9, pp. 1121 - 1145.

Krasovitskii, B.A. and Maron, V.I., 1981, "Growth of Paraffin Deposits on the Pipe Wall," *Inzhenerno-Fizichaskii Zhurnal*, Vol. 40, No. 4, pp. 683 - 689.

Lee H.S. and Fogler, H.S., 2001, "Combined Convective Heat and Mass Transfer Analysis of Wax Deposition under Turbulent Flow Conditions," *Department of Chemical Engineering, University of Michigan and Chevron Energy Technology Company, Housten.*

Lévêque, 1928, *Ann. des Mines*, Vol. 12, No. 13, pp. 201, 305, 381

Mills, A.F., 1979, *Journal of Heat Transfer*, Volume 101, Issue 3.

Perry, R.H. and Chilton, C.H., 1973, *Chemical Engineer's Handbook, Fifth Edition*, McGRAW-HILL.

Petukhov, B. S., 1970, "Heat Transfer and Friction in Turbulent Pipe Flow with Variable Physical Properties," *Advances in Heat Transfer*, Vol. 6, Academic Press, Inc., New York, pp. 504 - 564.

Quarmby, A. and Anand, R.K, 1969, "Axisymmetric Turbulent Mass Transfer in a Circular Tube", *J. Fluid Mech.*, Vol. 38, pp. 433 - 455.

Ramachandran, V. and Fogler, H.S., 2004, "Comments on Analogies for Correlated Heat and Mass Transfer in Turbulent Flow," *AIChE*, Vol.50, No. 7, pp. 1623 - 1626.

Ramirez-Jaramillo, E., Lira-Galeana, C. and Manero, O., 2004, "Modeling Wax Deposition in Pipelines," *Petroleum Science and Technology*, Vol. 22, No. 7-8, pp. 821 - 861.

Schulkes, R., 2006, "An Introduction to Multiphase Flow", *The University of Oslo, Compendium.*

Shah, R.K. and London, A.L., 1978, "Laminar Flow Forced Convection in Ducts," *Advances in Heat Transfer*, Academic Press.

Singh, P., 2000, "Gel Deposition on Cold Surfaces," *The Univeersity of Michigan, PhD Thesis.*

Srivastava, S.P., Handoo, J., Agrawal, K.M. and Joshi, G.C., 1993, "Phase-Transition Studies in n - Alkanes and Petroleum Related Waxes," *J. Phys. Chem., Solids*, Vol. 54, No. 639.

Svendsen, J.A., 1993, "Mathematical Modeling of Wax Deposition in Oil Pipeline Systems," *AIChE Journal*, Vol.39, No. 8, pp. 1377 - 1388.

Todi, S., 2006, "Experimental and Modeling Studies of Wax Deposition in Crude-Oil-Carrying Pipelines," *Offshore Technology Conference 18368.*

Venkatesan, R. and Fogler, H.S., 2004, "Comments on Analogies for Correlated Heat and Mass Transfer in Turbulent Flow," *AIChe Journal*, Vol. 50, No. 7.

White, F.M., 2006, *Viscous Fluid Flow, Third Edition*, McGRAW-HILL

Wilcox, D.C., 2006, *Turbulence Modeling for CFD, Third Edition*, DCW Industries